Fermi National Accelerator Laboratory

FERMILAB-TM-2061

Prospectus for an Electron Cooling System for the Recycler

J.A. MacLachlan, editor

Fermi National Accelerator Laboratory
P.O. Box 500, Batavia, Illinois 60510

November 1998

Operated by Universities Research Association Inc. under Contract No. DE-AC02-76CH03000 with the United States Department of Energy

Prospectus
for an
Electron Cooling System
for the
Recycler

October 20, 1998

Abstract

The Recycler ring was added to the Main Injector (MI) project in 1997 as means to recover the antiprotons remaining at the end of Tevatron stores and to serve as a second stage accumulator to raise the maximum stack current. This report describes an electron cooling system with substantially higher stack capacity than the Recycler stochastic cooling system which could be brought into operation toward the end of Run II. It is the major component of a program to double the design Run II luminosity and should have a positive effect on integrated luminosity soon after turn-on. The upgrade potential is intended to meet the longer term needs of the Laboratory's luminosity upgrade program. The current experience with electron cooling is discussed to provide the rationale for the choice of design parameters and to make clear the needs for additional development work. Both analytical and numerical development of the theory has been pursued to confirm that the limits in principle are well beyond foreseen need. The specific hardware described is not the only realization that has been considered, but it is in some ways the most conservative. The general scheme of using an electrostatic accelerator with high efficiency charge recovery was actively discussed in the 1980's. Recent developments have served to build confidence in this approach, but, by whatever means realized, a Recycler electron cooling system will require significant extension of current practice. The Prospectus incorporates the ideas and understanding current 15 September 1998. Rapid progress toward a comprehensive development plan at this time means that its details will already differ from ideas now current.

Contributors to the Recycler Electron Cooling Design
Alexi Burov (Budker Institute)
Curtis Crawford
Thomas Kroc
James MacLachlan, Prospectus editor
Sergei Nagaitsev, group leader
Charles Schmidt
Anotoli Sharapa (Budker Institute)
Alexander Shemyakin (Budker Institute)
Arden Warner

Contents

Chapter 1

Introduction

The Laboratory started in 1995 to investigate the application of electron cooling to 8 GeV antiprotons in the Recycler as a promising component of an upgrade of Tevatron luminosity beyond the Run II goals. The idea was not entirely new at that time; it had been proposed as an upgrade path for the Accumulator as early as 1985, [1] and there had been some experimental work as well as conceptual development.[2] The practice and principles are well established for ions with velocity less than 0.8 c, i.e., for p-bars of less than a GeV or so. For ions of higher velocity the fundamentals are the same, but hardware development is required and the technical problems differ.

The Recycler is a fixed 8 GeV kinetic energy antiproton storage ring installed near the ceiling of the Main Injector tunnel. It employs a stochastic cooling system to collect multiple batches from the Accumulator and re-cool antiprotons which remain at the end of Tevatron stores. Electron cooling will improve cooling performance in the Recycler, permitting faster stacking and larger stacks. In combination with other accelerator upgrades it will permit substantially greater luminosity in the collider.

A charged particle traveling in an electron beam undergoes Coulomb scattering with the electrons. The resulting friction and velocity diffusion tend to bring such particles into thermal equilibrium with the electrons. If the particle kinetic energy in the beam frame is high in the comparison with the electron temperature, diffusion is insignificant and the particles are cooled. The method of electron cooling was originally suggested by A. M. Budker. [3] It was developed and studied then both theoretically and experimentally; an ample list of the references can be found in Ref. [4], for example.

Electron cooling can reduce the spread in all three components of beam momentum simultaneously. Its primary advantage over stochastic cooling is that the cooling effect is practically independent of antiproton beam intensity. It's greatest disadvantage is that the effect is very weak until the antiproton emittances are already close to the values wanted in the collider. Thus, the two processes can be seen as complementary rather than competitive. Electron cooling will prove very powerful in the Recycler as an add-on to the stochastic pre-cooling in the Antiproton Source and Recycler.

1.1 Role of electron cooling in the collider upgrade

The Tevatron will continue to be the highest energy collider for several years. To apply this resource to the outstanding issues within its energy reach, Fermilab is committed to an upgrade program which will sustain the historical increase in luminosity. Figure 1.1 displays the history of

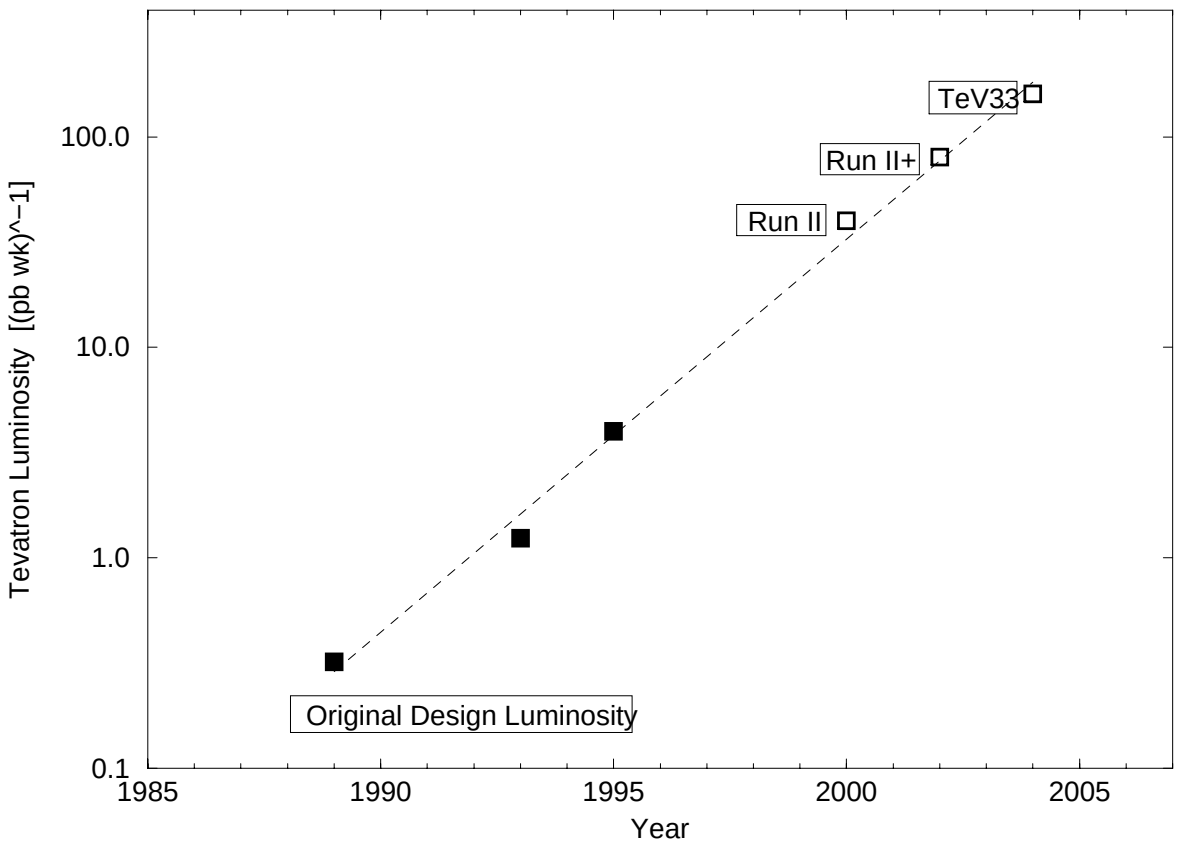

Figure 1.1: Tevatron collider luminosity history on a semi-log scale shows a 2.3 yr doubling time. The open circles are projections to Run II, Run II plus electron cooling, and later operation at $10^{33}\ \mathrm{cm}^{-2}\mathrm{s}^{-1}$.

the typical average luminosity since 1989 and a projection through Run II. Over the years 1989 – 97, average luminosity has increased from 0.32 to more than 2 pb^{-1}/week; the original design luminosity was 0.2 pb^{-1}/week. The increase has been exponential with a doubling time of ~ 2 years. The first open point on the projection is the Run II goal of the combination of Main Injector and Recycler. The second open point represents the initial goal for electron cooling at 80 pb^{-1}/week. The electron cooling approach described in this report is expected to be open to improvements that will support operation at the 160 pb^{-1}/week represented by the last point on the projection.

The projected luminosity growth depends on several developments. Electron cooling is part of a comprehensive program to increase collider luminosity. The Main Injector will supply a higher flux on the production target and brighter proton bunches for collision. It should also improve the efficiency of antiproton acceleration somewhat. The Recycler will make a major contribution to the antiproton supply by reclaiming those remaining at the end of stores and by allowing for the accumulation of larger stacks than the Accumulator can handle effectively. Before the Recycler was added to the Main Injector project, the Run II goal was 16 pb^{-1}/week; the factor 2 – 3 to reach 40 pb^{-1}/week comes directly from a corresponding increase in the number of antiprotons available for a store. The upgrade of the Recycler with electron cooling is key to further increase in the antiproton supply and consequent continued increase in the luminosity.

At each increment in luminosity the entire collider beam scenario will be empirically re-optimized

in accordance with the performance of each part of the accelerator chain at the new flux; that is what operators do. Therefore, it requires a number of assumptions to quantify the luminosity gain expected from the incremental improvement in any single component. For the purpose of illustrating the payoff for electron cooling, a highly simplified argument will be used. The Recycler Technical Design Report[5] indicates that it is possible to sustain a program at 40 pb^{-1}/wk with a flux of $2 \cdot 10^{11}$ $\overline{\mathrm{p}}$/hr and 10 eVs transfers from the Accumulator at two hour intervals. The maximum $\overline{\mathrm{p}}$ intensity in the Recycler is $4 \cdot 10^{12}$. Taking the total cross section σ_T at 2 TeV to be 75 mb, the $\overline{\mathrm{p}}$'s are consumed for physics at the rate of $5.4 \cdot 10^{10}\mathrm{h}^{-1}$, which is 27% of the nominal $\overline{\mathrm{p}}$ flux from the Antiproton Source. Assume that the utilization ratio remains fixed and that, therefore, luminosity is directly proportional to the number of antiprotons stored. Also assume that the Accumulator is limited to stack intensity of $4 \cdot 10^{11}$ or less to maintain rate. Then as flux increases, the Accumulator must be emptied more frequently. To handle higher flux at fixed bandwidth, the gain profile must be flattened to give a stack distribution which is proportionally wider but has the same number of $\overline{\mathrm{p}}$ per eV at the peak. This is because flux $\Phi \propto \psi/(\mathrm{d}\psi/\mathrm{d}E)$, and, for constant flux over the width of the distribution, the distribution is exponential $\psi(E) \sim e^{E/\Delta}$. Thus, the width Δ and the flux change in direct proportion. If the Accumulator stacks at twice the Run II rate, $4 \cdot 10^{11}$/hr, it can be emptied of $4 \cdot 10^{11}$ $\overline{\mathrm{p}}$ in 10 eVs once per hour.

It is shown in Chapter 4 that the electron cooling can reduce longitudinal emittance by 180 eVs/hr more or less independently of momentum spread. It is also shown in Chapter 5 that the equilibrium emittance is 7 eVs with a full stack, so that with desired stack emittance of 60 eVs, intrabeam scattering does not reduce the stacking rate. The emittance that needs to be cooled during an eight hour store cycle is approximately 10 eVs for every batch plus the recycled beam which could be at most 400 eVs. Run II projects 144 eVs recycled emittance in 36 bunch operation based on filling the Tevatron buckets; this is a worst-case upper limit. The emittance to be recycled is going to grow with luminosity. If the proton beam, store length, and the initial $\overline{\mathrm{p}}$ emittance remain the same, the emittance to be recycled will also grow linearly. Extrapolating from past experience and consistent with Recycler TDR projection, the values 133 eVs at initial peak luminosity $\mathcal{L} = 2 \cdot 10^{32}\,\mathrm{cm}^{-2}\mathrm{s}^{-1}$ and 400 eVs at 10^{33} are assumed. Granting all this, the relation between luminosity, $\mathcal{L}$, and amperemeters of electron beam, $\mathcal{C}$, is linear:

$$\mathcal{L} = 30\mathcal{C} \quad ,$$

where the luminosity is given in units of $\mathrm{pb}^{-1}\mathrm{wk}^{-1}$. Figure 1.2 plots this relation up to luminosity of $200\,\mathrm{pb}^{-1}\mathrm{s}^{-1}$, roughly equivalent to peak luminosity of $10^{33}\,\mathrm{cm}^{-2}\mathrm{s}^{-1}$. A floor of $\mathcal{L} = 40\mathrm{pb}^{-1}\,\mathrm{wk}^{-1}$ is shown on the plot because below this level the stochastic cooling in the Recycler is sufficient by itself; above this level the electron cooling will be used for the momentum cooling. The projection ignores the probability that electron cooling will likely be needed also for transverse cooling at some point before the upper end of the plot and also assumes ideal performance from a new technology. The assumptions are rather speculative. Furthermore, the assumption on the effectiveness of stochastic cooling in the Accumulator at higher flux is the most optimistic possible. Should emittances from the Accumulator be higher for higher flux, the relation between luminosity and cooling power would have a positive curvature, but in any case the recycled beam remains the predominant factor over a wide luminosity range. Therefore, it does not make sense to determine the design parameters directly from the preceding arguments. It appears more reasonable to work toward a slightly optimistic extrapolation of the limited experience at Fermilab and elsewhere; the cost of the cooler is not a strong function of the design current for currents of 500 mA or less. On the other hand, the projection implies that the proposed system could evolve to satisfy the needs of the collider well into the future. For example, the cooling necessary to recycle $3 \cdot 10^{-5}\,\pi$ mm mrad

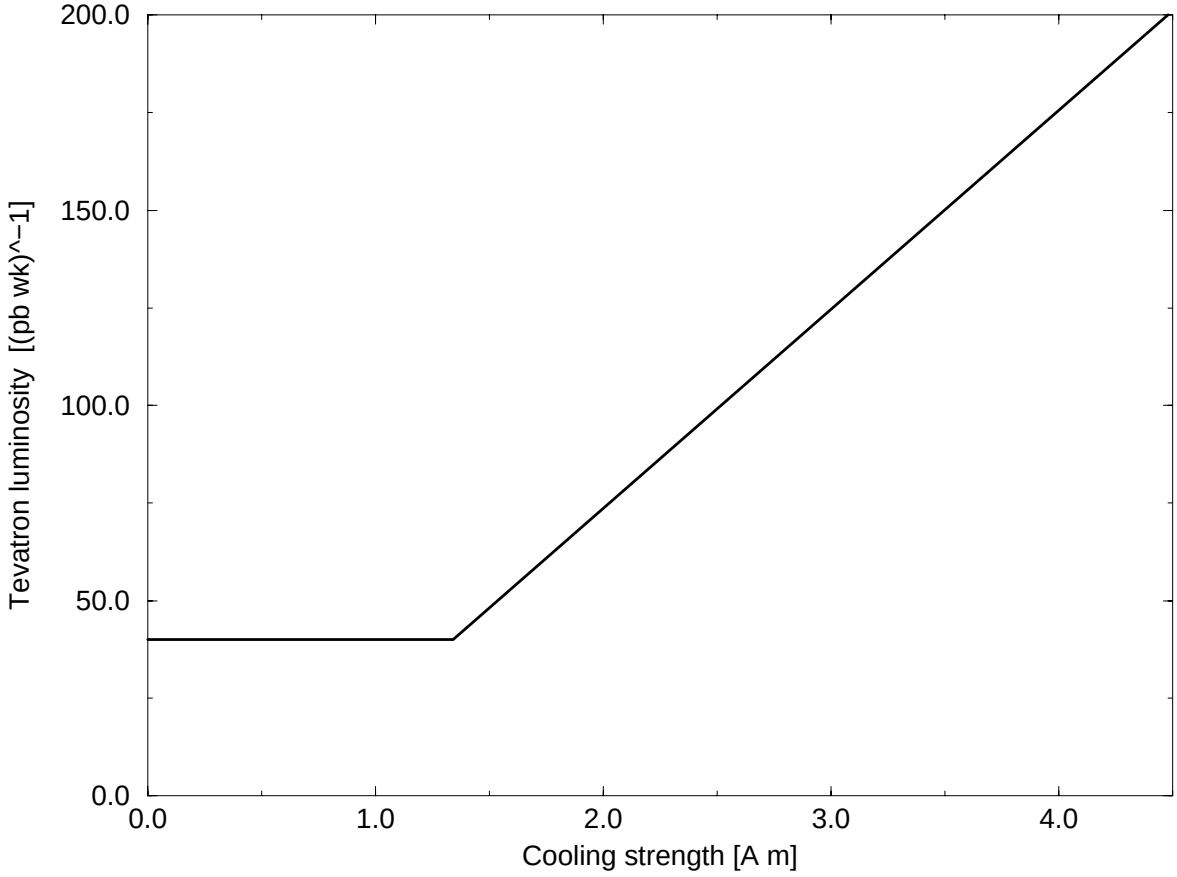

Figure 1.2: Tevatron luminosity $[\mathrm{pb}^{-1}/\mathrm{wk}]$ *vs.* electron beam current [A] $\times$ cooling section length [m] based proportionality between $\bar{\mathrm{p}}$ supply and luminosity and ideal cooler performance

transverse emittance is 20 A m with a cooling region β of 200 m.

1.2 Recent developments in recirculation technology

Electron cooling of the 8 GeV antiprotons in the Recycler ring requires high-quality dc electron beam with the current of several hundred mA and kinetic energy of 4.3 MeV. The only technically feasible way to attain such high electron currents is through beam recirculation (charge recovery). The recirculation principle is shown schematically in Figure 1.3. The primary current path is from the cathode at the high voltage terminal potential to ground where the electron beam interacts with the antiproton beam and cooling takes place, then to the collector located in the terminal, and finally through the collector power supply back to the cathode. Take, for example, a terminal potential of 5 MV, a collector power supply voltage of 5 kV, and a beam current of 500 mA. Providing there is no current loss to ground, the real power needed to circulate the beam is 2.5 kW given by the beam current times the collector voltage. The beam power, the 25 MW given by the beam current times the terminal potential, represents stored energy and is reactive.

One of the principal goals of the R & D program started in 1995 is to develop and demonstrate the technology to recirculate a suitable electron beam. The technical goal set for a proof-of-principle demonstration using mostly existing equipment was recirculation of a 200 mA beam for the period of one hour. This goal was reached in June 1998: currents of 200 mA were main-

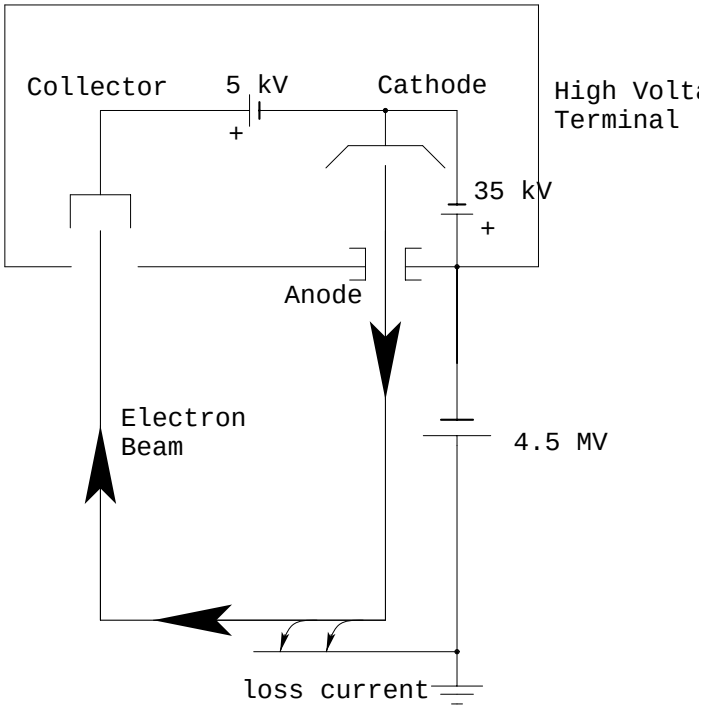

Figure 1.3: Simplified electrical schematic of the electron recirculation system

tained for the periods of one hour (typical) without a single breakdown, 300 mA for 20 minutes, and 680 mA for seconds. Although the recirculation tests used a 1-1.5 MeV electron beam and the Recycler electron cooling system requires a 4.3 MeV beam, the demonstration is relevant because the increased energy does not involve fundamental changes in technology.

This demonstration was performed using a 2 MeV Pelletron accelerator (Van de Graaff type) at National Electrostatics Corporation. The results of these tests demonstrate the feasibility of a Pelletron-based dc recirculating system capable of producing hundreds of milliamperes in the MeV energy range.

1.3 The complementary pieces of the upgrade program

There are three additional upgrades beyond those contained in the Run II plan which will be required to realize all of the luminosity gain which the electron cooling offers. Taken separately, they appear to be on a scale that would permit each to be carried out by an appropriate Beams Division department.

The dual use of the AP1 line as a 120 GeV line to the production target and as an 8 GeV antiproton line to the Recycler may limit the transfer frequency from Accumulator to Recycler to about once every two hours. When the production rate is increased it will be necessary to unload the Accumulator more often. If the existing AP3 line is extended all the way to the Recycler with a dedicated antiproton transfer line (AP5), the transfers could be carried out at whatever rate proved optimum for the Accumulator cooling system, even every few seconds if desired. The dedicated line relieves the Main Injector of time lost as an 8 GeV transfer line. When the Accumulator can be emptied frequently, the stack tail system can be re-optimized for higher flux.

The Accumulator must of course stack at a higher rate. Modest gains in protons on target, ac-

ceptance in the antiproton line to the Debuncher, ring acceptances, and cooling system performance can be combined to raise the stacking rate from 20 to 40 mA/hr.

The CDF and D0 experiments are being upgraded to handle peak luminosity of $2 \cdot 10^{32} \mathrm{cm}^{-2}\ \mathrm{s}^{-1}$. Therefore, as the antiproton supply is increased above the Run II design figure, the peak luminosity must be controlled. By making the focusing of the beam at the detectors stronger as the emittances increase and the intensity drops, it will be possible to maintain the luminosity near its initial peak value for a substantial fraction of the store. The average luminosity for the store will then increase nearly in proportion to the increased flux. This luminosity leveling can be achieved by a control system program which slowly changes the current in the low-beta quads around the detectors while controlling the Tevatron tunes, closed orbit, and chromaticities.

1.4 Scope of the project

The report describes the basic elements of an electron cooling system to be installed in the Recycler during the Run II period. Although electron cooling is well understood, the Recycler application represents a major step in beam energy, to 8 GeV from less than 1 GeV. The step is large enough that the high voltage generator, beam transport, and cooling region all require extension of the state of the art. Therefore, about three years of research and development activity are likely to precede introduction of any electron cooling equipment into the Recycler.

The R & D phase of the project has the following goals:

1. optimized system parameter set
2. a reliable 4.3 MeV electron beam
3. beam collector and transport to sustain a circulating current of at least 0.5 A
4. precise matching from discrete-element beam transport to continuous cooling region solenoid
5. a 20 m cooling section with uniform axial magnetic field with precision such that $\bar{\mathrm{p}}$ transverse angles $\lesssim 10^{-4}$
6. beam instrumentation and control to maintain alignment and equal mean velocity of electron and $\bar{\mathrm{p}}$ beams to precision $\lesssim 10^{-4}$, to measure beam temperature, to determine neutralization, *etc*.

The laboratory developments are now being carried out at National Electrostatics Corp. in Middleton WI and in the downstream end of the Wideband Lab experimental area at Fermilab. There is sufficient space at Wideband to carry out the development work envisioned for the Recycler cooling project. The hardware aspects of the development program are treated in detail in Chapters 6, 7, and 8 and the modeling aspects in Chapter 4. The goal of the development program is cooling system hardware ready for installation into the Recycler.

The remainder of the work constitutes an accelerator improvement projects of moderate scale. The basic tasks are

1. construction of an enclosure for the high voltage generator and an interconnection tunnel to the MI enclosure for the electron beam transport
2. installation of a Recycler lattice insertion for the cooling region

3. installation of cooling section and electron beam transport

4. commissioning of the cooling system

5. construction of a $\bar{p}$ transport line from the Accumulator to the Recycler (AP5 line)

6. incremental improvements to $\bar{p}$ Source to double throughput

Some aspects of these final phase tasks are considered in Chapters 5 and 9.

The emphasis in this report is on the R & D aspects of the project. That emphasis accounts for the substantial space devoted to fundamental principles and the discussion of numerical and analytical models. The modeling has yielded a self-consistent set of basic system parameters to represent the system concept and a general conclusion that the proposed realization is practicable. The R & D program consists of a continuation of the modelling studies in parallel with the experimental development program to produce an adequate cooling system within a useful time.

A suitable technique must be identified and developed to produce bright electron beam of 4.3 MeV at about 500 mA. Although more than one hardware scheme has been considered, the path with the fewest unresolved issues and reasonable prospects is the electrostatic accelerator with beam recirculation to which this prospectus is limited. It provides a nominal design from which it is reasonable to expect development of a cooler that meets the programmatic goals of the Laboratory. The provisional nature of some parameter choices is not so fundamental and represents less concern for the timely construction of a cooler facility than the need to establish experience with a suitable technology. Theoretical work and modeling studies are proceeding to optimize such parameters as p-bar beam radius, cooling section length, focusing strength for electron beam, electron current, *et al*. Current laboratory studies of the high voltage dc systems and space charge dominated beam optics need to be continued and intensified. Conceptually, there is a fair piece of parameter space open for a useful cooler. Practically, where the final design lands will be established most expediently by development tests.

The system concept which is described in Chapter 3 is a direct descendant of the original 1980's scheme using an electrostatic accelerator with lumped-element beam transport to and from the cooling interaction region. Although development of this technology is definitely needed, the apparent cost/benefit ratio justifies some technical risk. The cooling device is being developed to provide a multiplier of two or more on the collider physics productivity deriving from the Main Injector project at a few hundreths of the Main Injector cost.

Chapter 2

Recyler Operating Scenario with Electron Cooling

It is unnecessary to recapitulate the complete scenario for Collider operation with the Main Injector and Recycler rings because electron cooling in the Recycler is consistent with the general scheme described in Chapter 2 of the Recycler TDR[5] and Chapter 7 of the Run II Handbook[6]. In fact, because it is planned to introduce electron cooling into the end of Run II as it surpasses the performance of the stochastic cooling, the initial scenario will differ primarily in details of Recycler operation. Because the two cooling methods have different characteristics, the mode of Recycler operation will be significantly different from the outset. For early operation, however, Recycler inputs, outputs, and timing will be similar to the Run II specifications. As performance improves somewhat shorter stores may be preferred.

For descriptive purposes it is convenient to use approximate round numbers. Furthermore, although some parameters are known with great accuracy, precise performance numbers would be misleading at this stage of development. Later chapters deal with the confidence limits on important parameters and how to confront remaining open issues. In Table 2.1 one finds the basic timing and beam intensities related to Recycler operation without detail on efficiencies and losses. The three parameter sets are Run II Recycler, the initial goal for electron cooling, and cooling approaching goals of the TeV33 upgrades; they correspond approximately to the three open squares on the plot of collider luminosity versus time in Fig. 1.1. This report focuses on the the Run II+ parameters; the flanking columns provide relevant comparisons. In this table some parameters have a value for "recycling" and another value for "stacking". Recycling applies to the condition where the antiprotons from the Tevatron have just arrived, the stack has been transferred to the Tevatron for the next store, and the next batch from the Accumulator has not yet arrived. Stacking applies to the entire time from the injection of the first Accumulator batch to shot setup. These stages of the Recycler cycle are discussed individually below for the steady state that is attained after there has been a full intensity store and time to build up a full Accumulator stack. Since the aim of a cycle is to produce a stored beam, a new cycle will be considered to begin with the end of experimental use so that the first phase of a Recycler cycle will be shot setup. Figure 2.1 illustrates the number of antiprotons in the Recycler as a function of time. It is drawn for half hour transfer interval and $40 \cdot 10^{10}$ antiprotons/hour average stacking rate. The frequent Accumulator-Recycler transfers require the proposed antiproton line (AP5) to the Recycler so that the AP1 proton line and the MI are not used for antiproton transport. In the absence of the AP5 line, a less efficient mode of operation would be used; three or four Accumulator-Recycler transfers would be made per storage cycle, each interrupting

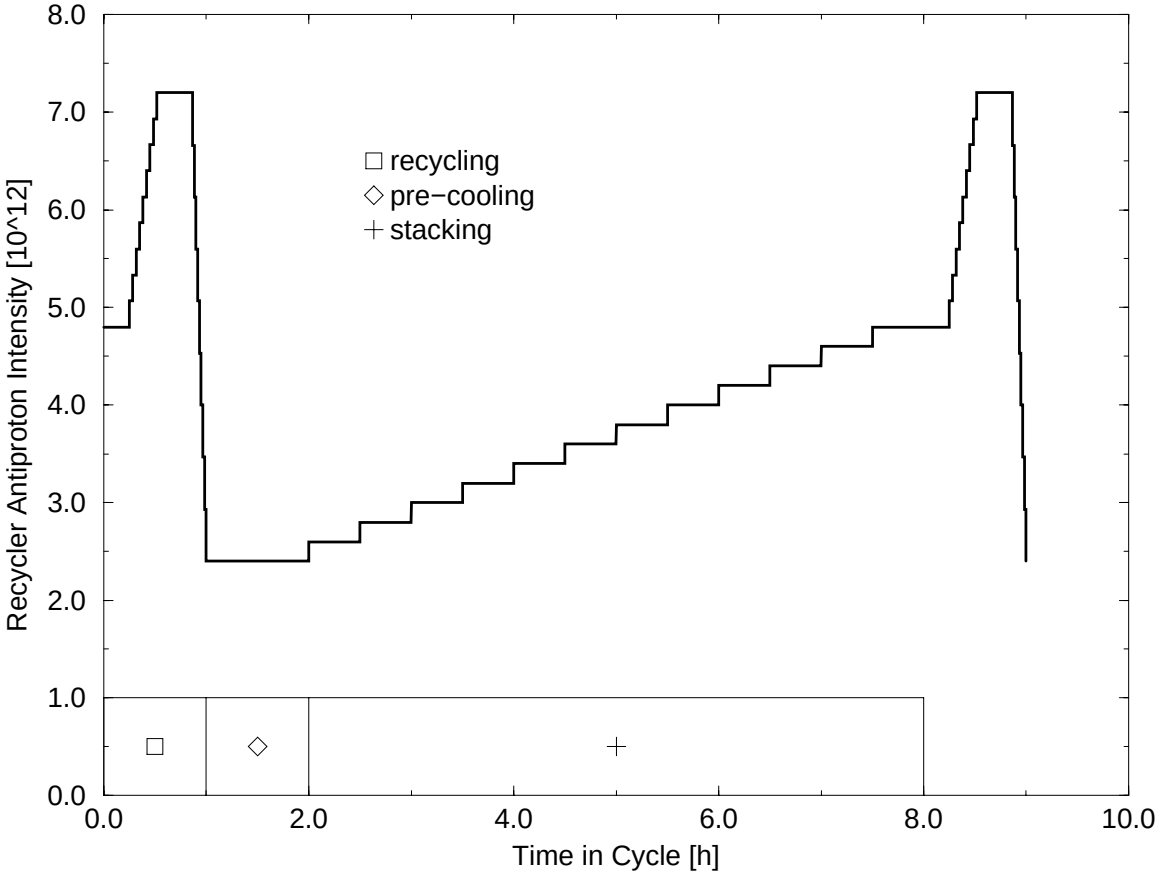

Figure 2.1: Recycler beam current over a full store cycle starting at the setup for a new store

antiproton production for an estimated fifteen minutes. The performance illustrated depends not only on the development of the electron cooling but also on the detailed management of the longitudinal phasespace of the several components of the beam with a broadband rf system. The use of so-called barrier buckets for this purpose is described at length in the Recycler TDR.[5]

2.1 Shot setup

At this stage the Recycler has a stack from $2 \cdot 10^{12}$ (Run II) to $4 \cdot 10^{12}$ (Run II+) uniform around the circumference except for an ion clearing gap. The gap is increased to about 3/4 of the circumference to receive nine Tevatron batches each containing on average eleven bunches with 132 ns spacing totaling $1 – 3 \cdot 10^{12}$ antiprotons. Protons are scraped at 1 TeV and antiprotons are decelerated to 150 GeV and then decelerated to 8 GeV in the Main Injector in nine separate cycles. By the time the bunches reach the Recycler their emittance can be nearly 2.5 eVs each. The barrier bucket rf system is used to adiabaticlly debunch and compress each batch into a ± 17 MeV segment roughly 800 ns long. For the ninth and final batch just the necessary 1.6 μs gap remains. Protons can then be reverse injected from the MI to check the tuneup for antiproton extraction. Once the Tevatron is filled with the proton bunches, the antiproton bunches can be extracted from the Recycler in nine batches with the correct bunch spacing for the MI and the Tevatron. The entire stack will be extracted, leaving only the recently returned antiprotons at the end of the shot setup sequence.

Table 2.1: Collider operating scenario with the Recycler and electron cooling

	Run II	Run II + e. c.	→TeV33	
Tevatron $\bar{p}$				
number of $\bar{p}$ in store	2.5	5.0	10.	$\cdot 10^{12}$
number of bunches	$36 \rightarrow 100$	100	100	
bunch spacing (minimum)	$395 \rightarrow 132$	132	132	ns
length of store	7	7	7	hour
length of nominal store cycle	8	8	8	hour
initial transverse emittance	2.5	2.5	2.5	$\cdot 10^{-6}$ m (rms)
initial bunch emittance	$1.5 \rightarrow 0.6$	0.6	0.6	eVs
final transverse emittance	3.3	4.2	5.0	$\cdot 10^{-6}$ m (rms)
final bunch emittance (maximum)	$3.0 \rightarrow 1.2$	2.4	4.0	eVs
number of $\bar{p}$ recycled	1.4	2.8	5.0	$\cdot 10^{12}$
time to load Recycler	15	15	15	min.
Antiproton Source				
average $\bar{p}$ production rate	20	40	80	$\cdot 10^{10}$/hr
time between extractions (typical)	2.0	0.5	0.25	hr
number of $\bar{p}$ per batch (typical)	40	20	20	$\cdot 10^{10}$
number of batches	3	14	26	
longitudinal emittance of batch	10	10	15	eVs
transverse emittance of batch	1.6	1.6	2.5	$\cdot 10^{-6}$ m (rms)
Recycler				
stochastic cooling time for recycling	7	1	1	hr
pre-recycling transverse emittance	3.3	4.2	5.0	$\cdot 10^{-6}$ m (rms)
post-recycling transverse emittance	1.6	1.6	2.5	$\cdot 10^{-6}$ m (rms)
pre-recycling longitudinal emittance	120	240	400	eVs
post-recycling longitudinal emittance	60	60	60	eVs
steady state transverse emittance	1.6	1.6	1.6	$\cdot 10^{-6}$ m (rms)
steady state longitudinal emittance	54	54	54	eVs
max. $\bar{p}$ beam	3.9	7.8	15.	$\cdot 10^{12}$

Historically, the shot setup has taken two hours or more; the goal for Run II is get this down to forty-five minutes. The length of the shot setup is taken as one hour in Table 2.1 consistent with the level of approximation adopted here. The total store cycle is taken as eight hours for initial operation because this is near the optimum established in the Recycler TDR and is operationally convenient.

2.2 Recycling

The beam returned from the MI has transverse normalized emittance of as much as $5 - 6 \cdot 10^{-6}$ m (rms). Thus by the time of the next shot it must be reduced by a factor of three or so. The cooling time for the outer part of this distribution using electrons is comparable to length of a store cycle. However, with no other beam in the ring, the stochastic cooling system can provide the desired transverse cooling in about an hour. Because the energy spread is substantial, as much as ± 12 MeV, intrabeam scattering will not be a limit; therefore for the recycling phase the beam is distributed over nearly the entire ring circumference to minimize the peak current. The transverse cooling is expected to remain useful at Run II+ levels, but the longitudinal cooling will become ineffective as the intensity is raised. The Accumulator continues to stack during this period. If the dedicated antiproton line from Accumulator to Recycler is available, the first transfer would be made at the end of the recycling period, about two hours into the cycle. Otherwise the first Accumulator batch would be taken at about three hours into the cycle. A variant of this procedure may be needed if the Accumulator can not continue to stack efficiently during the full stochastic pre-cooling period. It is possible to resume stacking from the Accumulator while the transverse pre-cooling of the recycled beam proceeds. The increments to the $\bar{\mathrm{p}}$ current will progressively degrade the stochastic cooling, but a few $\sim 10\%$ increments might be tolerable.

2.3 Stacking

Stacking in the Recycler is fundamentally a longitudinal phase space stacking of the Accumulator batches. The momentum cooling must clear enough phase space between injections to accommodate the the following one. The broadband rf system is used to open an azimuthal gap of about one Accumulator circumference to receive a batch. The length of the batch is then adjusted to match its momentum spread to that of the stack, after which the two are adiabatically combined by slowly reducing the rf barrier. In order to maintain a steady state stacking, the momentum cooling must reduce the spread of the augmented stack to its earlier value in the time between batches, a reduction in energy spread of 15 – 20 %.

The value of once per half hour given for the frequency of batch transfers from Accumulator to Recycler is an estimate for the optimum frequency. It limits the Accumulator stack to an intensity at which the stochastic cooling systems should be working close to their highest cooling rates. Electron cooling can be integrated more directly into the Run II scheme with less frequent transfers, every two hours for example. Then the transfers would likely be made at about three, five, and seven hours into the cycle. To get the full benefit of the electron cooling, more frequent transfers are required. For the half hour interval it is expected that it will be best to start transfers in the second hour and stop one hour before the end.

Chapter 3

Nominal System Parameters

The physics principles of the cooling process are described at greater length in Chapter 4, but most of the general features of an electron cooler can be understood from a qualitative description of the scheme. The electron beam is accelerated to the same mean velocity as the antiprotons and passed through a straight section in the Recycler. It is prepared with the lowest practicable momentum spread. In the coordinate frame moving at the common mean velocity there are a relatively small fraction of antiprotons moving randomly among many electrons of much lower momentum. The effect of the momentum exchange in the many Coulomb collisions of each antiproton is to pass the energy of the random motion from the antiprotons to the electrons. The antiprotons circulate for minutes or hours through this straight section while the electrons make a single pass and are collected at potential close the electron gun potential. In the co-moving frame the process looks like the exchange of heat between a hot, tenuous antiproton gas and a denser electron gas that is continuously circulated at low temperature. The kinetic energy of electrons that move at the same velocity as 8 GeV antiprotons is 4.3 MeV. The cooling rate is proportional to the electron current and the length of the cooling straight section. Unfortunately, the Lorentz transformations that convert the cooling rate in the beam frame to the rate in the laboratory frame introduce an inverse square dependance on the antiproton energy. For this reason a design for medium energy will push hard for high electron current and a long interaction region. However, the recycling scenario does not require very fast cooling nor a very high phase space compression, so cooling system parameters other than beam energy do not differ by a full order of magnitude from those already used for low energy ions.

3.1 Cooler description

In Figure 3.1 is shown the general layout for the Recycler electron cooling system. A 4.3 MV electrostatic accelerator is located in an underground enclosure just south of the MI-30 Service Building. The accelerator depicted is a Pelletron, similar to the one used for recirculating beam tests at National Electrostatics Corp. The electron beamline enters and leaves the MI tunnel through a side tunnel near Q306. The beam transport includes vertical achromatic bends at the bottom of the Pelletron, two right angle achromatic bends at the entrance into the Recycler tunnel, and a 180° achromatic bend to return the beam from the end of the cooling region to the side tunnel. Figure 3.2 shows a schematic of the Pelletron including the high voltage terminal containing the electron gun and collector, the acceleration and deceleration gradient columns, and the focusing solenoids

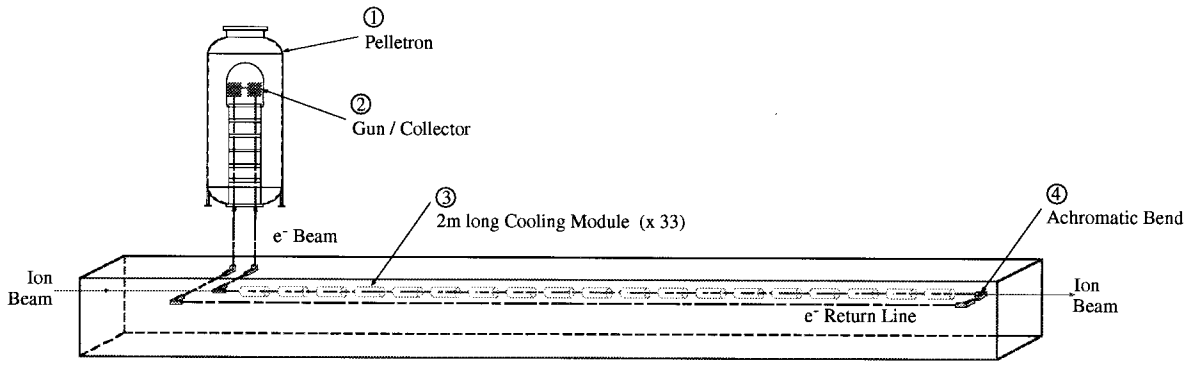

Figure 3.1: Plan of the 4.3 MV electron cooling system

on the columns. It contains many standard NEC components, but would be custom-built for its special application. The principal technical parameters of the cooler are given in Table 3.1.

The cooling section itself is shown as twenty meters in this scheme, but there is space to make it up to about 80 m. The cooling section length can be increased if that is more practical than raising the current to upgrade performance. Leaving open space has the advantage of providing for the convenient introduction and commissioning of a second-generation cooler at a later date, a development that would combine the advantages of enhanced performance with operational redundancy for continued operation in the event of the failure of either cooler. The cooling section is contained in a continuous solenoid with axial field of about 50 G. There is a matching section at the upstream end to adjust the beam to trajectories in the solenoid. The beam at the gun must enclose the same flux as the beam in the cooling section. Otherwise, the beam in the cooling section will have non-zero mechanical angular momentum to conserve generalized momentum. Thus, the electron gun is also surrounded with a solenoid as shown in Fig. 3.2. The equality of enclosed fluxes is an additional condition on the matching between the beam transport and the cooling section.

3.2 Antiproton beam parameters

As indicated in Chapter 2, the Recycler accepts 8 GeV antiprotons from the Accumulator and the Main Injector. Batches from the Accumulator and the recycled $\overline{p}$'s are stacked and cooled to the emittance required for the collider. The entire stack is used to fill the Tevatron except for the most recently returned $\overline{p}$'s, which have not had sufficient cooling time. The parameters for the three types of beam in the Recycler are summarized in Table 3.2. Although the electron cooling can operate during the hour of stochastic cooling of the returned $\overline{p}$'s, the effect is small because emittance is too large. The operation of the combined systems should be simulated, however, because the effect of the electron cooling should be to improve the ratio of signal to noise in the longitudinal stochastic cooling system by collecting the particles with low momentum error so that the signal produced by them is at the center of the filter notches. There may be useful enhancement of the transverse cooling as well.

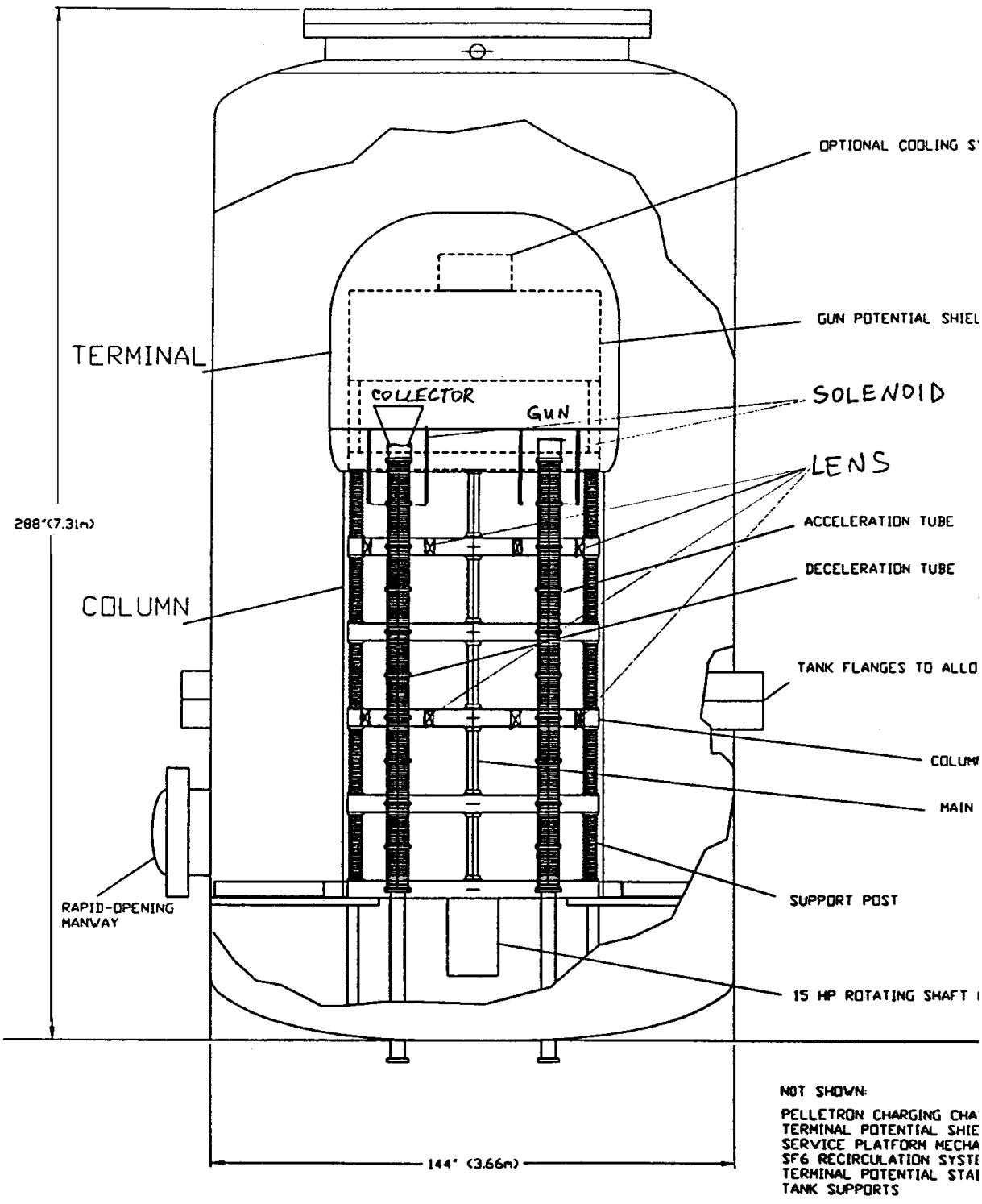

Figure 3.2: Schematic of a 5 MeV electrostatic accelerator of the Pelletron type configured for recirculating electron beam

Table 3.1: Technical parameters of the cooler

Electrostatic Accelerator		
terminal voltage	4.3	MV
terminal regulation	± 200	V
charging capacity	400	μA
terminal capacitance (est.)	350	pF
circulated current	0.5	A
gun solenoid field	200	G
gun cathode diameter	0.5	cm
gun-terminal bias	-50	kV
collector efficiency	99.995	%
collector-cathode bias	5	kV
beam diameter (typical)	0.8	cm
height of HV tank	7.3	m
outside diameter of HV tank	3.7	m
HV insulation - SF_6	6.4	atm. abs.
column vacuum	10	nT
time for tank access, in & out	4	hr
Cooling Section		
length	20	m
solenoid field	≤ 50	G
vacuum	0.1	nT
beam radius	0.6	cm
antiproton beam C-S β	20	m

Table 3.2: Antiproton beam parameters for the Recycler

Stack		
intensity (max)	5	$\cdot 10^{12}$
normalized rms emittance (h & v)	1.6	$\cdot 10^{-6}$ m
total longitudinal emittance	54	eVs
Accumulator Batches		
intensity (typical)	20	$\cdot 10^{10}$
normalized rms emittance (h & v)	1.6	$\cdot 10^{-6}$ m
total longitudinal emittance	10	eVs
number of batches in stack (typical)	14	
batch injection interval (typical)	30	min.
Recycled Beam		
intensity (typical)	2.2	$\cdot 10^{12}$
(before stoch. cooling)		
normalized rms emittance (h & v)	5	$\cdot 10^{-6}$ m
total longitudinal emittance	240	eVs
(after stoch. cooling)		
normalized rms emittance (h & v)	2.5	$\cdot 10^{-6}$ m
total longitudinal emittance	240	eVs

3.3 Recycler lattice

The Recycler described in the Technical Design Report[5] maintains nearly the same FODO focusing pattern in the MI-30 straight section as in the arcs, but the dispersion is matched to zero. To install electron cooling, a matched insertion of the desired length and β value will be introduced. The example shown in the TDR (Fig. 2.2.11) is for a 100 m length of 200 m β, which was developed to provide the highest practical β value. This choice was made to provide for the most effective transverse cooling. At that time, the electron beam was intended to do all of the cooling, and planning was intended to be compatible with the TeV33 requirements for a stack of approximately 10^{13} $\bar{\text{p}}$'s.

The design presented in this report is optimized for longitudinal cooling and has an initial goal for a stack of $5 \cdot 10^{12}$. For this intensity the transverse stochastic cooling is adequate for recycling. It is demonstrated in Chapter 4 that the length and the β value for the cooling insertion should be about equal to maximize the rate of longitudinal cooling. The optimum choice for the current plan is a 25 m clear section with $\beta = 20$ m. The optics for this case have not yet been calculated, but with plenty of space and the need to match only the β-functions, a solution is unlikely to be difficult. The added phase advance in the straight section should not be a dynamical problem if it makes an integer tune change. Such an insertion is less of a perturbation of the basic lattice than the TDR example. The Recycler phase trombone can be used to compensate for small change in the fractional tune. Because the tradeoff between cooling section length and electron beam current is one of the matters open to adjustment in developing a full design, the design of the high-beta insertion is also subject to change. However, because some permanent magnets have been made for the 200 m high-β insertion, one goal of the conceptual design effort will be to evaluate the consequences

of accepting the 200 m value as a design constraint.

Besides the elements for the β-matching, which can be permanent magnets, powered trims will be required to achieve precise alignment of the antiprotons with the cooler axis. The tune shift caused by the electron beam is small, $\Delta\nu \approx 4 \cdot 10^{-5}$, so local correction is not required. However, it may be desirable to correct locally the x-y coupling introduced by the solenoid.

3.4 Performance

The performance of the cooler in a general sense has been presented in terms of the scenario it facilitates. This section provides more specific information on the design goals for cooling rates, system reliability, *etc*. The Pelletron is favored as a high voltage generator because it is well proved at least as an ion accelerator for nuclear physics. The high-gradient acceleration tubes are free of organic materials and have good vacuum properties. Energy stability is excellent ($\pm 5 \cdot 10^{-5}$). MeV level negative terminal machines have been made, although the experience with electrons is more limited. Recirculation applications, *e. g*. free electron lasers, have not achieved the dc current that electron cooling requires. Therefore, development of a useable cooler can be expected to require thorough engineering throughout and months of commissioning. It is expected that the technical obstacles to circulating hundreds of milliamperes can be overcome, but it is not simply a matter of designing a suitably efficient collector. The whole system needs to be developed to efficiently transport currents at this level and to maintain stable operation for hours at a time. It is not the available charging current that limits acceptable beam loss but rather the need to maintain voltage stability. Fortunately, however, the antiproton beam should survive a sudden loss of high voltage with only slight disruption. The process of restoring the electron beam intensity will be slow enough to be adiabatic. Therefore, an occasional sparkdown would not render the cooler useless. However, longer loss of cooling would at least delay the program and in a matter of hours result in the loss of antiprotons.

So long as the transverse emittance of the $\bar{\mathrm{p}}$ beam is at the 10 π mm mrad specified in Table 3.2, the performance of the cooler for stacking can be summarized in a single number, 18 eVs/h/A/m, which gives the decrement in longitudinal emittance per hour normalized to an ampere of electron beam in a one-meter cooling region. This means, for example, that Accumulator batches of 10 eVs could be stacked at about half-hour intervals with 55 mA electron beam in a 20 m cooling region. The analysis of Chapter 5 shows the effect of intrabeam scattering (IBS) has a neglegible effect on rate or momentum width in either stacking or recycling mode. The level of IBS is one of the few accelerator physics issues causing uncertainty in performance projections. The apparent margin of safety for stacking in the nominal parameters would not be generous at the full design intensity if the IBS is correctly evaluated in Refs. [5, 7] However, there appears to be an error in the work which underlies both references (see Section 5.3).

Chapter 4

Analytical and Numerical Modeling Studies

Despite thirty years of theoretical and practical investigation (see for example the references in [4, 8]), there remain practically important questions to be resolved or, at least, requiring more detailed or accurate results. In particular, the optimization of the cooling of a specified particle distribution should be developed more fully.[9] This subject is addressed in Section 4.2.2. As an introduction the cooling system requirements are first estimated with a simplified version of the model used later in Section 4.2.

The focus of calculations in the conceptual design process has been to establish values for important system parameters, estimate acceptable tolerances, identify potential problems, and delineate the areas of greatest uncertainty. Recycler electron cooling is pushing far into a new regime of beam energy, but Run II goals do not lead to major extrapolation in other parameters or the underlying physics. The regime in which the proposed system will operate makes it more simple to analyze than a typical low energy cooling system. Even a simplified version of the model permits useful estimation of the cooling rates, longitudinal drag, and the sensitivity of these to parameter changes.

4.1 Elementary Model

What is a simplified physical model for low energy cooling is actually more realistic for the Fermilab proposal which does not employ a strong solenoid in the cooling region or carry the cooling process to the stage where $\bar{p}$ velocity spread is small compared to the spread in electron velocity. In this case the electron-antiproton collisions are simple Rutherford scattering, and the effect of the electron velocity distribution is minor. The cooling interaction is described in the beam frame, that is, in a coordinate system moving with the mean velocity common to the protons and electrons. In this frame a tenuous distribution of $\bar{p}$'s moving in random directions at low speed is scattered by more numerous electrons which are also moving in all directions but even more slowly. The situation is analogous to the introduction of a hot $\bar{p}$ gas into a cool electron gas. In this view the cooling hardware is a refrigerator which circulates an electron fluid to provide a heat sink of infinite capacity, hence the evocative name electron cooling. However, the system is a heterogeneous non-neutral plasma, and the velocity distributions are non-isotropic; the definition of temperature for relativistic beams and the concept of thermal equilibration do not simplify the analysis. It is sufficient to analyze the interaction as the non-relativistic Coulomb scattering of single $\bar{p}$'s with a distribution of electrons. The only collective plasma effect taken into account is limitation of the impact pa-

rameter for the collisions by the Debye screening radius. This approach has been described in both research papers and reviews, for example references [8] and [10]. No one reference derives all of the expressions used here, but reference [11] provides more detail from the same point of view and reference [8] is a rather complete review.

If a quantity $\mathcal{L}(u,\chi)$ is some function of the center of mass scattering angle χ and relative velocity u in the Coulomb scattering, the average rate of change of $\mathcal{L}$ is

$$\langle\dot{\mathcal{L}}\rangle = n^\star \int\int u\,\sigma(u,\chi)\,\mathcal{L}(u,\chi)\,g(\vec{v})\,\mathrm{d}u\,\mathrm{d}\chi \quad ,$$

where $n^\star$ is the volume density of the electrons, σ is the Rutherford cross section, and g is the normalized velocity distribution of the electrons. Quantities like the density n and $\overline{\mathrm{p}}$ momentum p_p which will be referred to both lab and beam frames will be given the superscript $\star$ for the beam frame. Other quantities like the electron velocity $\vec{v}$ and relative velocity $\vec{u}$ which always refer to the beam frame will not be superscripted. When $\mathcal{L}$ is $\Delta\vec{p}_p^\star$, $\langle\dot{\mathcal{L}}\rangle$ is the average frictional or cooling force $\vec{F}^\star$. The component of $\Delta\vec{p}_p^\star$ along $\vec{p}_p^\star$ gives the cooling, the transverse components add in quadrature to give a concomitant diffusion. The diffusion coefficients are given by the same integral with $\mathcal{L} = \Delta p^\star_{p,i}\,\Delta p^\star_{p,j}$. The diffusion of the $\overline{\mathrm{p}}$ by the electrons is not practically significant. However, the scattering of a $\overline{\mathrm{p}}$ by the $\overline{\mathrm{p}}$ — intrabeam scattering — is an important source of diffusion which is treated in Section 5.3 using this approach.

The angular integration for the friction force can be performed along with an approximate integration over impact parameter to give

$$\vec{F}^\star = F_\circ \Lambda \vec{I} \quad ,$$

where

$$F_\circ = 4\pi(r_e mc^2)^2 n^\star/m \quad ,$$
$$\Lambda = \log(b_{\max}/b_{\min}) \quad ,$$

and

$$\vec{I} = \int \frac{\vec{u}}{u^3}\,g(\vec{v})\,\mathrm{d}^3\vec{v} \quad .$$

$F_\circ$ is a scaling constant with dimensions force $\times$ velocity^2, the Coulomb log Λ contains the ratio of the maximum to minimum impact parameters b possible for the collisions, and the collision integral $\vec{I}$ embodies the integration over electron velocities. The constants c, m, and r_e have their conventional meaning of velocity of light, electron mass, and classical electron radius respectively. Λ is weakly dependent on u and is generally removed from the velocity integral as shown here. The argument of the log varies about as the cube of the relative velocity, but the appropriate velocity depends on whether one is considering the longitudinal or transverse component of the friction. The value generally lies in the range $\Lambda = 10 \pm 4$ with lower values for the longitudinal case and higher for the transverse.

It is very useful to observe that the velocity space integral $\vec{I}$ is the same as the coordinate space integral for the Coulomb force between a point charge at position $\vec{v}_p^\star$ and an extended distribution of charges at positions $\vec{v}$. This so-called Coulomb analogy makes a trove of potential theory results and familiar concepts applicable to the analysis of the cooling process. For example, one infers immediately that

$$\vec{I} = \vec{v}_p^\star/v_p^{\star 3} \quad (\text{for } \; u \gg v)$$

Table 4.1: Transformation of variables between laboratory and beam frames

	Lab Frame	Beam Frame
velocity	v_x	$v_x^\star/\gamma$
	v_y	$v_y^\star/\gamma$
	v_z	$v_z^\star + \beta c$
coordinates	$\mathrm{d}x$	$\mathrm{d}x^\star$
	$\mathrm{d}y$	$\mathrm{d}y^\star$
	$\mathrm{d}z$	$\mathrm{d}z^\star/\gamma$
	$\mathrm{d}t$	$\gamma \mathrm{d}t^\star$
density	$n = \mathrm{d}N/\mathrm{d}x\mathrm{d}y\mathrm{d}z$	$\gamma n^\star$
momentum	p_x	$p_x^\star$
	p_y	$p_y^\star$
	p_z	$\gamma p_z^\star$
force	F_x	$F_x^\star/\gamma$
	F_y	$F_y^\star/\gamma$
	F_z	$F_z^\star$
diffusion	$D_\perp$	$D_\perp^\star/\gamma$
	$D_\parallel$	$\gamma D_\parallel^\star$

regardless of g. The most important range of u in the Recycler application turns out to be $u \gtrsim v$ so calculations which include the integration over the electron velocity distribution will be somewhat more accurate than the cold electron beam formulas developed in this section. More significant, however, is the omission of variation in $\bar{\mathrm{p}}$ velocity arising from betatron oscillation. Average friction should include averaging over betatron phases; this deficiency is remedied in section 4.2.

More useful than the force $\vec{F}^\star$ itself in evaluating system parameters will be certain related quantities transformed to the lab frame. The beam frame is chosen with the $z^\star$ axis in the direction of the mean beam velocity $\bar{v} = \beta c$. The lab frame has the same orientation but moves with respect to the beam frame at a velocity $-\bar{v}$. A tabulation of the effects of the Lorentz transformation for this special case is collected in Table 4.1. In the preceding development no allowance has been made for the fact that cooling takes place only for $\bar{\mathrm{p}}$'s in the cooling section; the end results must include a reduction of the force by the ratio $\eta = \ell_c/\ell_R$ of cooling section length to Recycler circumference. This packing factor for the cooling unfortunately can hardly exceed a few percent for a storage ring; it is < 0.01 for the Recycler design. It will be a practice in this section to include the factor η when expressing quantities in the lab frame but not to include it in beam frame expressions.

Because force is $\mathrm{d}p/\mathrm{d}t$, the force on a particle divided by its momentum is the instantaneous fractional rate of change of momentum, *i. e.*, the cooling rate. For the large v_p case,

$$\vec{F}^\star = F_\circ \Lambda \vec{v}_p^\star / v_p^{\star 3}$$

so, using the non-relativistic expression for the momentum, the rate is

$$\alpha^\star = F_\circ \Lambda / (m_p v_p^{\star 3}) \quad .$$

In this case one can obtain the time dependence of the velocity by direct integration of the force

equation:

$$v_p^{\star 3} = v_{p\circ}^{\star 3} - \frac{3F_\circ \Lambda}{m_p} t^\star \quad .$$

For the $t^\star$ value

$$t^\star_{\rm stop} = m_p v_{p\circ}^{\star 3}/(3F_\circ \Lambda)$$

the $\bar{\rm p}$ velocity would be zero if the v^{-2} force law carried through to small $v_p^\star$. Even though it does not signify the time for complete cooling, $t_{\rm stop}$ is useful because it has the full scaling properties for the cooling time and because it approximates the time required to achieve the cooling needed for the Recycler system, *viz.*, the time to lower $\bar{\rm p}$ velocity spread to about that of the electrons. Notice that $t^\star_{\rm stop} = (\alpha^\star_\circ)^{-1}/3$, where the subscript $\circ$ denotes the rate evaluated at $v^\star_{p\circ}$. The lab frame expression is

$$t_{\rm stop} = \gamma m_p v_{p\circ}^{\star 3}/(3F_\circ \Lambda \eta) \quad .$$

It is not especially complicated to express $v_p^\star$ in terms of lab frame variables, but a convenient approximation is to replace $\vec{v}_p^\star$ with $v^\star_{p\perp}$ which typically constitutes the greater part of it and is expressible in the particularly simple form

$$v^\star_{p\perp} = c\varepsilon_\perp / r_b \quad ,$$

where $\varepsilon_\perp$ is the invariant emittance containing all of the beam of interest and r_b is the radius of the $\bar{\rm p}$ beam in the cooling section. The approximated $t_{\rm stop}$

$$t_{\rm stop} = \gamma m_p c^3 \varepsilon_\perp^3/(3F_\circ \Lambda \eta r_b^3)$$

has the same practical usefulness as the original expression. The constant $F_\circ$ incorporates the beam frame electron density $n^\star$ which introduces another power of γ when expressed in terms of lab frame density; see Table 4.1. Writing all of this out explicitly one has

$$t_{\rm stop} = \frac{\gamma^2 a^2 \beta e \varepsilon_\perp^3}{12\pi^3 r_p r_e \Lambda \eta I_e r_b^3} \quad ,$$

where quantities not previously defined are the electron beam radius a, electron charge (> 0) e, the classical radius of the proton r_p, and the electron beam current I_e.

The maximum rate of longitudinal drag, *i. e.*, the rate at which the $\bar{\rm p}$ beam as a whole can be accelerated or decelerated by sweeping the electron beam energy, is

$$R_D = \left.\frac{{\rm d}E}{{\rm d}t}\right|_{\rm max} = F_\parallel|_{\rm max}\bar{v} \quad .$$

Table 4.1 shows that $F^\star_\parallel \equiv F_\parallel$; however, the cooling fraction η must be introduced. Thus,

$$R_D = \eta F^\star_\parallel|_{\rm max}\beta c = \eta F_\circ \Lambda I_{\parallel{\rm max}}\beta c \quad .$$

$I_\parallel$ has a maximum value of approximately $\Delta_\perp^{-2}$ when the $\bar{\rm p}$ velocity and the maximum electron velocity are equal leading to

$$R_D = F_\circ \Lambda \eta \beta c/\Delta_\perp^2 \quad .$$

The longitudinal cooling rate $\alpha_\parallel$ is a somewhat different quantity. It is obtained by transforming the beam frame rate $\alpha_\parallel^\star$ given above to the laboratory frame and correcting for the fraction η of the circumference occupied by the cooling section:

$$\alpha_\parallel = \eta\alpha_\parallel^\star/\gamma = \frac{\eta F_\circ \Lambda I_\parallel}{\gamma m_p v_{p\parallel}^\star} \quad .$$

This quantity gives the rate at which the momentum spread is reduced and thus the effectiveness of the momentum stacking used to accumulate multiple injections from the Antiproton Source. The limit of longitudinal cooling is found by comparing this rate to the diffusion rates from various scattering and noise sources. The equilibrium with intrabeam scattering is evaluated explicitly in section 5.3. As for $t_{\rm stop}$, there is also the factor of γ^{-1} contained in $F_\circ$.

The roughest approximation for $I_\parallel$ is just $1/v^{\star\,2}$. In this approximation, the rate $\alpha_\parallel$ is $\propto (\Delta p/p)^{-1}$ or the force is *independent* of $\Delta p/p$. Therefore, the cooling will eliminate Δp at a constant rate regardless of the fractional spread, and the cooling proceeds *linearly* so long as the longitudinal $\overline{\rm p}$ velocity exceeds that of the electrons. This conclusion is not an accident of over-simplification; it remains true in the detailed analysis as well. The elimination of a non-essential parameter makes it simpler to specify an appropriate system and is the reason that it is convenient to express the longitudinal cooling rate in eVs/s in Table 4.3.

4.1.1 Estimating Recycler electron cooling system parameters

In Table 4.2 are listed the system and beam parameters representing a nominal design. Some of these parameters like beam energy and Recycler circumference are known to great precision and are not subject to optimization. Other quantities like input emittances are not so precisely known but are also taken as fixed for now, although they might be adjusted in a complete optimization of the scenario. Some parameters relating to the electron cooling system are set for the conceptual design on the basis of what appears practicable; it may be possible to relax some requirements in the course of a full design optimization. There is also a somewhat arbitrary selection of the both transverse and longitudinal emittance for the recycling mode. The longitudinal emittance is taken at the value expected for Tevatron beam at the end of stores while the transverse emittance is taken at half of the expected value, because the transverse stochastic cooling is expected to be effective even if the longitudinal cooling is not.

There is a discussion of the overall accumulation and recycling scenario in Chapter 2 which may be consulted for origins of, and caveats on, the injection frequency, cycle, *etc*. The results demonstrate that for recycling it is advantageous to exploit the complementary strength of the stochastic cooling until intensity needs swamp it and the electron cooling capability has been increased by something like a factor of three. The particular choice of electron beam current and cooling section length is provisional. The length has been taken considerably longer than what has been used for low energy coolers but less than a quarter of the available straight section. The 500 mA is chosen as a reasonable value to attempt on the basis of some preliminary experience. It should be understood that, except at a rather detailed level, the cooling rate scales only with the product of the two. Thus, the choice, for example, of higher current and proportionally shorter cooling section would not have a first order effect on the model analysis. However, technically the choice may be crucial. Higher performance than this conceptual design offers is likely to come more easily from higher beam current than larger diameter electron beam and a longer cooling interaction region.

Table 4.2: Beam and system parameters

E_p	$\bar{\text{p}}$ energy	8.94	GeV
$\varepsilon_\perp$	$\bar{\text{p}}$ $\varepsilon_\perp$ (6σ, normalized)		
	stacking	10	π mm mrad
	recycling	15	π mm mrad
ΔE_p	$\bar{\text{p}}$ energy spread ($\pm 2\sigma$)		
	stacking	± 3	MeV
	recycling	± 12	MeV
N_p	number of $\bar{\text{p}}$ (total)	5	$\cdot 10^{12}$
	number of $\bar{\text{p}}$ (per injection)		
	stacking	2	$\cdot 10^{11}$
	recycling	2.5	$\cdot 10^{12}$
a	electron beam radius	0.0060	m
r_c	cathode radius	0.0025	m
ε_e	elect. trans. emit. rms norm.	1	$\cdot 10^{-6}$ m
I_e	electron beam current	500	mA
ΔU	electron energy stability	± 200	eV
ℓ_c	length of cooling section	20	m
ℓ_R	ring circumference	3319	m
$\bar{\beta}$	$\bar{\text{p}}$ Courant-Snyder β_x and β_y	20	m
	Recycler injection frequency		
	stacking	2	h^{-1}
	recycling	0.12	h^{-1}
	ring vacuum	~ 0.1	nTorr

Table 4.3: Model parameters

input				
E_e	electron energy	4.87		MeV
β	Lorentz beta of beam frame	0.994		
γ	Lorentz gamma of beam frame	9.526		
$\Delta\beta^\star_{e,\|}$	long. el. vel. spread, beam frame	4.134	$\cdot 10^{-5}$	
$\Delta\beta^\star_{e,\perp}$	trans. el. vel. spread, beam frame	4.356	$\cdot 10^{-4}$	
x	max. $\bar{\text{p}}$ beam radius	0.0056		m
$\beta^\star_{p,\perp}$	trans. $\bar{\text{p}}$ vel., beam frame			
	stacking	1.777	$\cdot 10^{-3}$	
	recycling	2.176	$\cdot 10^{-3}$	
$\beta^\star_{p,\|}$	long. $\bar{\text{p}}$ vel. in beam frame			
	stacking	3.375	$\cdot 10^{-4}$	
	recycling	1.350	$\cdot 10^{-3}$	
output				
$t_{\rm stop}$	cooling time			
	stacking	22.85		min
	recycling	36.42		min
$\alpha_{\rm ec\|}$	longitudinal cooling rate	6.39	$\cdot 10^{-2}$	eVs s^{-1}
	(units discussed in text)			
	recycling	1.48	$\cdot 10^{-4}$	s^{-1}
R_D	longitudinal drag			
	stacking	4.82	$\cdot 10^{-2}$	MeV/s
	recycling	6.67	$\cdot 10^{-2}$	MeV/s

4.1.2 Cooling time

The cooling time ($t_{\rm stop}$) is given in Table 4.3 for both the recycling and the stacking modes. This table also records that

$$\vec{v}^\star_{p\perp} > \vec{v}^\star_{p\|} \gtrsim \Delta_\perp \gg \Delta_\| \quad ,$$

but only in the last inequality is there a full order of magnitude difference. Therefore, the formula for $t_{\rm stop}$ is approximate on account of both the first two relations, especially for stacking from the Accumulator. However, little or no transverse cooling is needed in this mode, so $t_{\rm stop} = 0.38$ hr serves primarily to reassure that there is no gross inadequacy in the cooling power. For the recycling mode, the .61 hr estimate is relevant to the time required to restore the transverse emittance of used $\bar{\text{p}}$'s after the stochastic precooling. Recycling with just the electron cooling of this power would be marginal; however, the stochastic cooling makes the proposed scenario an acceptable initial mode. The third power dependance of $t_{\rm stop}$ on $\bar{\text{p}}$ velocity makes it clear that transverse emittance is a critical consideration, especially for recycling.

4.1.3 Longitudinal drag and longitudinal cooling rate

The purpose of the electron cooling in the stacking mode is to reduce the momentum spread of a batch from the antiproton source plus the initial stack back to the initial stack momentum spread

before the next batch comes along. In this condition stacking is in equilibrium with cooling and can in principle proceed for many batches. The longitudinal cooling rate is given in Table 4.3. Expressed in the more usual unit s^{-1} it is close to $t_{\rm stop}^{-1}/3$ as one expects from the simplest estimate of the cooling force (see Section 4.1).

The system parameter list might be augmented by a quantity f representing the fraction of the azimuth occupied by the stack. This number will be affected by the size of gap needed for ion clearing and, during injection, by the injection gap. There is freedom to adjust the momentum spread of the cooled stack, the cooling recycled beam, and the newly injected batch which can each be maintained in separate azimuthal sectors by the barrier bucket rf. Because the longitudinal cooling force is practically independent of $v_{p,\|}$ or, equivalently $\Delta p_{p,\|}$, the rate of longitudinal phase space area reduction is proportional to the length of the sector occupied. Therefore, as much of the circumference should be used for the beam as possible. All of the beam should be combined in a single partition except during the injection process during which the momentum spread of injected batch and stack must be equalized.

Another mode in which stacking could be carried out is by sweeping the electron beam energy through the batch momentum, using the beam as an accelerator or decelerator in much the same way as rf stacking is carried out but without the disruption of the stack. The drag rate R_D given in Table 4.3 gives the maximum rate at which the energy can be changed. If barrier bucket manipulation is used to lay the batch above and below the full length of the stack, the required sweep is the batch energy spread divided by the ratio of batch to stack length, half from below and half from above. The sweep rate in the table appears to make this mode advantageous for getting the highest possible stacking rate, but part of the stack is not being cooled during the electron beam energy change. Furthermore, the tendency for the beam to develop a high momentum density just at the electron β may lead to intrabeam scattering strong enough to scatter some $\bar{\rm p}$'s back into the range from which they had been removed. The sweeping mode is not considered further in this report, but it should not be summarily dismissed without a better understanding. It could be a viable alternate approach if available cooling power falls short of expectations.

4.1.4 Sensitivity of performance to the choice of parameters

System performance has been evaluated with a particular choice of system parameters for two sets of beam parameters, one for stacking from the Antiproton Source and one for recycling from the Tevatron. Treated here is the sensitivity of that performance to major system parameters.

The specification on accelerating voltage regulation as ± 200 V was based on what the manufacturer and users of Pelletron type Van de Graaff accelerators quote as the present state of the art. However, until the longitudinal velocity error, either slow or fast, becomes comparable to the transverse velocity spread, the effect on performance is small. Because

$$v_{\|} = c\Delta U/(\beta U) \quad ,$$

an energy drift or jitter of $\mathcal{O}(10^{-4})$ or 500 V would be acceptable.

The transverse temperature in the cooling section could in principle be lower than the cathode temperature because the beam radius is larger than the cathode radius, but there are various likely sources of transverse velocity growth including non-uniform emission, nonlinear fields near the cathode, redistribution of spacecharge free energy, transport aberrations, *etc*. The specified value is such that the transverse electron velocity is comparable to the longitudinal $\bar{\rm p}$ velocity in the beam

frame. For large $\Delta_\perp$,

$$\alpha_{\rm ec} \propto \Delta_\perp^{-2} \propto T_\perp^{-1} \quad ,$$

but as long as $\Delta_\perp$ is a factor of two or so smaller than $\beta_{p,\perp}$, the loss in longitudinal cooling is small. Thus, from the standpoint of stacking time the temperature could be several times greater. To preserve transverse cooling capability for recycling, $\Delta_\perp$ should be less than $5 \cdot 10^{-4}$ allowing $T_\perp$ up to $\lesssim$2000 K. Therefore, even though electron beam temperature is a sensitive parameter, there is considerable margin for non-ideal electron transport.

Besides random thermal velocity, there are other ways in which the electron beam can have greater transverse velocity in the beam frame. These include beam-beam alignment, stray magnetic field, and space charge spread. Allowing transverse velocity from beam alignment to be no more than $\Delta_\perp/2$ gives an alignment requirement of $\Delta\vartheta < \beta_\perp/2$. This is 100 μrad for nominal parameters but could be relaxed to 250 μrad or so with a relaxed requirement for $T_\perp$. The results obtained in Section 4.2 are just a bit more restrictive than these estimates.

The preceding approximate analysis shows that the provisional parameters, *i.e.*, conceptual design choices, lie in an appropriate region of the parameter space with room in every direction to refine and optimize. The confidence in the adequacy of the available parameter space is founded on the margin by which the predictions exceed minimum requirements and the sensitivity of the predictions to the parameters. The next section describes the current state of the modelling work and supports the generalizations above. An important message from the results of the simple model is that the challenge of the project is stable, dependable electron current, not exquisitely small electron emittance, incredible voltage regulation, or few microradian level beam alignment. In each of these latter matters there are incremental quantitative gains to be made over time. However, to get the show on the road, it is electrostatic accelerator technology that must be mastered first and foremost.

4.2 Detailed Analysis

Longitudinal and transverse cooling rates are calculated analytically for a particle executing betatron oscillations in a storage ring. The formulas obtained are compared with numerical results. Particular attention is paid to the case where transverse relative velocities dominate over longitudinal. Exact analytical results for finite electron temperatures are presented. Longitudinal cooling time for a Gaussian beam is calculated as a function of a percentage of un-cooled particles; the optimum size of the electron beam is calculated. The results obtained are applied to the Recycler cooler parameters; the cooling time, the optimum parameters and the tolerances are calculated.

Various particles are cooled at different rates, but practically it is important to know how long one has to wait until all or almost all the particles are cooled. In fact, the answer depends on the definition of "almost all". Electron cooling acts such that the higher the particle velocity relative to the electron beam, the less efficiently it is cooled. Thus, however long the particles are cooled, a portion of them could have practically the same velocities as at the beginning of the process. In other words, the time required for the beam cooling depends on the acceptable percentage of the insufficiently cooled particles; it increases without bounds when this percentage goes to zero. These un-cooled tails of the particle distribution are referred to here as a loss percentage.

The calculation of the beam cooling time is the first goal of this chapter. To this end, accurate formulas for single particle rates are needed. For the particles executing the betatron oscillations, these formulas are derived in the Section 4.2.1; the analytical expressions obtained are compared

with numerical results, and an agreement better than 10% is demonstrated. The electron longitudinal and transverse temperatures are taken into account there. One of the results is existence of an optimum transverse temperature of the electrons, where the longitudinal cooling rate is 40% higher than at the zero-temperature limit. The results of this chapter refine some of the known rate estimations [4].

The beam loss as function of the time of cooling is calculated analytically in Section 4.2.2 for the longitudinal cooling. This allows finding an optimum electron beam radius, minimizing the required time of cooling for a given loss. The optimum beam radius and the required cooling time are calculated there for a homogeneous electron density distribution within the beam radius.

In Appendix A, the shape of the electron beam profile optimizing the longitudinal cooling is found for cold electron beam. The gain in a comparison with the homogeneous density optimization is found to be about 60%.

In Sections 4.2.3 and Appendix B the results obtained are applied to the Recycler cooler scheme[12, 13]. The optimum parameters and tolerances are calculated, the results are summarized in the tables.

4.2.1 Single particle rates

The friction force acting on the particle in the beam frame can be expressed as follows:

$$\overrightarrow{F} = -\frac{4\pi n e^4 L_C}{m}\frac{\overrightarrow{\Delta u}}{\Delta u^3} \ , \tag{4.1}$$

where n is electron density, e^2 is the product of the electron and the particle charges, m is electron mass, L_C is the Coulomb logarithm and $\overrightarrow{\Delta u}$ is the particle-electron velocity. This force causes a slow change of the actions for the particles due to their interaction with the electron beam within a certain part of their trajectory in the storage ring. The transverse actions $J_{x,y}$ and phases $\psi_{x,y}$ are defined to correspond to normalized emittances:

$$x = \sqrt{2J_x\beta_f/(\gamma\beta)}\cos\psi_x, \quad x' = -\sqrt{2J_x/(\beta_f\gamma\beta)}\sin\psi_x \tag{4.2}$$

and similarly for the y direction. Here $\beta_f = \beta_x = \beta_y$ is the Courant-Snyder beta-function. With $\beta_f' = 0$ in the cooler, only the transformation (4.2) is needed. The actions $J_{x,y}$ are defined so that the rms normalized emittances $\epsilon_{x,y}$ are the average values:

$$\langle J_{x,y}\rangle = \epsilon_{x,y} \ .$$

Particle velocities in the beam frame are given by the Lorentz transformation; in the units where the velocity of light $c = 1$ they become

$$u_x = \gamma\beta x' = v_x\cos\psi_x; \ u_z = \beta\delta p/p = v_z; \ u^2 = u_x^2 + u_y^2 + u_z^2 \ . \tag{4.3}$$

When the longitudinal motion of the cooled particles is free, the role of the longitudinal action is played by the momentum deviation $\delta p/p$. In this case, the cooling rates can be determined as logarithmic time derivatives of the actions

$$\tau_x^{-1} = -\frac{1}{J_x}\frac{dJ_x}{dt} \quad \tau_z^{-1} = -\frac{1}{\delta p/p}\frac{d\delta p/p}{dt} \tag{4.4}$$

averaged over the betatron oscillations.

Because of the friction (4.1), the rates have nonzero values. For the cold electron beam they can be expressed as

$$\begin{aligned} \tau_x^{-1} = & -\frac{2}{\gamma v_x^2}\langle F_x u_x\rangle = \frac{4(I_e/e)r_e r_p \eta}{\beta\gamma^2 a^2}\left\langle \frac{L_C}{u^3}\frac{2u_x^2}{v_x^2}\right\rangle \\ \tau_z^{-1} = & -\frac{1}{\gamma}\langle F_z\rangle = \frac{4(I_e/e)r_e r_p \eta}{\beta\gamma^2 a^2}\left\langle \frac{L_C}{u^3}\right\rangle \ , \end{aligned} \tag{4.5}$$

where a is the electron beam radius, I_e is the electron current, e is the electron charge, r_e, r_p are the electron and particle classical radii and η is the fraction of the orbit occupied by the cooler. The angle brackets stand for the betatron averaging:

$$\langle ...\rangle = \int_{-\pi}^{\pi}\int_{-\pi}^{\pi} ... \frac{d\psi_x d\psi_y}{(2\pi)^2}.$$

Longitudinal Rate for Cold Electrons

Here the electron beam is mainly considered to be cold, meaning that the electron velocities in the beam frame are small in comparison with the corresponding velocities of the cooled particles. The longitudinal rate (4.4) is proportional to the averaged inverse cube of the particle velocity:

$$\left\langle \frac{1}{u^3}\right\rangle = \frac{1}{\pi^2}\int_{-\pi/2}^{\pi/2}\int_{-\pi/2}^{\pi/2} \frac{d\psi_x d\psi_y}{(v_x^2\sin^2\psi_x + v_y^2\sin^2\psi_y + v_z^2)^{3/2}} \ . \tag{4.6}$$

This integral can be calculated analytically for both limiting cases: $v_x \gg v_z$ and, alternatively, $v_x \ll v_z$. In the first case, the integral over phases converges at $|\psi_x| \le v_z/v_x \ll 1$, and can be calculated by the substitution $\sin\psi = \psi$ and an expansion of the integrations on the whole real axis:

$$\left\langle \frac{1}{u^3}\right\rangle = \frac{1}{\pi^2}\int_{-\infty}^{\infty}\int_{-\infty}^{\infty} \frac{d\psi_x d\psi_y}{(v_x^2\psi_x^2 + v_y^2\psi_y^2 + v_z^2)^{3/2}} = \frac{2}{\pi v_x v_y v_z} \ . \tag{4.7}$$

In the opposite case, $v_x \ll v_z$. The result is obvious: $\langle 1/u^3\rangle = 1/v_z^3$. The transition between these alternatives is smooth; a simple way to join them can be tried as

$$\left\langle \frac{1}{u^3}\right\rangle = \frac{1}{v_z\sqrt{(\pi v_x^2/2 + v_z^2)(\pi v_y^2/2 + v_z^2)}} \ . \tag{4.8}$$

This gives for the longitudinal rate

$$\tau_z^{-1} = \frac{2}{\pi}\frac{(I_e/e)r_e r_p \eta L_\parallel}{\gamma^2\beta^2 J_e\sqrt{\tilde{J}_x\tilde{J}_y}(\delta p/p)} \tag{4.9}$$

with

$$\tilde{J}_x = J_x(1 + (2/\pi)(v_z^2/v_x^2)) = J_x + (2/\pi)\beta\beta_f(\delta p/p)^2/\gamma \ . \tag{4.10}$$

Here $L_\parallel$ is the Coulomb logarithm calculated with the longitudinal velocity as the argument, and J_e is the invariant corresponding to the electron beam radius: $a = \sqrt{2J_e\beta_f/(\gamma\beta)}$.

The Coulomb logarithm is a function of the relative velocity between the particle and the electron beam; its argument normally scales as the velocity cubed. If the longitudinal velocity is small

in comparison with the transverse velocity amplitudes, the particle is mainly cooled when its transverse velocity is smaller or comparable with the longitudinal one. Therefore, the logarithm has to be calculated with the longitudinal velocity as its argument in this case. In the opposite situation, the relative velocity is equal to the longitudinal one; hence, again, the logarithm has to be calculated for the longitudinal velocity. Thus, it can be concluded that in any case the longitudinal cooling rate must be evaluated with the Coulomb logarithm taken for the longitudinal velocity as its argument [14]. The integral (4.6) was calculated numerically for $v_z = 0.1$ and $0.03 \leq \sqrt{v_x^2 + v_y^2} \leq 1,\ 0.03 \leq \arctan(v_y/v_x) \leq \pi/2 - 0.03$ and compared with the analytical approximation (4.8); the results are presented in Figs. 4.1, 4.2. The agreement between the analytical and numerical calculations allows the use of the analytical expressions (4.8, 4.9) for any relations between longitudinal and transverse velocities of the cooled particles.

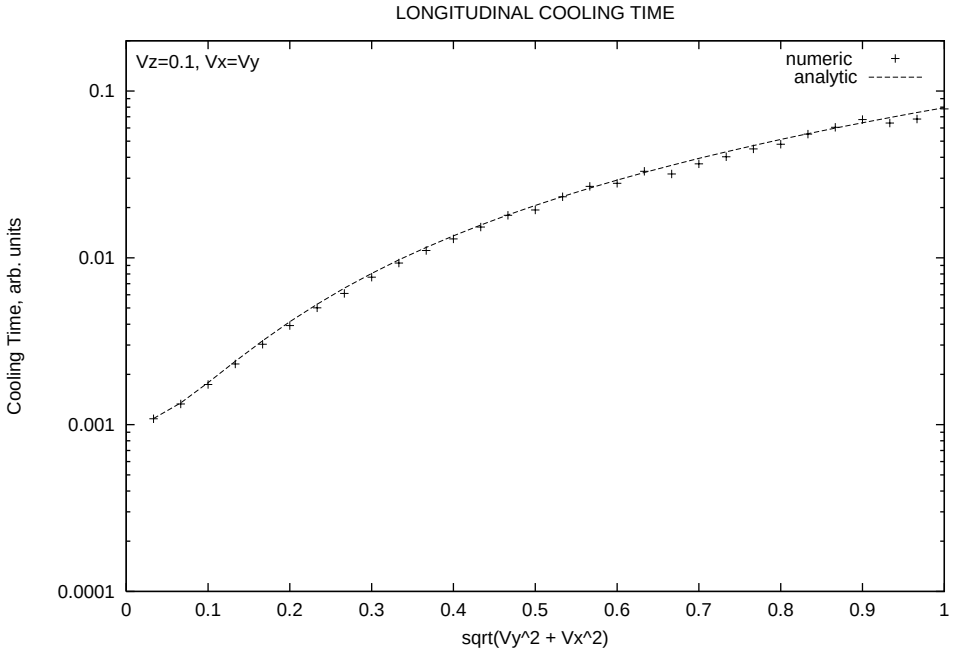

Figure 4.1: Longitudinal cooling time as a function of the total transverse amplitude $v_\perp = \sqrt{v_x^2 + v_y^2}$, for $v_x = v_y$, $v_z = 0.1$, arbitrary units.

Longitudinal rate for flattened distribution

When the longitudinal velocity is small, $v_z^2 \ll v_{x,y}^2$, the expression for the longitudinal rate (4.9) is simplified:

$$\tau_z^{-1} = \frac{2}{\pi} \frac{(I_e/e) r_e r_p \eta L_\parallel}{\gamma^2 \beta^2 J_e \sqrt{J_x J_y} (\delta p/p)}. \tag{4.11}$$

The dependence $\tau_z^{-1} \propto (\delta p/p)^{-1}$ means that the longitudinal cooling force actually does not depend on the momentum offset. It also means that the locally determined cooling time τ_z (Eq. 4.4) is equal to the integral full-stop cooling time. In fact, the result (4.11) comes mainly from those phases of the particle betatron oscillations where it almost stops, $\psi_{x,y} \leq v_z/v_{x,y}$. That is why the electron

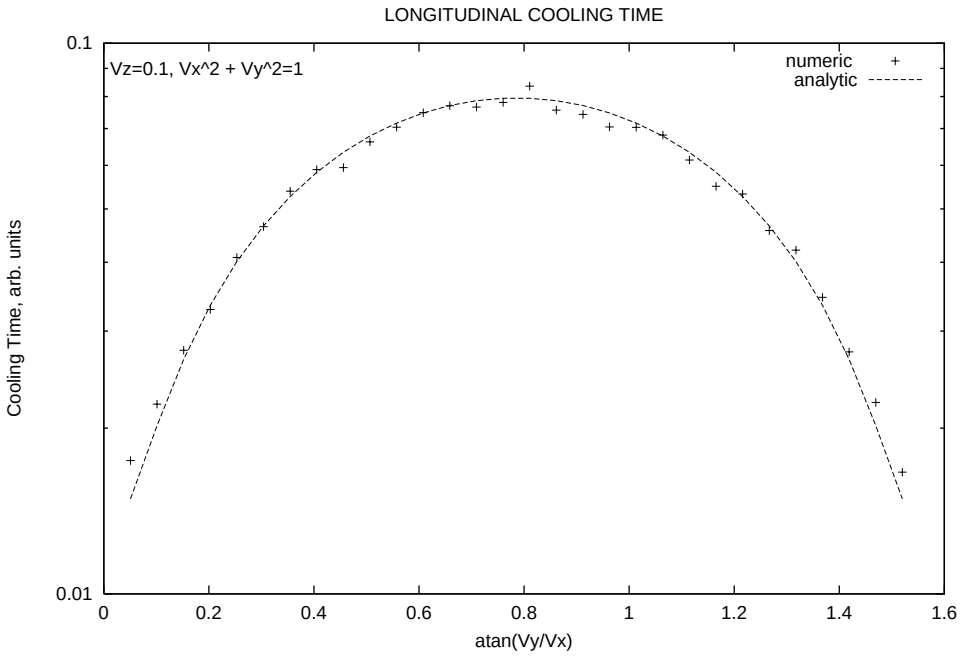

Figure 4.2: Longitudinal cooling time as a function of a distribution of the transverse energy among the two degrees of freedom with $v_x^2 + v_y^2 = 1.$, $v_z = 0.1$, arbitrary units.

beam has to be wide enough to cover the amplitudes of the cooled particles. The particle cooling time as a function of the electron beam size has a singularity at the maximum particle offset, when $a = \sqrt{x_m^2 + y_m^2}$, with $x_m = \sqrt{2J_x\beta_f/(\gamma\beta)}$. For $a > \sqrt{x_m^2 + y_m^2}$, the cooling time grows with the radius in proportion to a^2 because of the electron density decrease. It grows much faster when the radius goes down below the singularity, $a < \sqrt{x_m^2 + y_m^2}$. This dependence is shown on Fig. 4.3 for a case of equal betatron amplitudes, $v_x = v_y$ at $v_z = 0.1\, v_x$ and $v_z = 0.25\, v_x$. It can be concluded that the particles with oscillation amplitudes greater than the electron beam are lost from the useful stack.

Up to this point, the electron velocities in the beam frame were considered negligible. When both particle and electron longitudinal velocities are small in comparison with both of their transverse velocities, the cooling rate can be calculated analytically for arbitrary relations between the transverse velocities. This case can be referred to as a flattened distribution. Assuming $f(\vec{w}, \vec{r}_\perp)$ to be a normalized electron distribution over the 3D velocities $\vec{w} = (w_x, w_y, w_z)$ and the transverse (2D) coordinates $\vec{r}_\perp = (x, y)$, the longitudinal rate (4.5) can be presented as follows:

$$\tau_z^{-1} = -\frac{1}{\gamma}\left\langle F_z \right\rangle = \frac{4\pi(I_e/e)r_e r_p \eta L_C}{\beta\gamma^2}\left\langle \int \frac{d\vec{w} f(\vec{w}, \vec{r}_\perp)(u_z - w_z)}{|\vec{u} - \vec{w}|^3 u_z} \right\rangle \tag{4.12}$$

with

$$\int d^3w d^2r_\perp f(\vec{w}, \vec{r}_\perp) = 1 \ .$$

For the flattened distribution, $|u_{x,y} - w_{x,y}| \gg |u_z - w_z|$, the integral over the electron transverse velocities $\vec{w}_\perp$ is mainly contributed by the vicinity of the particle transverse velocity $\vec{w}_\perp = \vec{u}_\perp$, and

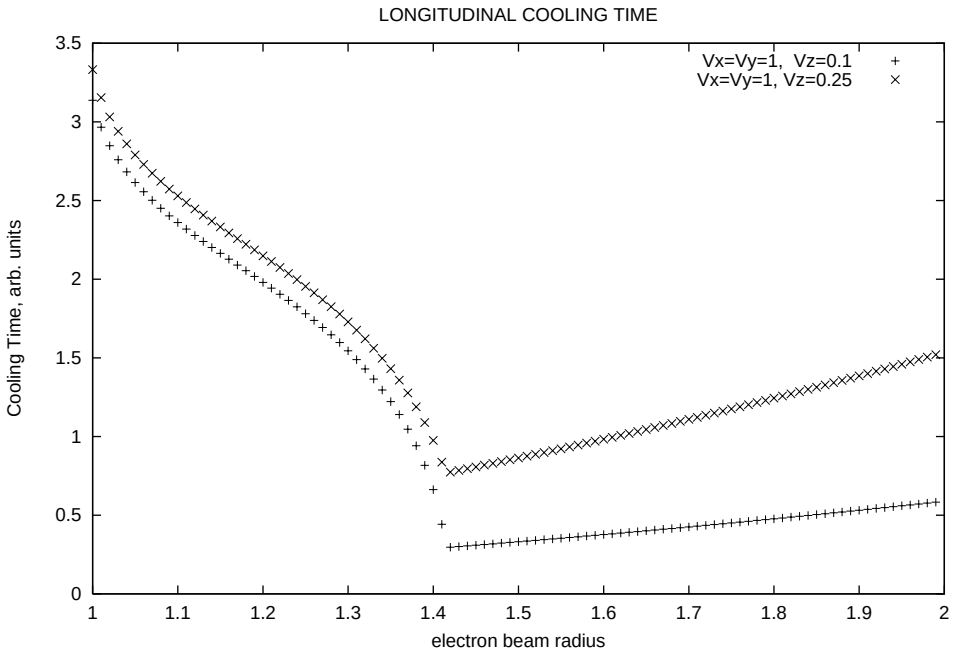

Figure 4.3: Longitudinal cooling time as a function of the electron beam radius. The betatron amplitudes assumed to be equal, $v_x = v_y$. Two sets of the plotted points correspond to different longitudinal velocities, $v_z = 0.1v_x$ and $v_z = 0.25v_x$. The time is taken in arbitrary units, the radius is in the units of the amplitude offset $x_m = v_x\beta_f/(\beta\gamma)$.

this integral can be taken:

$$\tau_z^{-1} = \frac{8\pi^2(I_e/e)r_e r_p \eta L_C}{\beta\gamma^2} \left\langle \int dw_z f(u_x, u_y, w_z) \text{sign}(u_z - w_z)/u_z \right\rangle \quad . \tag{4.13}$$

Assuming the distribution to be factorized as $f(\vec{w}, \vec{r}_\perp) = f_\perp(\vec{w}_\perp, \vec{r}_\perp) f_z(w_z)$, the longitudinal integral $\int dw_z f_z(w_z)\text{sign}(u_z - w_z)/u_z$ can be taken separately for the limiting cases of one or another longitudinal velocity dominating:

$$\int dw_z f_z(w_z)\text{sign}(u_z - w_z)/u_z = \begin{cases} 1/|u_z| & \text{if } |u_z| \gg \Delta w_z \\ f_z(0) & \text{if } |u_z| \ll \Delta w_z \end{cases} \tag{4.14}$$

where Δw_z is the width of the longitudinal electron distribution. It is convenient here to determine this width as $\Delta w_z = 1/f_z(0)$. Then, the two limits in the Eq. 4.14 can be joined by an approximate formula:

$$\int dw_z f_z(w_z)\text{sign}(u_z - w_z)/u_z = 1/\tilde{u}_z, \tag{4.15}$$

with

$$\tilde{u}_z = \sqrt{u_z^2 + \Delta w_z^2}\,, \quad \Delta w_z = 1/f_z(0)\,.$$

For a Gaussian distribution with the rms velocity $\hat{w}_z$, this effective width is $\Delta w_z = \sqrt{2\pi}\hat{w}_z$. Substituting Eq. 4.15 in 4.13, the result is

$$\tau_z^{-1} = \frac{8\pi^2(I_e/e)r_e r_p \eta L_C}{\beta\gamma^2 \tilde{u}_z} \langle f_\perp(\vec{u}_\perp, \vec{r}_\perp)\rangle \quad . \tag{4.16}$$

The last result expresses the cooling rate in terms of the electron distribution function taken at the particle's trajectory and averaged $\langle ... \rangle$ over the particle oscillations. This formula may be used for both homogeneous and inhomogeneous electron distributions $f_\perp(\vec{u}_\perp, \vec{r}_\perp)$ as well.

For certain cases, the betatron averaging in Eq. 4.16 can be performed analytically. In particular, it can be done for the homogeneous distribution over the transverse coordinates $\vec{r}_\perp$ within the radius a, and Gaussian distribution over the transverse velocities $\vec{w}_\perp$ with the rms $\hat{w}_\perp$, i.e.

$$f_\perp(\vec{w}_\perp, \vec{r}_\perp) = \frac{\exp(-\vec{w}_\perp^2/(2\hat{w}_\perp^2))}{2\pi^2 \hat{w}_\perp^2 a^2}. \tag{4.17}$$

Using an integral representation of the modified Bessel function,

$$\mathrm{I}_0(\kappa) = \langle \exp(\kappa \cos\psi) \rangle \quad ,$$

the result for the rate can be expressed as

$$\tau_z^{-1} = \frac{2(I_e/e) r_e r_p \eta L_C}{\pi \beta \gamma^2 v_x v_y \tilde{u}_z a^2} \sqrt{\mathrm{A}(v_x^2/(4\hat{w}_\perp^2)) \mathrm{A}(v_y^2/(4\hat{w}_\perp^2))} \quad , \tag{4.18}$$

where the special function $\mathrm{A}(x) = 2\pi\, x\, \exp(-2x)\, \mathrm{I}_0^2(x)$ has been introduced. The plot of this function is shown in Fig. 4.4. The asymptotic $\mathrm{A}(\infty) = 1$ corresponds to zero-temperature electron beam, described by Eq. 4.11. It is interesting that the rate from Eq. 4.18 increases with the electron transverse temperature up to $\hat{w}_\perp^2 = v_{x,y}^2/3$, where the rate has a temperature maximum. When the temperature increases more, the rate goes down as the inverse temperature. At this temperature optimum, the rate is 40% higher than at zero-temperature limit. Such rate enhancement with higher transverse temperature has not been reported, but it appears that there may be something to gain by looking for the optimum.

Transverse rate for cold electron beam

A general analytical expression for the transverse integral in Eqs. 4.5, *viz.*, $\langle (1/u^3)(2u_x^2/v_x^2) \rangle$, probably does not exist. It can be evaluated, however for various limit cases, where one of the velocities is much higher than others. Then, one or another variant to join these limit solutions can be tried and compared with the exact numerical results. Without going into details of the calculations, an approximate formula of such a kind is presented below:

$$\left\langle (1/u^3)(2u_x^2/v_x^2) \right\rangle = \frac{1}{\tilde{v}_x^3} \begin{cases} 1 + \ln(\tilde{v}_x/\tilde{v}_y) & \text{if } \tilde{v}_x > \tilde{v}_y \\ \tilde{v}_x/\tilde{v}_y & \text{otherwise} \end{cases} \quad , \tag{4.19}$$

with $\tilde{v}_{x,y} = \sqrt{v_{x,y}^2 + v_z^2}$. A comparison of the numerical and the analytical calculations is shown in Figs. 4.5, 4.6.

4.2.2 Beam cooling time

Up to this section, the rates of single particles were of the interest. The values calculated above are functions of the particle actions. However, the cooled particles have a certain distribution over the actions, and a rather high percentage of the particles must be cooled. Thus, the beam cooling times need to be calculated when the single-particle times are already known. Then, the parameters of the cooler can be optimized to have a minimum for the beam cooling time within given

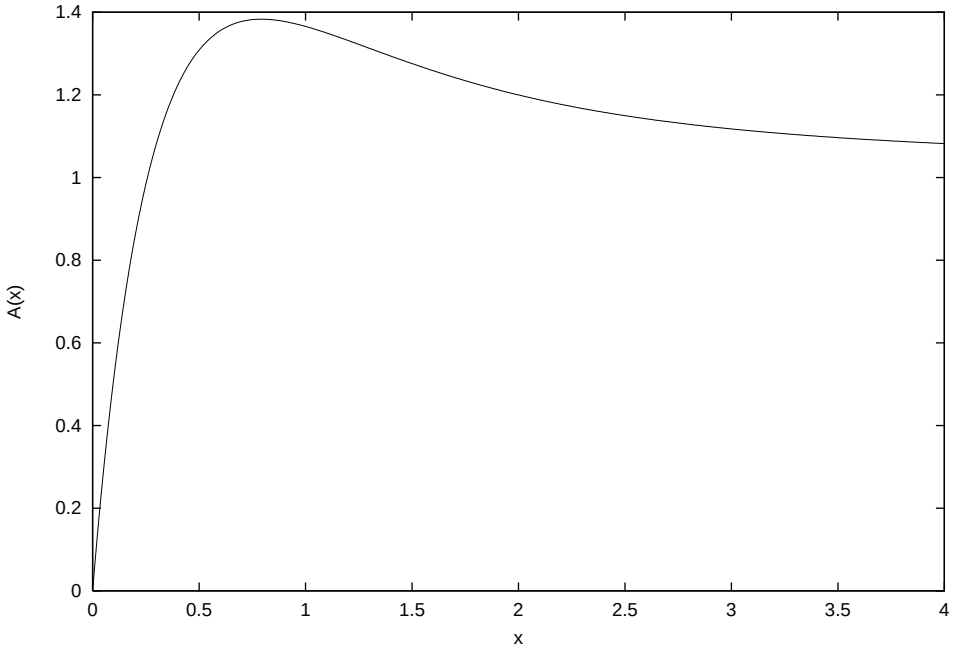

Figure 4.4: Function $\mathrm{A}(x) = 2\pi\ x\ \exp\ (-2x)\mathrm{I}_0^2(x)$

constraints, and also tolerances can be found. The problem is rather extensive; the consideration is limited here to the case of the longitudinal cooling with small longitudinal velocity,

$$v_z^2 \ll v_{x,y}^2\ \ , \tag{4.20}$$

a typical case for relativistic beams.

Various particles are cooled with different rates. For a given time t, only a certain part of the beam can be cooled; particles with low rates $\tau^{-1} < t^{-1}$ are not cooled sufficiently and would be lost if the cooling were stopped at that time and the beam were removed from its phase space. The longer the cooling, the less are the losses, and visa-versa. Thus, the beam cooling time is a function of the tolerable losses. This time can be calculated in the following way: first, for a given time the loss percentage is evaluated and, second, the time is found from here to give the desirable losses.

To accomplish this program, the cooled particle distribution has to be specified as well as the properties of the cooling electron beam. The losses are evaluated below with the assumption of a Gaussian distribution for the cooled particles and constant density within the circle $x^2 + y^2 \leq a^2$ for the electron beam. Small losses are of interest; this gives a small parameter for the problem and allows almost all the calculations to be carried out analytically.

Because of the small longitudinal velocity, particles are effectively cooled longitudinally only when they are almost stopped transversely, that is when they have a maximum offset from the axis. That is why the particles which stop transversely beyond the electron beam boundary have rates a factor of $\simeq v_z/v_{x,y} \ll 1$ lower than the particles stopping within the electron beam. This condition of the effective cooling can be expressed as

$$x_m^2 + y_m^2 \leq a^2, \tag{4.21}$$

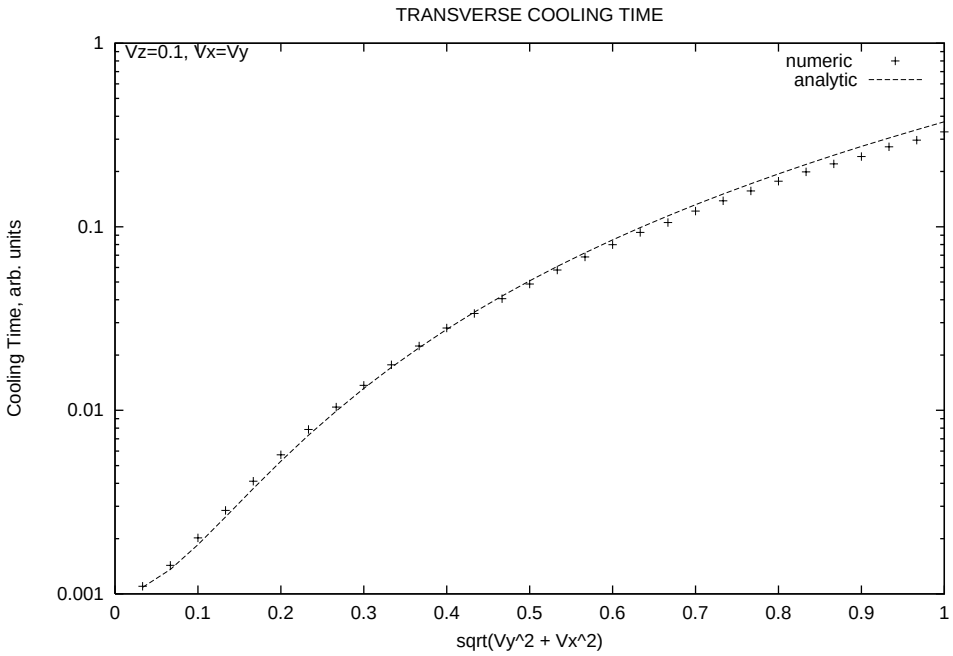

Figure 4.5: Transverse (x) cooling time as a function of the total transverse amplitude $v_\perp = \sqrt{v_x^2 + v_y^2}$, for $v_x = v_y$, $v_z = 0.1$, arbitrary units.

with x_m, y_m standing for the amplitudes of the betatron oscillations in the cooler. The particles stopping outside the electron beam can be considered as lost; for more details see the subsection 4.2.1 and Fig. 4.3.

Therefore, the losses consist of two parts. The first one includes the inside particles Eq. 4.21 with velocities too high to be cooled in a given time. The second part includes the outside particles, i.e. ones satisfying the condition opposite to Eq. 4.21.

To simplify the formulas, it is convenient to go to dimensionless variables, expressed in units inherent to the problem. The transverse actions $J_{x,y}, J_e$ will be assumed to be expressed in the units of the rms normalized emittance $\epsilon = \epsilon_x = \epsilon_y$; the longitudinal velocity v_z can be expressed in terms of its rms value $v_{zrms} = \beta(\delta p/p)_{rms}$. The radius of the electron beam a (or the corresponding action J_e) has to be optimized; therefore, the time unit should be independent of it. The time unit $t_\circ$ can be taken as an inverse rate (Eq. 4.11) with $J_x = J_y = J_e = \epsilon$:

$$t_0^{-1} = \frac{2}{\pi} \frac{(I_e/e) r_e r_p \eta L_\parallel}{\gamma^2 \beta^2 \epsilon^2 (\delta p/p)_{rms}} \quad . \tag{4.22}$$

This scaling time has the dependence $(\delta p/p)^{-1}$ characteristic of the single particle rate noted in Section 4.1. Therefore, the beam cooling rate will also have the property that the decrement in δp (or δE) is independent of δp and constant in time.

Assuming all the values are expressed in dimensionless variables, the particle's cooling time is

$$\tau = v_z \sqrt{J_x J_y} J_e \quad . \tag{4.23}$$

For a fixed cooling time t, the particles with $v_z > \bar{v} = t/(J_e \sqrt{J_x J_y})$ are not sufficiently cooled and are effectively lost. The corresponding portion of the loss percentage Δ_{in} is calculated by

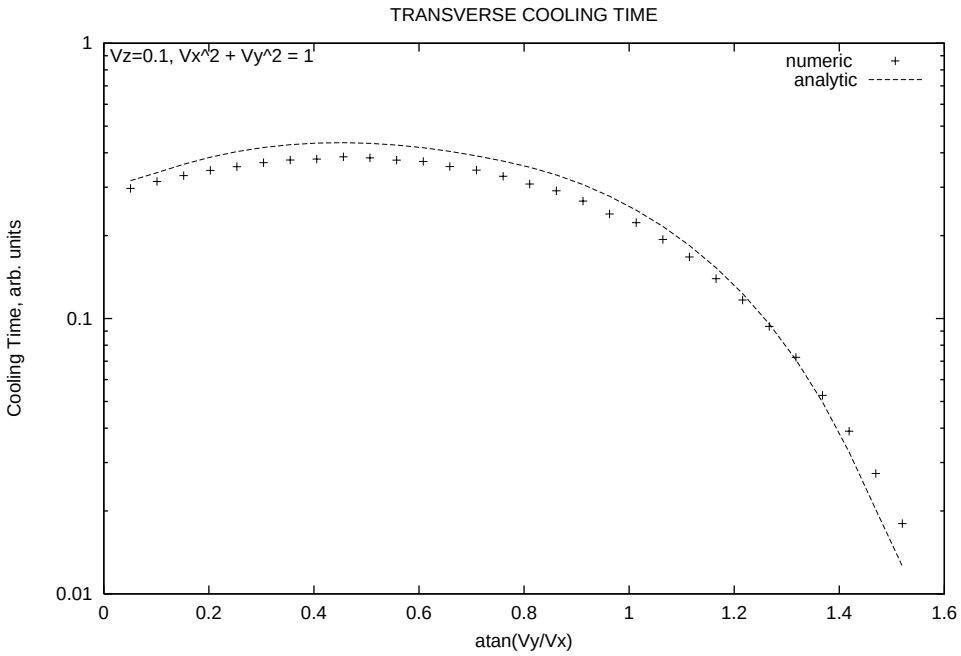

Figure 4.6: Transverse (x) cooling time as a function of a distribution of the transverse energy among the two degrees of freedom with $v_x^2 + v_y^2 = 1.$, $v_z = 0.1$, arbitrary units.

means of an integration over the particle distribution:

$$\Delta_{in} = \sqrt{2/\pi} \iint_{J_x+J_y<J_e} dJ_x dJ_y \exp\left(-J_x - J_y\right) \int_{\bar{v}}^{\infty} dv_z \exp\left(-v_z^2/2\right) \ . \tag{4.24}$$

When the losses are small, $\Delta_{in} \ll 1$, the value of the longitudinal integral is dominated by the contribution from the vicinity of its lower limit $v_z = \bar{v}$, and the resulting transverse integrals can be evaluated by the saddle-point method. It then follows that

$$\Delta_{in} = 2\sqrt{\pi J_*/3} \exp\left(-3J_*\right) \ . \tag{4.25}$$

The value

$$J_* = 2^{-1/3}(t/J_e)^{2/3} \tag{4.26}$$

is the saddle-point of the integral over the transverse actions (Eq. 4.24). The losses come mainly from the vicinity of the saddle-point, where $J_x = J_y = J_*$ and

$$v_z = v_* = t/(J_e J_*). \tag{4.27}$$

The second part of the losses arises from the particles stopping outside the electron beam, as was noted above:

$$\Delta_{out} = \iint_{J_x+J_y>J_e} dJ_x dJ_y \exp\left(-J_x - J_y\right) \ . \tag{4.28}$$

This integral can be evaluated exactly; keeping the same accuracy as for Eq. 4.25, it becomes

$$\Delta_{out} = J_e \exp\left(-J_e\right) \ . \tag{4.29}$$

The total losses Δ_t results from the sum of both inside and outside parts:

$$\Delta_t = 2\sqrt{\pi J_*/3}\exp\left(-3J_*\right) + J_e \exp\left(-J_e\right) \quad . \tag{4.30}$$

From Eq. 4.26 and $J_e = a^2/x_m^2$ the right hand side of the expression obtained is a function of both the electron beam radius and the time of cooling, (Note that x_m is the betatron amplitude associated with the rms emittance ϵ, so $x_m^2 = 2x_{rms}^2$.) Assuming the losses to be fixed at a certain tolerable level, the cooling time as a function of the electron beam radius can be found. The radius corresponding to the minimum cooling time is the optimum. The plots for the cooling time versus the electron beam radius are presented in Fig. 4.7, for $5\%, 10\%$ and 15% of losses. The electron beam radius is in units of the cooled beam rms amplitude $x_m = \sqrt{2\epsilon\beta_f/(\beta\gamma)}$, the time is in units of the parameter t_0, introduced in Eq. 4.22. The optimum electron beam radius lies within the rather narrow interval $2.1 < a/x_m < 2.4$ for any loss percentage between 5% and 15%.

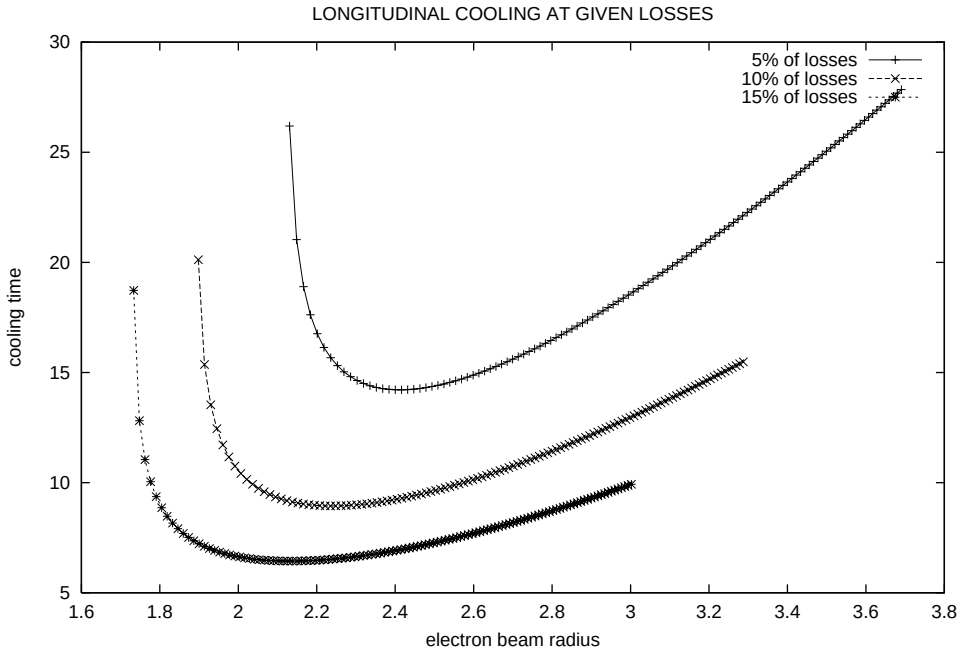

Figure 4.7: Time of cooling required for the given losses as a function of the electron beam radius. The time is in units of the parameter t_0 (Eq. 4.22), the electron beam radius is in units of the rms amplitude of the cooled beam $x_m = \sqrt{2\epsilon\beta_f/(\beta\gamma)}$.

4.2.3 Results for the conceptual design parameters

Electron cooling is to be used for longitudinal stacking of anti-protons in the Recycler storage ring.[5, 12, 13] After stacking, the $\overline{\text{p}}$'s are injected in the Tevatron. The consideration of the previous section gives the optimum for the electron beam radius and for the resulting beam cooling time.

Certain results can be derived for misalignment tolerances. Assume that because of misalignments the electron beam acquires a coherent angle θ_e giving a transverse velocity for the electron in the beam frame $u_{e\perp} = \gamma\beta\theta_e$. Its effect is a suppression of the cooling rates for the small velocity

particles, $v_{x,y,z} \leq u_{e\perp}$ given by Eq. 4.5 with $\langle(1/u^3)\rangle = 1/u_{e\perp}^3$. The result would still be tolerable, if the cooling time for these particles were smaller then the beam cooling time considered in the previous section. This condition can be expressed in terms of the rms betatron amplitudes $v_{x,y} = \sqrt{2\beta\gamma\epsilon/(\beta_f)}$, longitudinal velocity $v_z = \beta(\delta p/p)_{rms}$ and the dimensionless electron emittance J_e:

$$u_{e\perp} \leq (\pi v_x^2 v_z t/(2J_e))^{1/3}, \quad \theta_e = u_{e\perp}/(\gamma\beta), \tag{4.31}$$

where t is the (optimized) dimensionless beam cooling time. This formula gives the tolerable level for the stray electron velocity $u_{e\perp}$. With a given emittance, it scales as $\beta_f^{-1/3}$.

The sources for the stray electron velocity $u_{e\perp}$ mainly depend on the cooler specifications; a detailed consideration of this item goes beyond the scope of this chapter. However, some sources can be considered without going into details of the electron cooler construction; such is a stray transverse magnetic field $B_\perp$ on the electron trajectory. To suppress such fields, the correctors can be installed with a certain periodicity l_s, which gives a minimal wave number for the stray field space harmonics $k = 2\pi/l_s$. From here, the amplitude of the forced electron oscillations can be found:

$$u_{e\perp} = (B_\perp/e) r_e l_s/(2\pi), \tag{4.32}$$

where electrons are assumed to have a Larmour period $\gg l_s$. Eq. 4.31 gives the tolerable level for the stray field $B_\perp$.

The parameters obtained for the electron cooler calculated at the nominal design electron current and cooling length are given in Table 4.4, where some general parameters of the Recycler and the $\overline{\text{p}}$ beam are presented for convenience. From the point of view of longitudinal cooling, the optimum value for the beta-function at the cooler is the length of the cooling section. For higher values of the beta-function, the cooling rate does not depend on it, but all the sizes increase as $\beta_f^{1/2}$ and the tolerances decrease as $\beta_f^{-1/3}$. The entry for the longitudinal cooling rate is just the reciprocal of the given cooling time in units that manifest the independence of energy decrement on energy spread.

4.2.4 Numerical model for complete scenario

The numerical integration used to obtain the results tabulated in the Table 4.4 is too detailed to use for following a distribution of particles through hours of cooling to provide an overall process simulation. However, it was shown that the analytical single particle rate formulas are rather accurate. Using these formulas in a macroparticle phase space tracking routine makes a good numerical model practical. When only cooling is taking place, the time steps can be scaled according to cooling rates; when rf manipulations are being carried out, the time steps have the scale of the synchrotron oscillation period. Even the shorter time intervals can be many beam circulation periods. By considering the full six-dimensional phase space distribution, such a calculation will reflect the progressive improvement in longitudinal rate as the transverse components are cooled. The utility of such a model is to check that the whole scenario fits together as advertised and that choices made along the way don't have unanticipated disadvantages. It will be helpful in tightening up performance predictions, checking important Recycler parameters like rf voltage limits, evaluating stack dilution during the injection process, *etc*.

Table 4.4: Electron cooling in the Recycler

Parameter	Symbol	$\beta_f = 200$m	$\beta_f = 20$m	Unit
Circumference	C	3319.4		m
Pbar momentum	p	8.9		GeV/c
Normalized rms emittance	ϵ	1.6		mm·mrad
Cooler length	l_c	20		m
Electron current	I_e	0.5		A
Losses	Δ_t	5		$\%$
Beam cooling time	t	15		min
constant longitudinal cooling rate	$\mathrm{d}\delta E/\mathrm{d}t$	180		eV/h
Electron beam radius	a	1.9	0.57	cm
Electron angle	θ_e	≤ 40	≤ 80	μrad
Electron temperature, tolerable	$m\hat{w}^2$	≤ 0.1	≤ 1	eV
Electron temperature, optimum	$m\hat{w}^2$	0.03	0.3	eV
Electron momentum spread	$(\delta p/p)_e$	$\leq 1 \cdot 10^{-4}$		
Corrector-corrector interval	l_s	1		m
Stray magnetic field	$B_\perp$	≤ 40	≤ 80	mGs

Chapter 5

Related Accelerator Physics Issues

The push toward higher luminosity raises important accelerator physics questions not only about electron cooling in the Recycler, but also about other components of the collider complex that must be modified or improved to cope with higher flux and closer bunch spacing. All of these matters have received attention at some level under such labels as TeV33,[15] luminosity upgrade,[16] and Fermi III.[17] The cited references provide substantial material on the overall scenario and critical issues for subsystems. This chapter draws from the references to provide a coherent setting for the electron cooling project. The issues which directly impinge on electron cooling are treated in some detail.

5.1 Antiproton production enhancement

It is the perspective of this report that electron cooling is the technological means to surpass the luminosity goals of the Run II plan. However, the cooling, of course, serves only to open the pipeline, not to fill it. A number of possibilities have been identified for increasing raw antiproton production and the usable fraction of it for Run II. Some of the same measures can be further developed and exploited to provide flux beyond Run II specifications. The most practical means to a factor of two or so in net flux is likely to be a combination of small gains from several approaches. What follows in this section is basically a catalog of the means under development or being discussed along with estimates of potential gain. A summary of the measures intended for Run II is provided in Table 5.1. Critical discussion of the merits and economics of the techniques is largely beyond the scope of this report; the aim is primarily to establish that issues are being addressed and that the outlook is favorable.

An immediate source of gain is the Main Injector itself. Its larger aperture and faster cycle time increase the number of protons per hour on the $\bar{p}$ target by 150% and someday, using multiple Booster batches, by as much as 400% over Run Ib parameters. Not all of this gain is immediately useable. In order to minimize damage to the target, the spot size of the proton beam will have to be increased, thereby reducing the antiproton yield. The scenarios listed below address regaining this yield as well as increasing the acceptance and improving the handling of the antiprotons produced.

5.1.1 Target Station Upgrades

The increase in energy deposited in the target because of the Main Injector increases in protons on target force an enlargement of the size of the beam hitting the antiproton target. A sweeping

system is planned to spread the energy deposition over a larger area of the target. This allows the addition of a proton focusing lithium lens to return the spot to 0.1 mm.

5.1.2 Antiproton Acceptance Upgrades

In order to accept more of the antiprotons produced, several changes are being considered for the systems between the target and the Debuncher. The optics of the AP2 line does not seem to be well matched between the target and the Debuncher. If this is addressed it should increase the admittance of the Debuncher from 17π mm mr to $26\ \pi$ mm mr. Further improvements may increase this to $32\ \pi$ mm mr. A scenario has been identified to increase the momentum acceptance from 4.0 to 4.9%. There is a proposal to increase the gradient in the Li lens from 750 T/m to 900 T/m and possibly as high as 1300 T/m. Taken together, these steps would ideally result in a 223% increase in antiproton acceptance.

5.1.3 Debuncher cooling

Through Run Ib, the Debuncher stochastic cooling systems (horizontal, vertical and momentum) all worked at 2–4 GHz. It is planned to change this to 4–8 GHz to be able to handle antiproton fluxes planned for Run II and beyond.

5.1.4 Accumulator Stacktail Upgrade

The stacktail system in the accumulator has previously operated at 1–2 GHz for both betatron and momentum. Work is being done to increase this to 2–4 GHz which would double the maximum flux it could handle. A change in the lattice is necessary to facilitate this. An increase to 4–8 GHz is possible but would require more extensive redesign and development.

5.1.5 Accumulator Core Upgrade

The core cooling systems in the Accumulator must cool the stack to 10π mm mr for transfer within 5–10 minutes (5% of stacking time). The performance of this system at the end of Run Ib was not sufficient for the requirements of the future. Meeting those requirements is planned through improvements in the performance of various components of the existing system rather than implementing a new one.

5.2 Stochastic Cooling Calculations

Electron cooling and stochastic cooling are complementary in principle, and, at least during the earliest operation of the electron cooling system, that complementarity will be exploited by using the stochastic cooling for the large transverse emittance of the recycled antiprotons whereas the electron cooling will be optimized for longitudinal cooling to increase the stacking rate and maximum stack current.

This report considers the performance of stochastic cooling for the purpose of establishing criteria for electron cooling. It is important to know what the beam parameters will be for the beam

Table 5.1: Run II accelerator improvements to enhance $\bar{p}$ flux

target for improvement	value	improved value	$\bar{p}$ flux gain factor
$\bar{p}$ on target	$4.8 \cdot 10^{15}$/h	$1.2 \cdot 10^{16}$/h	1.5
proton lens and beam sweeping	none	yes	1.15 – 1.20
optics match of AP-2	17π mm mr	26π mm mr	1.56
misc. admittance improvements	26π mm mr	32π mm mr	1.30
momentum acceptance	4.0 %	4.9 %	1.23
collection lens gradient	750 T/m	900 T/m	1.11
further gradient increase	900 T/m	1300 T/m	1.17
Debuncher cooling	2–4 GHz	4–8 GHz	needed with above
Accumulator stack tail cooling	1–2 GHz	2–4 GHz	needed with above
Accumulator core cooling	4–8 GHz	optimize gain	needed with above
ultimate stacking rate	$7.2 \cdot 10^{10}$/h	$30.3 \cdot 10^{10}$/h	3.20

Note that timing of implementation of these steps varies, that some are not independent of others, and that the final gain is not necessarily the product of the preceding gains.

injected from the Accumulator at the Run II level and beyond. Also the effectiveness of the longitudinal stochastic cooling in the Recycler determines the stacking rate and ultimate sustainable stack. Therefore, the level at which the electron cooling project should plan to switch from development to an operational system depends on how well the stochastic system can do. In the longer term it will also be necessary to understand at what intensity the transverse stochastic cooling may be completely incapacitated. At that point the electron cooling system must provide cooling of large transverse velocities, and the hardware requirements become substantially more challenging.

5.2.1 Recycler stochastic cooling revisited

The same program used in modeling the antiproton stacking in the Accumulator[18] has been applied to the Recycler stacking of Accumulator batches. Table 5.2 tabulates the Recycler ultimate stack and, in parentheses, the fraction thereof within the design goal of 54 eVs to be injected into the Tevatron. The four rows are for four different intervals between injection into the Recycler. The first two columns correspond to Accumulator stacking as specified for Run II (see Table 2.1). The first reflects the use of azimuthal compression to 25% of the full circumference in the Recycler to reduce the effect of intrabeam scattering. This mode and the diffusion constant chosen to represent the longitudinal IBS are consistent with the understanding of IBS contained in the Recycler TDR[5]. The analysis in Section 5.3 establishes that the constant is too large and the scaling with azimuthal compression questionable. In columns two and three the azimuthal compression remains constant at 79% where the remaining 21% is kept clear for transfers and barrier bucket manipulation. The third column corresponds to double the Run II flux, the initial goal of electron cooling. The emittances of the injected beam are the same for all cases. Because only a fraction of the stack lies within the target longitudinal emittance, the simulation must take into account not only the beam being stacked from the Accumulator and that returned from the Tevatron, but also the tails left behind when the new beam was put into the Tevatron.

One concludes from the Table that the Recycler with stochastic cooling can achieve Run II goals

Table 5.2: Ultimate stack intensity and ultimate intensity within 54 eVs in units of 10^{12} antiprotons combining Accumulator injection and return from Tevatron

Acc. Inj. Intrvl.	Run II compr.		Run II no compr.		Twice Run II flux	
min.	total	54 eVs	total	54 eVs	total	54 eVs
40	3.28	2.26 (.69)	4.87	2.92 (.60)	8.20	3.28 (.40)
60	3.25	2.60 (.80)	5.07	3.04 (.60)	8.49	3.48 (.42)
120	3.21	2.89 (.90)	4.95	3.17 (.64)	7.96	3.74 (.47)
140	3.01	2.74 (.91)	-	-	-	-

by receiving beam every one to two hours with or without the compression technique. More frequent transfers, which some of the source improvements depend on, will not not be as effective. As demand for antiprotons increases beyond initial Run II fluxes, stochastic cooling falls behind and plateaus well below what is required for double the Run II flux. A large part of the problem is the un-extracted tails. According to the simulations, when the recycled beam is returned from the Tevatron, the tails remaining from the transfer to the Tevatron are pushed farther out in momentum space to make room for the returned beam. It requires eight hours to smooth out the distribution, just in time for the next transfer. Approximately half of the beam is in this situation, essentially lost, being pushed back and forth on the outer edges of the distribution. With electron cooling there will be no un-extracted stack tails to interfere with cooling the beam returned from the Tevatron. Taken at face value, the figures for twice the input flux show that the stochastic cooling fails to achieve the stacking goals.

5.2.2 Initial Cooling of Recycled Beam

As explained in Section 2.2, antiprotons returned to the Recycler from the Tevatron may be cooled for one to two hours before transfers from the Accumulator are resumed. Earlier injection from the Accumulator is possible with some loss in effectiveness of the pre-cooling; a trade-off can be made between pre-cooling and Accumulator performance. The longitudinal stochastic cooling program used above, was applied to this situation as well. The results are shown in Figure 5.1 for stacking at 20 minute intervals.

With Run II parameters, $1.48 \cdot 10^{12}$ antiprotons returned from the Tevatron, about 80% of the beam is cooled into the central 54 eVs within an hour and a half. This matches well with the operating scenario stated. For twice the amount returned, $2.5 \cdot 10^{12}$, the scenario does not work; it requires three hours of cooling to sweep 80% of the beam into the central 54 eVs.

Figure 5.2 further illustrates the difficulties the system has dealing with the increased amount of beam. The top left plot shows the cooling of $1.48 \cdot 10^{12}$ particles returned from the Tevatron. The curves are plotted at 20 minute intervals for three hours. The momentum is binned in 0.4 MeV bins. The initial distribution is approximately ± 10 MeV in 80% of the circumference of the Recycler. The pair of dashed lines delineate the central 54 eVs within which the particles should reside to be sent back to the Tevatron for the next store. As shown in Fig. 5.1, about 88% of the beam makes it within that window in two hours.

The top right plot shows the cooling of $2.5 \cdot 10^{12}$ particles. The plot is about the same as the top left except for vertical scale. It takes 3 hours to cool just 80% of the beam to within the central

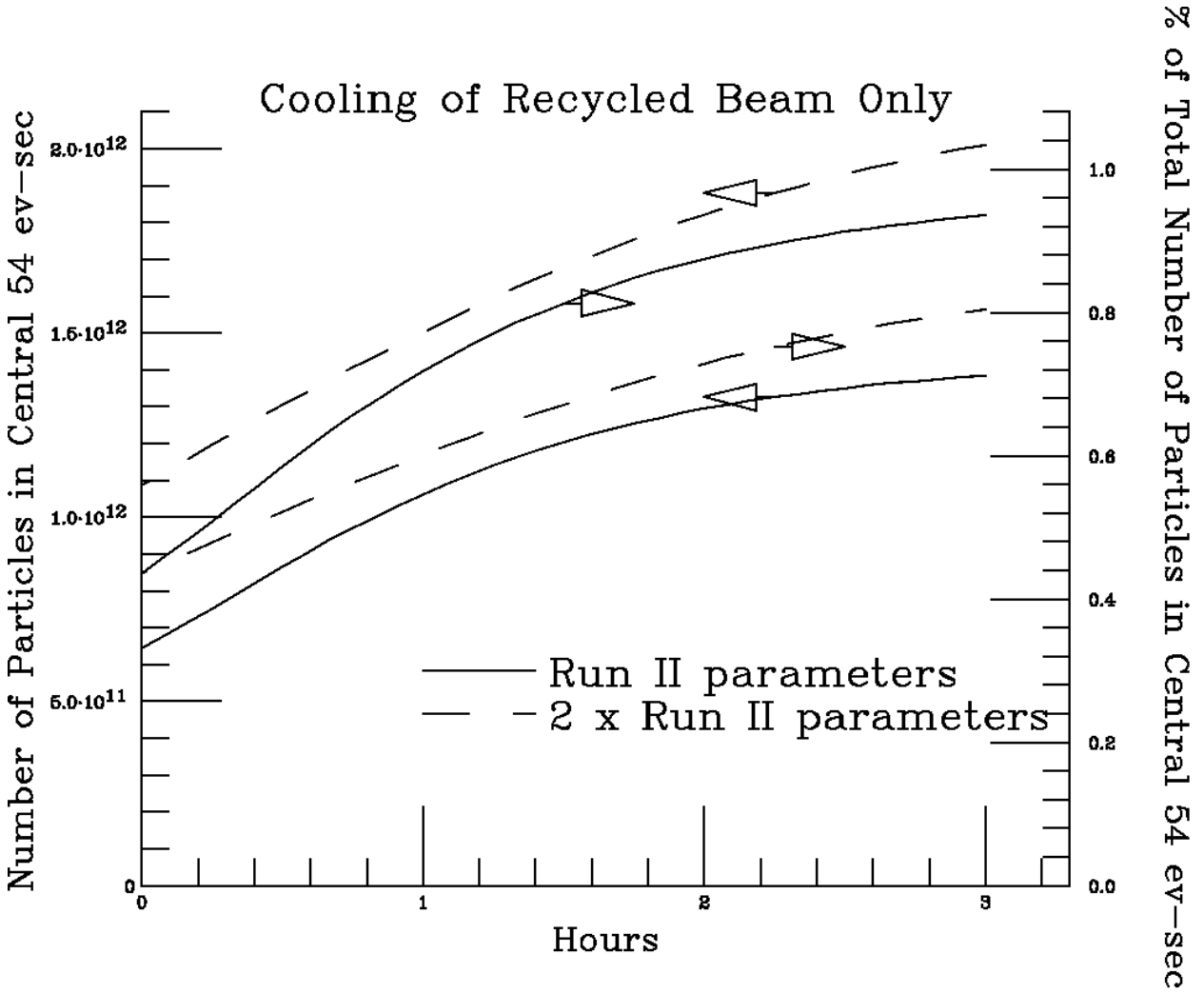

Figure 5.1: Stochastic momentum cooling of $\bar{p}$'s recycled from the Tevatron, intensity and fraction of intensity useable *vs.* time for $1.4 \cdot 10^{12}$ recycled (Run II) and $2.8 \cdot 10^{12}$ (Run II+).

54 eVs. The lower plot is a bin-by-bin ratio of the two upper plots for each of the time intervals. Initially, the ratio is 1.68 across all bins. As time progresses, the higher intensity tails lag their lower intensity counterparts and the ratio in the tails increases. Similarly, the movement into the central bins is slower for the high intensity case and the ratio is depressed.

The stochastic cooling calcuations for the Recycler reported in this subsection were made on the basis of the understanding of the longitudinal intrabeam scattering represented by the Recycler TDR.[5] They must be repeated with the new IBS evaluation described in section 5.3. These and the corresponding transverse cooling cases are needed to provide a better basis for the design by indicating the minimum useful performance for the electron cooling and providing early information on the effectiveness of the stochastic precooling.

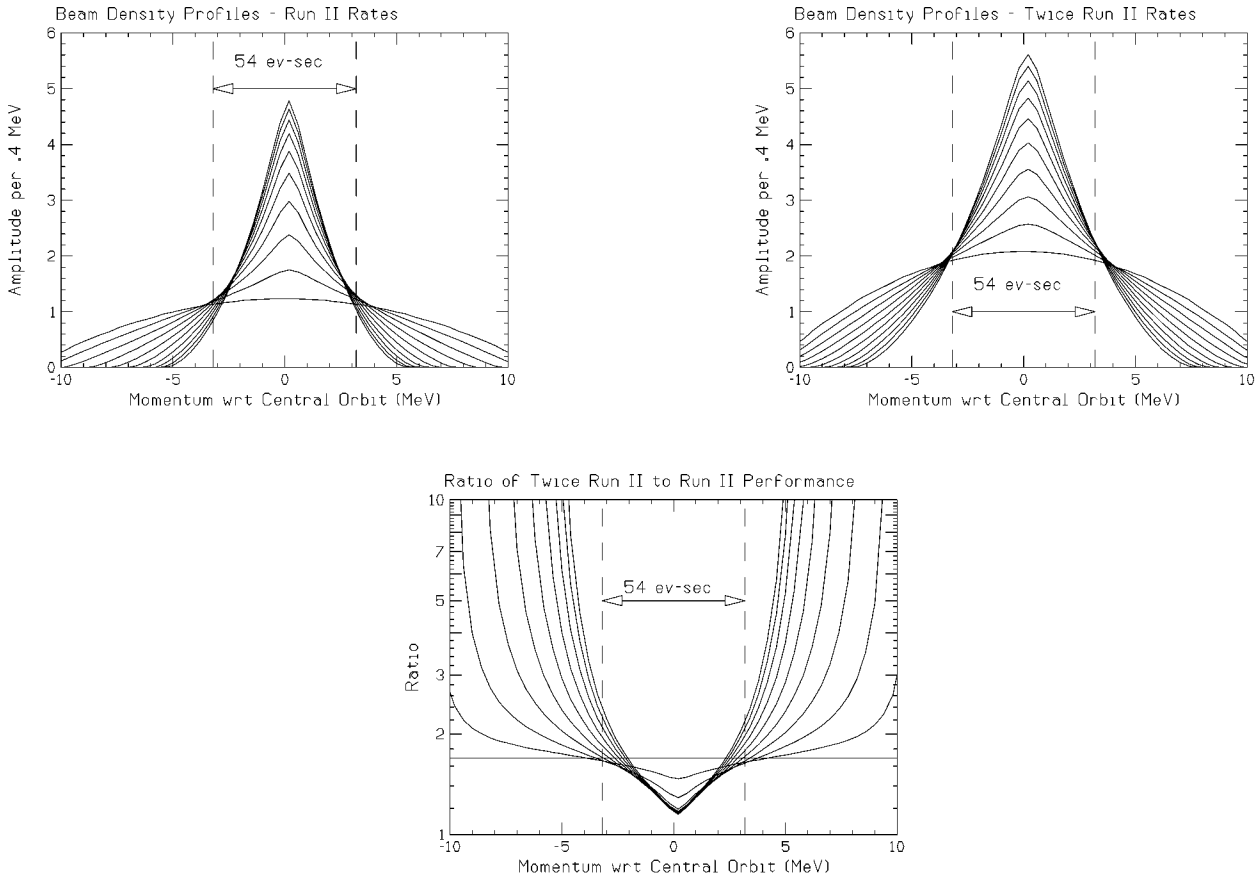

Figure 5.2: Same case as Fig. 5.1, density profiles at 20 min intervals. Lower plot is ratio of Run II+ profiles to Run II profiles.

5.2.3 Anticipated emittance from the Accumulator at 40 – 100 · 10^{10} $\bar{p}$ / hr

The Run II Handbook[6] states that the emittances must be less than 10π mm mrad and 10 eVs. These emittances apply to a flux of $20 \cdot 10^{10}$ $\bar{p}$/hr. As it becomes necessary to increase Accumulator throughput, it will be emptied more frequently and the gain profile modified to enhance stacking. Under these conditions one expects that the transverse emittance to be higher, but whether it will be possible to compensate this with the amount of transverse electron cooling planned is not certain without more information on the Accumulator upgrades. It is currently assumed that improvements to the present systems plus frequent transfers will maintain transverse emittance near the historical value at the $40 \cdot 10^{10}$/hr rate. As the rates go higher, it may be practical to improve the transverse cooling along with the necessary improvements in the longitudinal cooling.

5.3 Intrabeam scattering in the Recycler

The intrabeam Coulomb scattering (IBS) drives the antiproton distribution toward thermal equilibrium. Consequently, the relatively hot degrees of freedom (for the Recycler, transverse) are cooled, and the cold one (longitudinal) is heated. General formulas for the intrabeam scattering [19, 20] are rather complicated and are generally used by means of computer programs. The purpose of this section is to derive a handy formula for the IBS longitudinal diffusion. The following approximations are used:

- The longitudinal temperature of antiprotons is much lower than the transverse. In fact, they differ by a factor of 4 – 40.
- The dispersion size of the antiproton beam can be neglected. For the longitudinal 95% phase space area $\mathcal{A} = 240$ eVs, the rms momentum spread $\Delta p/p = 7 \cdot 10^{-4}$, assuming the whole ring occupation. The average dispersion of the Recycler $D = 70$ cm, which gives 0.5 mm of dispersion size, while the betatron rms beam radius is 4 – 6 times higher.
- The smooth approximation is applied. Actually, the Recycler lattice is rather smooth; the beam envelope oscillates with an amplitude $\approx \pm 30\%$.

In a collision a particle gets a longitudinal velocity kick; in the beam frame

$$\delta v_z = 2r_p \cos\theta/(\rho u), \quad \overline{\delta v_z} = 0, \quad \overline{(\delta v_z)^2} = 2r_p^2/(\rho^2 u^2),$$

where r_p is the classical proton radius, θ is the angle between the longitudinal axis and a plane of the relative motion, ρ is the impact parameter, u is the relative velocity, the bar $\overline{(...)}$ stands for the averaging over θ; all the expressions assume $c = 1$. From here, the IBS diffusion coefficient $D = d(\Delta p/p)^2/dt$ in the laboratory frame is found as a result of an integration over the impact parameter and over the velocities of the scattered particles $\vec{v}_2$. This result has to be averaged over the betatron phases ψ_x, ψ_y of the antiproton considered:

$$D = \frac{4\pi r_p^2 L_{\bar{p}}}{\gamma\beta^2} \int_{-\pi/2}^{\pi/2} \int_{-\pi/2}^{\pi/2} \frac{d\psi_x d\psi_y}{\pi^2} \int \frac{d^2 v_2 f_\perp(\vec{r}, \vec{v}_2)}{|\vec{v} - \vec{v}_2|} \tag{5.1}$$

$$\vec{v} = (v_x \sin\psi_x, v_y \sin\psi_y); \quad \vec{r} = -(v_x \cos\psi_x, v_y \cos\psi_y)/(\gamma\omega_b)$$

with $L_{\bar{p}}$ as the IBS Coulomb logarithm and ω_b as the betatron frequency for the both degrees of freedom. The relativistic factor γ appears here because of the time transformation in going to the laboratory frame. The transverse distribution of the antiprotons is assumed to be Gaussian,

$$f_\perp(\vec{r},\vec{v}_2) = n_p \exp(-r^2/(2a_p^2)) \exp(-v_2^2/(2v_\perp^2))/(2\pi\gamma v_\perp^2)$$

where $n_p = (I_p/e)/(2\pi\beta a_p^2)$ is the beam density at the axis in the laboratory frame, I_p is the peak antiproton current. In this case, the diffusion coefficient is rewritten as

$$D = \frac{4\pi n_p r_p^2 L_{\bar{p}} \mathcal{I}}{\gamma^2\beta^2 v_\perp}. \tag{5.2}$$

Here a dimensionless transverse factor was introduced:

$$\mathcal{I} = \int_{-\pi/2}^{\pi/2}\int_{-\pi/2}^{\pi/2} \frac{d\psi_x d\psi_y}{\pi^2} \exp(-r^2/(2a_p^2)) \int \frac{d^2 v_2 \exp(-v_2^2/(2v_\perp^2))}{2\pi v_\perp |\vec{v}-\vec{v}_2|} \tag{5.3}$$

with $a_p = v_\perp/(\gamma\omega_b)$. This factor can be easily calculated for the limit cases $v \gg v_\perp$ or $v \ll v_\perp$; then the results might be joined by a proper analytical expression. The following formula

$$\mathcal{I} = \frac{2}{\pi} \frac{v_\perp^3}{\sqrt{(v_x^2 + v_y^2 + 2v_\perp^2/\pi)(v_x^2 + 2v_\perp^2/\pi)(v_y^2 + 2v_\perp^2/\pi)}} \tag{5.4}$$

gives an exact result for the limit cases; its inaccuracy in the intermediate area, $v \simeq v_\perp$, is not worse than 20%.

The longitudinal distribution of the antiprotons is determined by the competitive action of the diffusion and the cooling force rewritten below for the sake of convenience:

$$\frac{d(\Delta p/p)}{dt} = -F, \quad (\Delta p/p) > 0 \tag{5.5}$$

with

$$F = \frac{8(I_e/e) r_e r_p \eta L_\parallel}{\pi\beta^2\gamma^2 a^2 v_x v_y} \tag{5.6}$$

The evolution of the longitudinal distribution function $f_\parallel$ is described by the Fokker-Planck equation:

$$\frac{\partial f_\parallel}{\partial t} + \frac{\partial}{\partial w}\left(-F f_\parallel - \frac{D}{2}\frac{\partial f_\parallel}{\partial w}\right) = 0 \ . \tag{5.7}$$

Here the symbol $w = \Delta p/p$ is introduced to simplify the notation. Taking into account that both the cooling force F and the diffusion do not depend on the momentum w, a stationary solution of this equation is found:

$$f_\parallel^0(w) = \exp(-w/\bar{w})/\bar{w}, \quad \bar{w} = D/(2F) \ . \tag{5.8}$$

From here, the lower limit for the longitudinal 95% emittance (phase space area) $\mathcal{A}_{\min}$ is presented as

$$\mathcal{A}_{\min} = 6\bar{w} l_p = 3 D l_p / F \ , \tag{5.9}$$

where l_p is the length of the antiproton beam bounded by the barrier voltage pulses. Substitution the expressions for the diffusion coefficient (5.2) and the force (5.6) permits rewriting this limit in the following form:

$$\mathcal{A}_{\min} = \frac{3\pi v_\perp p l_p I_p}{4 I_e \eta} \frac{r_p}{r_e} \frac{L_{\bar{p}}}{L_\parallel} \frac{a^2}{a_p^2} \mathcal{J}, \quad \mathcal{J} = \frac{\mathcal{I} v_x v_y}{v_\perp^2} \quad . \tag{5.10}$$

According to this result, the limit emittance $\mathcal{A}_{\min}$ does not change with the longitudinal compression of the antiproton beam; it depends only on the product $I_p l_p = \bar{I}_p C$. Thus it applies also equally to the stacking and recycling processes. The maximum value of the transverse velocity factor $\mathcal{J}$ is reached at $v_x = v_y = \sqrt{(1+\sqrt{5})/\pi} v_\perp \approx v_\perp$ with $\mathcal{J}_{\max} = 0.24$, which gives for the project basic parameters $\mathcal{A}_{\min} = 7$ eVs.

5.4 Stability of the Antiproton Beam

In general, antiproton beam stability is considered in the Recycler Technical Design Report.[5] Here, only the influence of the electron beam on these phenomena is discussed. The stability of the electron beam itself is discussed in the context of a cooling section with lumped focusing elements in Appendix B. The factors which could be relevant for $\bar{\text{p}}$ stability are listed below.

1. The space charge of the electron beam causes a betatron tune shift for the circulated antiprotons:

$$\Delta\nu_e = \frac{(I_e/e) r_p l_c \beta_f}{2\pi c a^2 \beta^2 \gamma^3} \tag{5.11}$$

   where I_e is the electron current, r_p is the proton classical radius, l_c is the cooler length, β_f is the beta-function in the cooler, a is the electron beam radius. Substitution here of the basic project parameters shows that this tune shift is not significant, $\Delta\nu_e = 0.4 \cdot 10^{-4}$.

2. The longitudinal cooling shrinks the momentum spread. This, in general, could reduce Landau damping and drive coherent instabilities. To prevent longitudinal microwave instability, it is sufficient to have the rms momentum spread $\Delta p/p$ satisfying to the Keil-Schnell condition

$$\Delta p/p \geq \sqrt{\frac{N r_p c |Z/n|}{2\pi\gamma\eta}} \tag{5.12}$$

   where $|Z/n|$ is the reduced longitudinal impedance, and $\eta = 1/\gamma^2 - 1/\gamma_t^2$ is the phase slip factor. For the project parameters, with the space charge impedance $|Z/n| = 12\Omega$ it gives $\Delta p/p \geq 5 \cdot 10^{-5}$.

3. The longitudinal cooling can hardly influence the transverse beam stability in the Recycler case. The reason is that the relative spread of the revolution frequencies is insignificant even without cooling. For the resistive wall instability, the most dangerous longitudinal mode number is the integer part of the betatron tune, $n = 25$, which corresponds to the longitudinal frequency spread factor

$$n\Delta\omega_0/\omega_0 = n\eta\Delta p/p \leq 1 \cdot 10^{-4}. \tag{5.13}$$

This value has to be compared with the shift of the incoherent betatron tune from the coherent tune due to the antiproton beam space charge (Laslett tune shift):

$$\Delta\nu_L = \frac{Nr_p}{4\pi\beta\gamma^2\epsilon_n} \tag{5.14}$$

where ϵ_n is the normalized rms emittance. For the nominal design, one finds $\Delta\nu_L = 0.5{\cdot}10^{-2}$. The revolution frequency spread factor (5.13) is only $\simeq 0.02$ of this number; such a small value can hardly be significant.

4. The electron beam introduces in the ring additional longitudinal and transverse impedances [21]. Both of these values are much smaller than the corresponding expected values for the ring, so they can be neglected.

5. The transverse cooling rate is inversely proportional to the relative electron-antiproton velocity cubed; the slow antiprotons are cooled very fast. If the electron beam is of a good quality, these fast-cooled antiprotons are condensed in a small core. This core could be space-charge dominated and so unstable. Recent experiments at CELSIUS, Uppsala [22], support this explanation for the cooled beam instabilities observed on several cooling facilities. To prevent such instabilities, the transverse velocity of the electron beam could be regulated at the entrance of the cooling section.

Chapter 6

Laboratory Studies

6.1 Electron beam recirculation

This section describes the successful recirculation of a dc electron beam at energies 1 – 1.4 MeV and currents in excess of 300 mA with typical relative losses of $1 - 2\times10^{-5}$. Currents of 200 mA were maintained for the periods of one hour (typical) without a single breakdown, 300 mA for 20 minutes.

In 1995 Fermilab started an R&D program in electron cooling that has two principal goals: (1) to determine the feasibility of electron cooling the 8 GeV antiprotons; and (2) to develop and demonstrate the necessary technology. The primary technical problem is to generate a high-quality, monochromatic, dc, multi-MeV electron beam of 200 mA or greater. The only technically feasible way to attain such high electron currents is through beam recirculation (charge recovery). High-efficiency recirculation of a 1 MeV, 1 A, dc electron beam was first demonstrated in 1987 [23] by INP, Novosibirsk using a continuous solenoidal field which provided beam focusing. Presence of a solenoid makes such a system cumbersome and not easily extendible to the several MeV range. Another approach, suggested and tested by a group from UCSB [24], is to utilize an electrostatic accelerator with discrete focusing elements. The UCSB group has demonstrated recirculation of a pulsed (several microseconds) 1.25 A electron beam using a 3 MeV Pelletron accelerator (Van de Graaff type) at National Electrostatics Corporation (NEC). The results of this demonstration became a basis for a Fermilab-led collaborative effort which attained recirculation of a 2 MeV, 105 mA beam with 11 μA losses sustainable for one to ten minutes [25]. Recirculation tests, described in the present paper, were performed on the same accelerator as described in Refs. [24] and [25] with shorter 2 MV acceleration and deceleration tubes, a new electron gun and collector [26], as well as a different beam line. Figure 1.3 shows a simplified electrical schematic of the recirculation test. Figure 6.1 shows the test beamline layout. Table 6.1 summarizes the important system parameters.

This system employs an electrostatic HV supply like a Van de Graaff with maximum charging current of a few hundred microamperes. The electron gun can be operated in both emission and space charge limited regime with a control electrode being always negatively biased with respect to the cathode. Figure 6.2 shows the mechanical schematic of the electron gun. The electron beam line consists of a 7.5 m long channel with discrete focusing elements (lenses and a bending magnet) flanked by small aperture (2.54 cm id) acceleration and deceleration tubes.

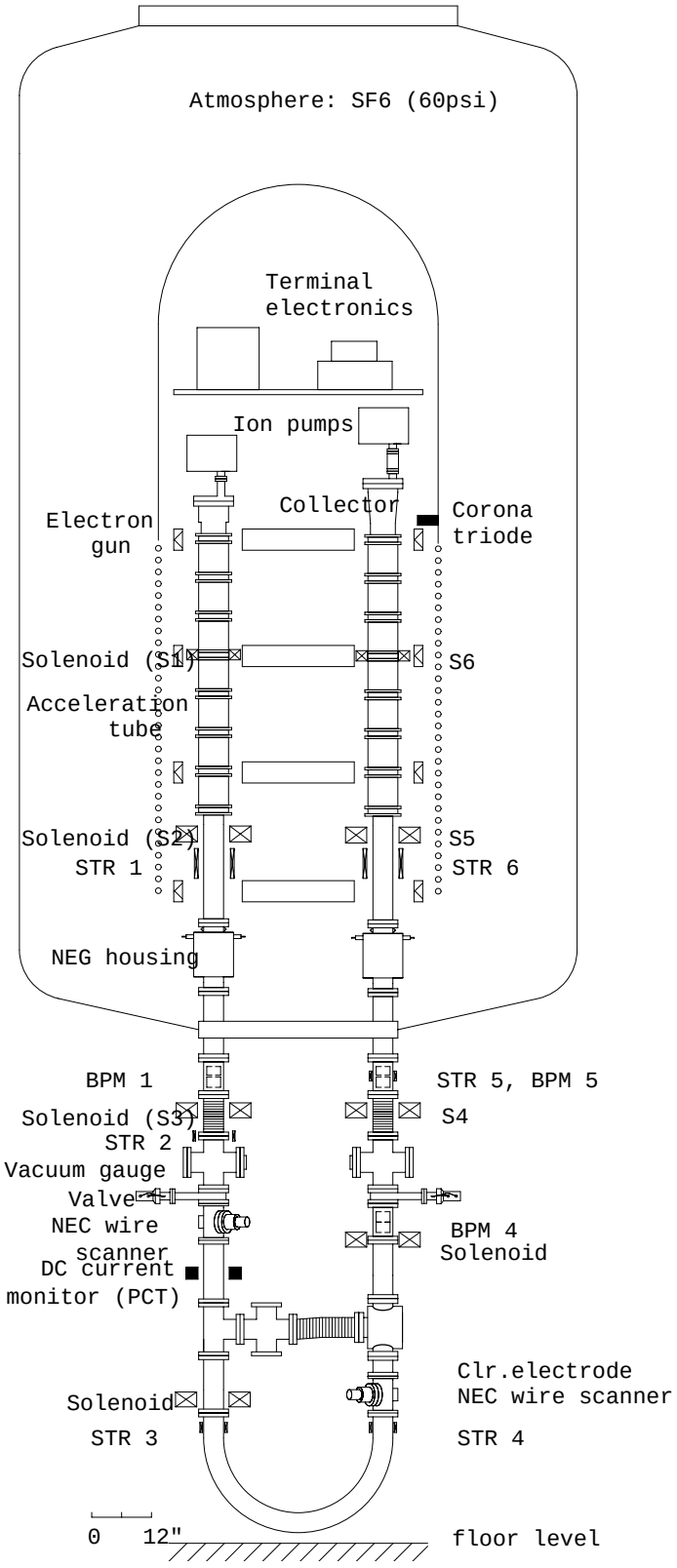

Figure 6.1: Recirculation system beamline layout

Table 6.1: Recirculation system parameters

Parameter	**Symbol**	**Value**	**Units**
Pelletron Voltage	U_0	1–1.4	MV
Max. Recirculated Beam Current	I_b	680	mA
Typical Vacuum	p	1×10^{-7}	Torr
Relative Losses	$\Delta I/I_b$	$1–2\times10^{-5}$	
Electron Gun			
Cathode Radius	r_c	1.7	mm
Gun Perveance	P	0.07	μPerv
Anode Voltage	U_A	$\leq$50	kV
Control Voltage	U_C		
beam off		$-U_A$/13	
beam on		$-U_A$/100	
Electron Collector			
Collector Voltage	U_{COL}	$\leq$5	kV
Relative Losses (30 keV test bench)		3×10^{-6}	

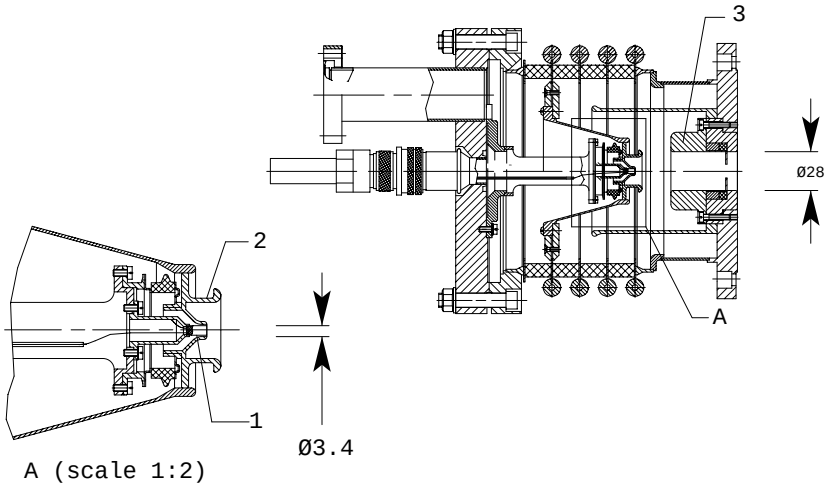

Figure 6.2: Mechanical schematic of the electron gun: 1 - cathode, 2 - control electrode, and 3 - gun anode. Dimensions are in millimeters.

6.1.1 Stability

A salient attribute of this recirculation test is relatively weak focusing: typical focal length of the beamline elements is about one meter. Note, that in traditional low energy electron cooling systems this value is 1 – 10 mm and electron trajectories do not depend on the beam energy. The system, described in Ref. [23], had a typical focal length of 5 cm and this allowed it to sustain 3% energy fluctuations. One of the consequences of the weak focusing is that particle trajectories, as well as beam losses, strongly depend on the particle's energy (Fig. 6.3). In the event of an energy fluctuation that exceeds several kilovolts, the voltage on the Pelletron drops instantly ("crashes") to a very low level. The mechanism of a crash can be described as follows. An energy fluctuation or other perturbation causes some initial beam loss. If losses occur in the acceleration or deceleration tube, it takes only a couple of microamperes to significantly redistribute grading potentials on the tube. As the tube electrodes charge up, the divergence of the beam increases, which in turn increases beam losses and so on. During this process the Pelletron voltage drops to a typical level of 200 kV. If the gun is not shut off immediately after such a crash, the system becomes stable at this low voltage: some of the tube electrodes become charged up to the cathode potential, nearly all the beam current that the anode supply is capable of producing is returned to the anode, and a few microamperes fall on the tube electrodes and even pass all the way down to ground. These crashes were of primary concern in the test because the final electron cooling system has to operate 24 hours a day without substantial intervention.

One of the most common mechanisms leading to large energy fluctuations is a partial or full tube breakdown. In these tests the Pelletron voltage has been lowered from a nominal 2 MV to 1 – 1.5 MV to both reduce the frequency of breakdowns and to minimize the damage to the terminal electronics caused by them. Even with the lowered voltage it takes at least one week to condition the tube with the beam on after opening the tube to the atmosphere.

Operation without crashes for the periods of one hour or longer is possible only when the beam boundary is far away from the apertures. In this mode of operation all the beamline settings can be varied (to some extent) without a significant increase in current loss. Figure 6.3 illustrates the dependence of losses on the beam energy for such a regime. The best stability is achieved at the minimum of loss curve (33 – 34 kV for the conditions of Fig. 6.3).

The behavior of the system significantly differs for the operation below and above the most stable energy. Figure 6.3 shows that the energy increase above the stable point leads to higher losses, reducing the mean time between crashes. On the other hand, the energy decrease below the stable range leads to an immediate crash: the increase of losses leads to further decrease of beam energy, which, in turn, increases losses, etc. This mechanism is valid on time scales shorter than the response time of an energy regulation (corona triode) circuit.

The time period between crashes decreases with beam current: typical time between crashes for 200 mA is one hour, 20 minutes for 300 mA, and seconds for 350 mA. The main reason is that the beam size generally increases with current. This reduces the range of sustainable fluctuations of various beamline settings and, consequently, the stability of the system. Also, the beam losses increase with the beam current (see Fig. 6.4), and the best stability is achieved with the lowest level of losses.

Stability with respect to the beam position inside the collector is also very important because of the electron-induced gas desorption from the collector surface [27]. The coefficient of desorption from the collector surface initially lay between one and ten molecules/electron. Even a small steering of a high current beam inside the collector onto a new location can be accompanied by a burst

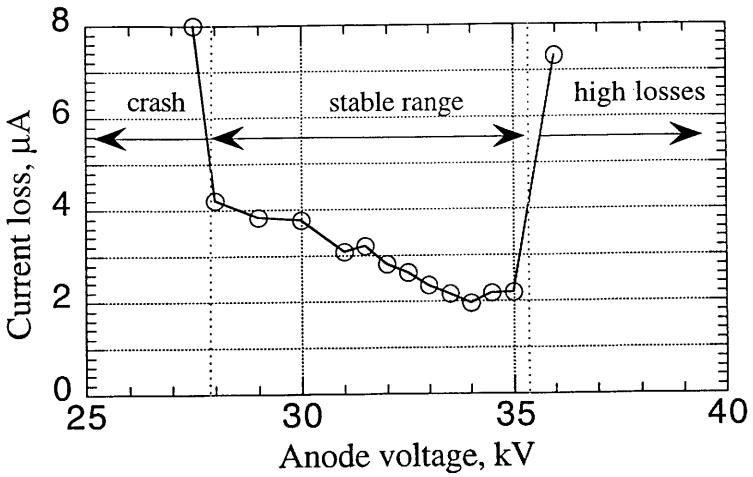

Figure 6.3: Measured dependence of losses on anode voltage U_A. Pelletron voltage was kept at $U_\circ = 1.135$ MV, beam current was 200 mA. Beam kinetic energy is $eU_\circ + eU_A$.

of the desorbed gas and subsequent HV breakdown. After a long operation period and uniform exposure of the collector surface to the electron beam, the coefficient of desorption fell to the level of 10^{-3} and this effect disappeared. The estimate of the acquired dose by the collector surface is on the order of 10 mA hr/cm^2. This effect puts the limit on how fast one can establish a recirculating beam after letting the collector up to the atmosphere. The best results were achieved with the collector being under vacuum for more than one year. Thus, there are at least three necessary conditions for a stable recirculation: (1) losses in the tubes should be significantly lower than the tube resistive divider current, typically equal to 10 – 20 μA; (2) fluctuations of the beam energy and the bending magnetic fields should not exceed 0.2% — this requirement is less stringent than the requirement of 0.01% energy regulation for efficient electron cooling; and (3) the beam boundary should be far away from the apertures.

6.1.2 Beam losses

The typical dependence of current losses as a function of beam current is shown in Fig. 6.4. This dependence has two reproducible parts: linear and exponential.

The exponential growth of losses is often observed because of beam scraping during initial beam steering as one tries to establish the recirculation. The exponential part in Fig. 6.4 also most likely corresponds to the scraping of primary beam. Figure 6.4 was obtained while operating the gun in a space-charge limited regime where the beam current is determined by the control electrode potential. We observed that the voltage on the control electrode that corresponds to the knee point in Fig. 6.4 increases linearly with U_A. This corresponds to a fixed beam size in the anode while the beam current scales as $U_A^{3/2}$.

The linear part of the losses in Fig. 6.4 might have three contributions: (1) collector losses, (2) residual gas scattering, and (3) beam halo formed in the gun region. At observed level of losses 1 – $2 \cdot 10^{-5}$ it is difficult to distinguish between these mechanisms. The collector losses probably do not play a major role because on a low energy test bench the loss was $\Delta I/I_b = 3 \cdot 10^{-6}$ for the beam current of 600 mA.[26]

At high beam currents the linear part of the losses have approximately linear dependence on vacuum. Figure 6.4 shows the measured beam losses as a function of beam current for two different

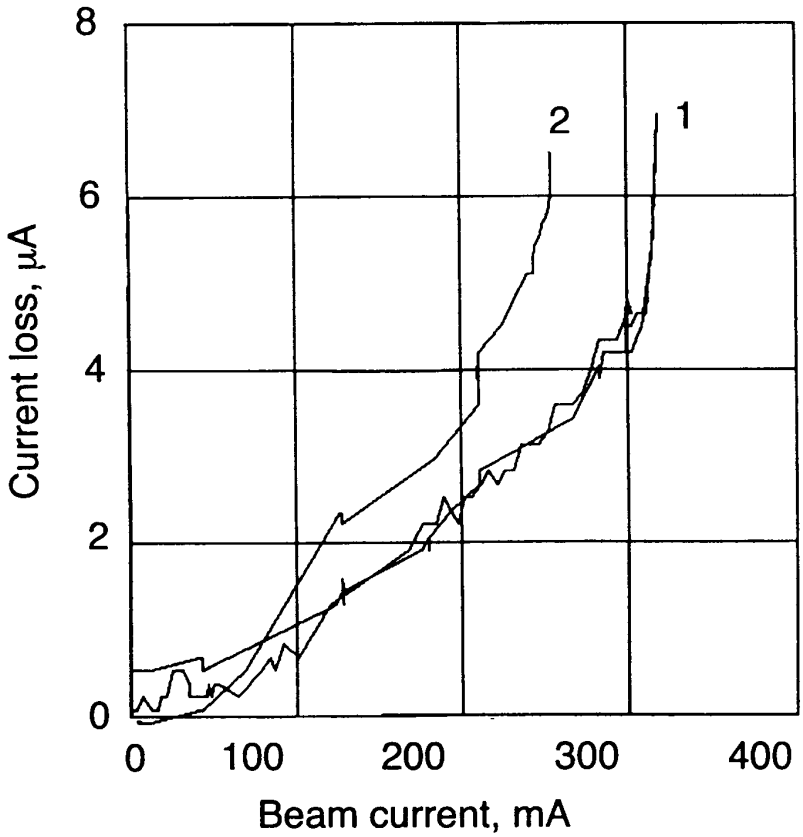

Figure 6.4: Measured current loss as a function of electron beam current. Curve (1) - p = 0.8–1.0 $\cdot 10^{-7}$ Torr, (2) - 2.3 – 3.3$\cdot 10^{-7}$ Torr. U_0 = 1.135 MV, and U_A = 39 kV for both curves. Two lines of curve (1) correspond to the increase and decrease of the beam current.

vacuum pressures. However, it does not appear that the residual gas scattering is a primary reason for current losses. Typical scattering cross sections for electrons of MeV energy yield losses too low to support such a mechanism.

"Beam halo" is used here to mean particles with longitudinal energy nearly equal to the primary beam energy and with the transverse energy orders of magnitude higher. The best understood source of this halo is an emission from the cathode edge and side surface. For the gun used in these tests, such emission is suppressed by employing a negatively biased control electrode, adjacent to the cathode. Voltage on this electrode (typically ranging from -400 V to -3 kV) determines the emitting area on the cathode face.[26]

A possible halo mechanism that would give a linear dependence on vacuum is secondary electron emission produced by the backstreaming ion bombardment. This mechanism is supported by the fact that during the initial HV conditioning with a cold cathode one could often observe a stable electron beam coming out of the accelerating tube. It has also been observed that the losses do not depend on the vacuum in the gun and collector region but only on the vacuum in the beamline.

To attain stable recirculation of electron beams with currents of 200 mA and greater in a system with relatively weak focusing it is necessary to ensure small current losses, on the order of 10^{-5}. This requires a gun carefully designed gun for small halo and a very efficient collector. Preferably beam tube pressure should be kept under 10^{-7} Torr. Electron beam size should be much smaller than the tube's aperture. Energy and bending magnet field stability should be better that 0.2%. Based on the recirculation tests, it appears feasible to build a Pelletron-based dc recirculating system capable of producing hundreds of milliamperes in the MeV energy range.

6.2 Vacuum study — electron beam surface conditioning

It is well known that in devices employing electron beams one observes intense electron-induced gas desorption from the vacuum chamber surfaces. This kind of desorption is often one of the most important factors limiting the performance and stability of such a device. The electron-induced desorption phenomenon is important for electron cooling devices. In the beginning of operation the vacuum deteriorates dramatically because of desorption from the collector surface, and one needs time to establish a maximum beam current. After the conditioning the pressure becomes a linear function of the current losses (see, for example [28, 29]). As a rule, these losses determine the vacuum level during routine operation.

The recirculation test setup at NEC shows a similar behavior; after long operation the pressure increases by 10 nTorr per microampere of loss. Such a high outgassing rate is inappropriate for cooler operation, because the vacuum in the Recycler ring must be kept under 0.1 nTorr.[5]

The electron stimulated desorption coefficient as well as the vacuum chamber outgassing rate can be decreased by a preliminary conditioning with a low energy electron beam. Ref. [27] reports reduction of both these values by several orders of magnitude after beam cleaning. The application of this method for cleaning of the cooling section seems to be very promising because of the rather simple shape of the section and a possibility to use its solenoids for the low energy beam transport.

Figure 6.5 shows the mechanical schematic of the laboratory setup for the surface conditioning studies. This all-metal setup consists of an electron gun (1) with a 2.54 cm diameter cathode, a six-way vacuum and instrumentation cross, and a 5 m long 3" od stainless steel beamtube with an ion gauge (IG2) at the far end. One short focusing solenoid near the gun (2) and five separately powered one-meter-long solenoids (3) along the beamtube alow the beam to bombard any given

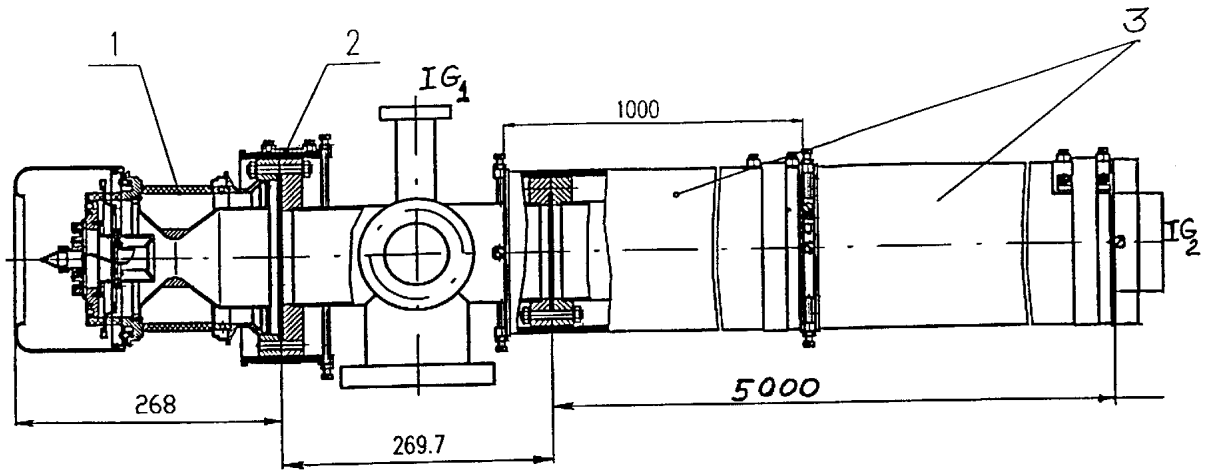

Figure 6.5: Beamline layout for the surface conditioning studies.

area of the vacuum surface. Position of the bombarded area is monitored by twelve equally spaced thermocouples. This device was commissioned in May of 1998. During the first operation a 3 keV beam of 0.25 A was transported along the 5 m long tube in magnetic field as low as 40 G. After applying of a specific dose of about 2 mA/h/cm^2 the electron stimulated desorption coefficient is 10^{-3} molecules/electron and the beam-off outgassing rate of the tube is about $7 \cdot 10^{-14}$ Torr-l/s/cm^2. The later value is significantly better than what is achievable by a bakeout procedure.[5, 30]

The following studies will be performed with this device:

1. measurements of the specific doses needed to outgas the vacuum surface
2. measurements of the outgassing rates and residual gas spectra with and without the electron beam
3. studies of the effects of opening the vacuum chamber to the atmosphere and subsequent exposure to the electron beam.

Solenoids used in this study will be a prototype for the electron cooling test beamline that will be installed in the Wideband Laboratory building.

6.3 Space charge dominated beam optics

For any beam of interest for electron cooling, the spacecharge term in the equation for the beam envelope is greater than the term depending on the transverse emittance by a factor $\mathcal{O}(10^3)$; that is, the beam is spacecharge dominated. Beam optics for spacecharge dominated beams differs from that familiar from the emittance dominated regime, especially where dispersion is involved. To facilitate development of optics for the cooler, a 12.5 kV proton beam line has been installed in the Wideband Laboratory.[31] When the current is scaled down by the square of the mass ratio, the proton beam becomes a close analog of a 4.3 MeV electron beam of the same physical emittance. Although the proton model does not correspond perfectly, it has the advantages of radiation-free operation and absence of the complications of high voltage. Before a 5 MV electron accelerator is

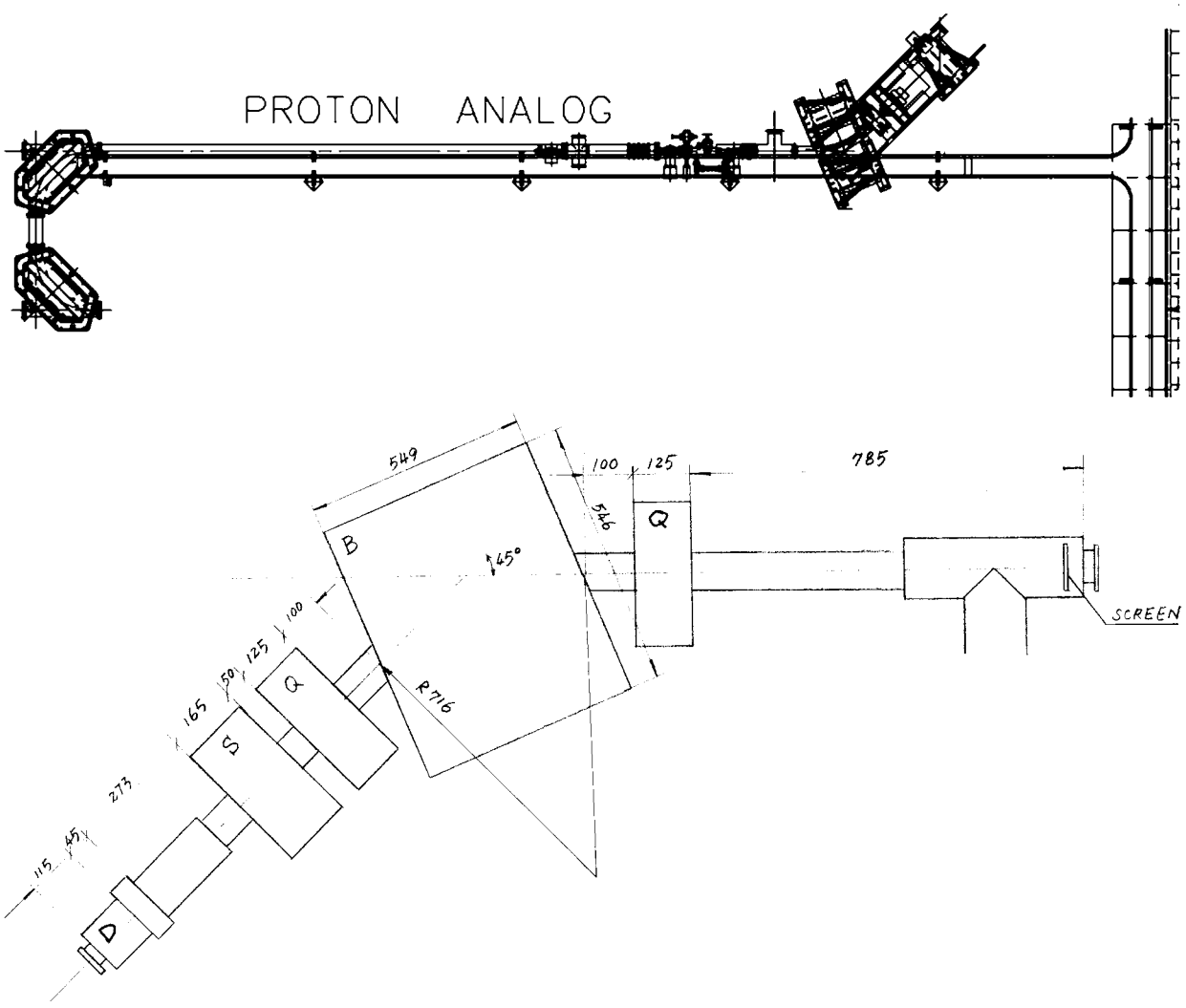

Figure 6.6: Schematic plan view of the 12.5 keV proton analog for a 4.3 MeV electron beam (top) and (bottom) sketch of duoplasmatron (D), solenoid (S), trim quads (Q), and mass selection dipole (B) left-right reversed with respect to the plan view

available, the proton analog will allow tests of beam optics and some instrumentation. The components for the $180°$ achromatic bend required to turn the beam in the cooler back toward the Pelletron have all been fabricated. A beamline containing the $180°$ bend will be built up at the Wideband Laboratory and investigated with the proton beam.

The proton analog, shown in Fig. 6.6, consists of a duoplasmatron modified for low intensity, high brightness, dc operation followed by a solenoid, a mass selection selection dipole, and an adjustable iris. Horizontal and vertical moving-slit emittance probes, Faraday cups, and an instrument carousel mounted on a precision longitudinal screw are available. The carousel rotates to place any of three instruments into the beam. It will generally have horizontal and vertical profile grids mounted.

Chapter 7

Development Program

The laboratory studies, the modelling, and conceptual development have opened a number of specific issues that will be addressed in building an operational cooler. Much of this report is devoted to identifying and discussing the more general or important of them. This brief chapter is intended to provide a reasonably comprehensive summary of the issues focused on specific elements of the hardware; it is basically a list of what needs to be done.

The ultimate goal for the development program at Wideband building (WB) is to build a system that differs little from the final electron cooling system (maybe, by the number of bends). A final adjustment to the beam can be made only by the electron cooling process itself, but the beam parameters appropriate for the cooling are to be reached at Wideband. These parameters are summarized in Table 7.1.

These parameters differ significantly from what was achieved during the electron beam recirculation (EBR) test at NEC. Many scientific and technical problems must be solved to have such a device in a reliable operation. The most important of them are listed below.

7.1 High voltage dc

Generally, technical difficulties increase with an increase of voltage. The high voltage in the WB experiment is approximately three times higher than that in the EBR test. The design acceleration gradient is also 1.5 times higher. Another difference is the presence of an inhomogeneous magnetic field along the acceleration and deceleration tubes. Consequently, the first problem to be

Table 7.1: Goal parameters for the experiment at Wideband building.

Electron current	0.5 A
Electron energy	4.5 MeV
Measured beam angles in the drift section	0.1 mrad
Energy stability	500 eV
Pressure in the drift section	1×10^{-10} Torr
Average time between crashes	1 hour
Time to reestablish the beam	2 min
Typical time between tank openings	1 month

solved in WB is reliable operation of the Pelletron at high gradient (17 kV/cm) with inhomogeneous magnetic field.

The EBR test shows that geometry of the gun and a region near the gun is critically important for the stability of operation. The origin of the HV crashes is thought to be a beam halo formed in the gun. This halo is electrons knocked from the cathode and control electrode placed near the cathode by high energy ions. These electrons have large transverse velocities and can reach acceleration tube walls and, thus, provoke breakdowns. Electron trajectories are changed by applying the magnetic field, and the accelerator stability can also change. Therefore, it is very important to find what the conditions are for stable operation with a magnetized gun.

A necessary condition for stable operation is low current losses. In the EBR test it was observed that the time between crashes decreases dramatically if the current losses exceed 10 μA. Apparently, a similar value will be an upper boundary for a 4.5 MeV device as well. To decrease the relative losses to such a low value, one needs to understand in general what determines current losses and, in particular, what is the efficiency of a partly magnetized collector.

A very important issue is the reliability of electronics operating at high voltage. This electronics will be placed on four platforms: one with potential equal to the cathode potential of -4.5 MV with respect to ground, one at anode potential, one at -3 MV, and one at -1.5 MV. Each level is powered by a separate generator and connected to a grounded computer system by optical cables. All in all, the system of the beam generation and recuperation consists of more than ten separate power supplies situated at high voltage. Achieving good reliability for such a complicated system is a difficult task needing a lot of time and effort. During the operation in the Wideband building, steps will be taken both to ensure that the electronics survive the HV sparks and to provide a mode of operation with the fewest possible sparks.

Another important technical problem which will be examined in the experiment is stability of electron energy. This question is addressed in Section 8.1.2.

7.2 Beam transport

As discussed in Chapter 8, the choice of a nearly standard accelerator results in a need for R & D in the beam optics, because the combination of a magnetized beam and a lumped focusing system is an untried solution. The primary concern are aberrations and distortions of the beam phase space because of misalignments. The beam transport line consists of solenoidal magnetic lenses, bends and steerers. An accurate analysis of the lenses can be done by a computer simulation because of their axial symmetry. A much more complicated problem is emittance growth due to passing the beam with non-zero angular momentum through 90 degree bends. It is difficult to simulate such a truly three-dimensional geometry. Perhaps these aberrations can be estimated most efficiently by measurements.

7.3 Cooling interaction region

A final goal of the WB efforts is a round beam propagating through the cooling section with angles below 0.1 mrad. The information about electron angles can be extracted from the beam size measurements. The wavelength of the electron gyromotion is approximately equal to the length of the cooling section. Therefore, five sets of scrapers installed five meters apart will provide enough information to determine the beam envelope.

Beam quality in the cooling section depends also on the magnetic field quality. The intention is to make magnetic measurements, analyze the influence of the field errors on the cooling process by a computer simulation, and, further, to correct the field errors.

Instabilities in the electron beam can be dangerous for the efficiency of the electron beam device performance as well as for stability of the antiproton beam. Information about instabilities and, more generally, about electron beam noise level can be obtained from pick-up electrodes used as BPMs.

To reach a vacuum level in the nTorr range, the technique of cleaning by low energy electron beam (see Section 6.2) will be used. Also, it will be necessary to measure the residual gas spectra with the 4.5 MeV beam on, because the residual gas content can be changed by the electron stimulated desorption.

7.4 Instrumentation and control

Effective implementation of electron cooling requires several diagnostic devices to align and characterize the anti-proton and electron beams. Because of the value of the anti-proton beam it is desirable that these diagnostics be non-intercepting or at most cause small loss to the beam. For the electron beam it is necessary that the diagnostics be nondestructive because loss of the recirculating electrons must be $\sim 10^{-5}$ to operate the Pelletron. Thus the various devices for measuring beam position, beam profile, velocity, momentum spread, instabilities, *etc*. should cause minimum loss of beams. For the most part the requirements for measuring the beams are not severe and fairly standard devices will provide the necessary precision. Across the ~ 20 m of the electron cooling section, an angular precision of $\sim 10^{-4}$ between the two beams and the solenoid field are desirable. The beam centers need to be determined to a few tenths of a millimeter with beams of about one centimeter diameter.

7.4.1 Anti-proton beam diagnostics

The stochastic cooling instrumentation will provide information on the antiproton beam directly applicable to electron cooling operations. There will be devices within the Recycler for diagnosing general cooling effects and the anti-proton beam which will be useful for electron cooling.

Several specific devices will be needed within the electron cooling straight section for aligning and observing the profile of the anti-proton beam. Position of the antiproton beam within the electron cooling section can be determined using RF beam position monitors (BPM) at each end of the cooling section. The profile of the anti-proton beam can be determined from knowledge of the beam and known lattice parameters or through measurements with fast scanning wires.

7.4.2 Electron beam diagnostics

Diagnostics for measuring and aligning the electron beam will be needed, and much of this information can be obtained by relatively simple and available devices. Beam current is measurable by precision DC current monitors, beam loss via the change in charging current of the Pelletron generator, and beam position by modulating the electron beam and sensing the position with RF beam position monitors. These devices are not destructive to the electron beam and may be used as necessary along the beam line and in the cooling section. Between the cooling solenoids, adjustable

scrapers can be used to determine the beam envelope. To some intensity flying wires are useable for measuring the density profile. These devices will be used during the R & D phase for measuring the electron beam to study recirculation with the Pelletron.

7.4.3 Advanced diagnostic possibilities

Several specialized diagnostic devices have been proposed or tried for specific needs. Many are very complex and require considerable development to implement. They may have utility for future studies of electron cooling, but many of these may be beyond the scope or needs of the initial program.

Laser scattering from the ionized background gas has been proposed for measuring the density profile.[32] The Fermilab electron cooling group has considered passing a narrow multi-keV H^- beam through the electron beam and measuring the dissociated neutral hydrogen atoms that emerge to give a density profile.

Longitudinal temperature and velocity profiles are often determined from cooling experiments. Under some conditions these values have been measured by the frequency shift and spread of backscattered laser light.[33, 34]

The transverse temperature has been estimated for lower energy electron beams by measuring the microwave radiation emitted from electrons spiraling in the magnetic field of the solenoid.[34] Whether this can be made to work would require much study.

Instabilities may be a problem with intense electron beams and will need to be monitored. Fortunately instabilities lead to RF effects in an otherwise DC beam. Standard techniques using RF, Schottky, and electrostatic measurements would be applicable.

Chapter 8

Technical Components

At the time of this report some parts of the cooler system are in the general concept stage while a few have been built in what may prove to be final form. This chapter describes component parts in terms as concrete as their state of development warrants. Because of its cost, procurement time, and installation/commissioning time, the high voltage generator has outstanding importance in planning for a project.

8.1 HV dc accelerator

The choice of the HV accelerator design is determined by two principles:

1. The design of the HV terminal components should be as simple as possible.

2. The proposed design should differ as little as possible from existing machines.

The first item on this list is a recognition of the fact that the engineering problems related to HV spark protection and hardiness of the terminal electronics could determine the time scale of the whole experimental program. In the recirculation tests, described in Section 6.1, it took more than a year to protect the electronics in the terminal to the degree that spark damage could be limited to one occurrence per month. Part of the solution was to reduce the average accelerating gradient from 15 kV/cm to 10 kV/cm, which resulted in less frequent sparks. However, these problems are solvable. The University of California, Santa Barbara (UCSB) facility operating with a 6 MV Pelletron accelerator in a recirculating mode reports superb reliability: almost no spark damage, scheduled tank openings twice a year for preventive maintenance.

The second item on the list is a recognition of the fact that large steps from existing HV technology normally take a large amount of time and effort to develop. It is clear that the traditional way to focus the electron beam with a kilogauss-range continuous magnetic field is incompatible with the existing HV technology. If one chooses to use a strong magnetic field in a combination with an MeV range accelerator, a new HV technology would be required. An example of such a proposal can be found in Ref. [35]. On the other hand, the desire to use existing HV technology leads into untried focusing schemes. A choice has been made to minimize HV R & D by finding a commercially available solution such as a Pelletron accelerator and concentrate the R & D effort on the beam transport.

Table 8.1: Pelletron accelerator parameters.

Maximum Voltage, MV	5
Maximum Charging Current, μA	400
Electrical Power, kVA	41
Tank Height, m	7.3
Tank Diameter, m	3.7
Tank Volume, m^3	71.4
Accelerator Weight (total), ton	30
SF_6 Weight, ton	3.3
HV Terminal Diameter, m	2
Column Height (incl. terminal), m	4.8

8.1.1 Accelerator design

The National Electrostatics Corporation (NEC) has constructed and commissioned over one hundred Pelletrons in the energy range from 0.5 to 30 MeV. Consequently, the HV generator itself is not expected to be troublesome. Figure 3.2 shows the Pelletron accelerator that has been proposed by NEC physicists to fit the requirements of the Fermilab electron cooling R & D program. The accelerator design incorporates several features that are not standard in NEC machines allowing for maximum flexibility in the choice of the electron beam optics. These features are:

1. **Gun and collector solenoids at terminal level** These 200 G, 50 cm long solenoids are powered by power supplies located at terminal potential. The gun solenoid creates a necessary magnetic flux through the cathode and focuses the beam for the first 500 kV of acceleration tube.

2. **Four focusing lenses** (two in each tube) These lenses are needed to keep the beam size in the tube small and to provide an optical matching between the gun (collector) solenoid and the solenoid at ground potential as described in Section 8.4. They are similar to lenses S1 and S6 used in the recirculation test (Fig. 6.1).

3. **Larger tank diameter** (12 feet as opposed to a standard 10 feet) This option allows installation of large diameter magnetic lenses and solenoids along the accelerating tube.

4. **Two rotating shafts in addition to the standard shaft that powers the gun and collector electronics** This option provides for the power for the solenoids if they are needed. However, the scheme with a solenoid and two discrete focusing lenses (items 1 and 2 above) does not require any power beyond what is normally provided by one rotating shaft.

5. **Tank flange** This option allows extending the accelerating tube length if lower operating gradient is needed; the typical gradient on NEC tubes is 16 kV/cm.

These features, of course, require development on the part of both NEC and Fermilab but seem feasible and require no new technology. Some relevant Pelletron parameters are specified in Table 8.1.

8.1.2 Pelletron voltage regulation

Pelletrons can be regulated by different techniques:

1. The amplified output of a capacitive pickoff (CPO) is applied to a tank liner for a high-bandwidth (1 to 300 Hz) feedback system. Alternately, the CPO signal can be used to drive a fast slew rate bias supply inside the HV terminal.

2. The output of a generating voltmeter (GVM) provides an error signal to the corona probe system in a slower (<1 Hz) feedback loop to provide long-term stability.

3. When beam is operating, an external system, *e. g*. slits or a beam position monitoring (BPM) system, can be used instead of the GVM to provide long-term stability.

NEC guarantees the short-term terminal ripple <1000 V FWHM for a 5 MV Pelletron without a liner system and <350 V FWHM with an optional liner system. However, the reported measured voltage stability is significantly better. UCSB reports[36] a 100 V (peak) ripple on a 6 MV Pelletron over a wide range of frequencies. Their feedback loop consists of a fast GVM (700 Hz BW), comparator, optical link (80 Hz BW), and corona triode (16 Hz BW).

The long-term Pelletron voltage stability is primarily determined by thermal effects. Since the GVM measures the electric field rather than the actual terminal voltage its calibration depends on the specific geometry of the tank and the HV terminal. As the Pelletron tank heats up, it expands and, thus, changes the GVM calibration. The dependence of the electric field, E, on temperature, T, can be expressed as follows:

$$\frac{1}{E}\frac{\mathrm{d}E}{\mathrm{d}T} = \frac{1}{\ln\frac{R_t}{R_s}}\left[-\left(\ln\frac{R_t}{R_s}+1\right)\alpha_t + \alpha_s\right] \quad , \tag{8.1}$$

where $R_t = 1.8$ m and $R_s = 1$ m are the radii of the tank and terminal shell and $\alpha_t \approx 1.4 \cdot 10^{-5}$ deg[C]$^{-1}$ (steel) and $\alpha_s \approx 2.5 \cdot 10^{-5}$ deg[C]$^{-1}$ (aluminum) are their coefficients of thermal expansion. This formula yields $0.5 \cdot 10^{-5}$ deg[C]$^{-1}$ relative thermal coefficient for the GVM calibration.

In summary, the standard short-term Pelletron regulation should be more than adequate for use in the Recycler electron cooling system. The long-term stability will also be adequate providing that the temperature variations do not exceed 10°C.

8.2 Electron gun and collector

Successful electron beam recirculation (EBR) tests at the National Electrostatics Corp. show that the gun and collector used are appropriate for operation in a beam current range of hundreds milliamperes.[37] On the test bench at Budker Institute the gun and collector were tested with current up to 600 mA.[26] Therefore, this equipment is considered as a basis for the gun and collector of the electron cooling system.

8.2.1 Electron gun

An important distinction of the present design from the original intention is the homogenous longitudinal magnetic field along the cooling section. Optimization of cooling parameters performed in Chapter 4 finds the optimum beam radius in the cooling section about 5 mm and the magnetic

Table 8.2: Gun description and parameters

Gun type	Triode with negative control electrode
Cathode type	dispenser
Cathode diameter	5 mm
Perveance	$\leq 0.07\mu$perv
Current	≤ 0.8 A
Voltage	30 – 50 kV
Magnetic field on cathode	200 G

field of ~ 50 G. As noted above (Section 3.1), Busch's theorem dictates that the gun cathode must be immersed in the same magnetic flux as the beam in the cooling section. For the chosen cathode diameter of 5 mm, magnetic field on the cathode should be 200 G. Gun parameters are summarized in Table 8.2.

Guns in traditional electron cooling devices are operated in the so-called adiabatic regime[38] in which the flight time of the electron from the cathode to the gun exit is at least several times the period of Larmour oscillation. In such a regime, electrons follow magnetic field lines, and transverse velocities created by the radial electric field of the gun are small at the gun exit. On the other hand, these transverse velocities acquired by the electrons at the gun turn into the effective temperature and can not be corrected by means of linear optics. The reason for that is the beam spacecharge; flight times are different for electrons travelling on different radii and phase advances of the Larmour rotation differ as well. The total transverse momentum remains proportional to the radius, but its radial component might be a complex function of radius and can not be decreased significantly across the entire beam by applying a lens.

In the gun under consideration, the magnetic field at the cathode is significantly lower than that in traditional coolers. As a result, the flight time is several times smaller than the Larmour period, and the anode electrostatic lens gives to the electron trajectories approximately the same angle as it does without the magnetic field. It is assumed that the beam exits the longitudinal magnetic field in the acceleration tube (see Section 8.4). The phase advance between the gun exit and the beginning of the field-free region is about two radians (120°). Radial velocities produced by both the anode and acceleration tube entrance electrostatic lenses remain proportional to the radius. They add to the axial velocities created by the solenoid fringe fields and can be compensated by a system of magnetic lenses, considered in Section 8.4. To avoid problems from the anode electrostatic lens, some conditions should be fulfilled:

1. Resulting increase of the beam size in the acceleration tube must not exceed a couple of millimeters so that the beam boundary is far from the tube electrodes.

2. Emittance growth due to gun aberrations must not exceed the emittance from the thermal electron velocities.

3. An increase of the effective emittance because of the difference in the phase advances must be made smaller than the thermal emittance.

The result of a simulation of the gun that satisfies these constraints is shown in Fig. 8.1. The simulation was performed using a SuperSAM code [39].

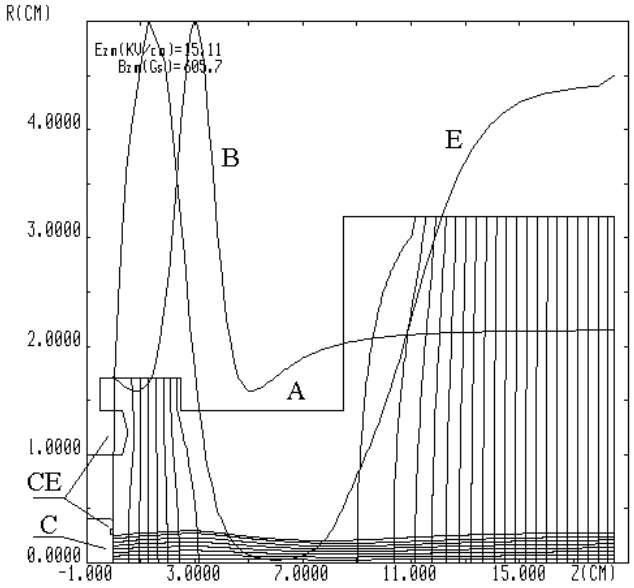

Figure 8.1: Result of the gun simulation. Anode potential is 38 kV, potential of the electrode near the cathode (control electrode) is -0.35 kV, beam current is 580 mA, magnetic field at the cathode is 200 G. Equipotentials are spaced every 5 kV.

This gun differs from the version tested in EBR test by the presence of the longitudinal magnetic field. A magnetic lens (a ring-shaped permanent magnet) mounted near the anode entrance establishes an optimum Larmour phase at the exit from the solenoid. The beam diameter at 138 keV is 5.4 mm, the angle of divergence is 2.5 mrad, and the increase in effective emittance is less than the thermal emittance.

8.2.2 Electron collector

The main challenge for a collector of an electron cooling device is to achieve a low current loss from secondary electrons. The EBR test has shown that stable operation is possible only when the current loss is less than 10 μA. For beam current of 500 mA, the relative value of the secondary electron flow from the collector must be kept less than $2 \cdot 10^{-5}$. Figure 8.2 shows the collector used in the EBR test with a solenoid added near its entrance. This collector appears to be suitable for the Recycler cooling system. The magnetic field of the entrance solenoid (about 100 G) keeps the beam at the collector entrance approximately parallel and the same size ($\sim$ 7 mm) as it was in the EBR test. Similar geometry was tested on the test bench at Budker Institute. The relative current loss was $3 \cdot 10^{-6}$ for beam current up to 600 mA. The loss value did not depend on the magnetic field strength in the entrance solenoid in a range of 0–100 G. The reason for this independence is rather clear: the secondary electron flow is suppressed in this collector by the transverse magnetic fields inside the collector cavity. The typical value of these fields is one hundred Gauss, significantly more than the field created in the cavity by the entrance solenoid. Therefore, electron trajectories are changed only a little by applying the entrance solenoid field.

Thus, the gun and collector used in the EBR test are appropriate for the electron cooling device, if they are immersed in a longitudinal magnetic field of 100–200 G. As far as the processes defining

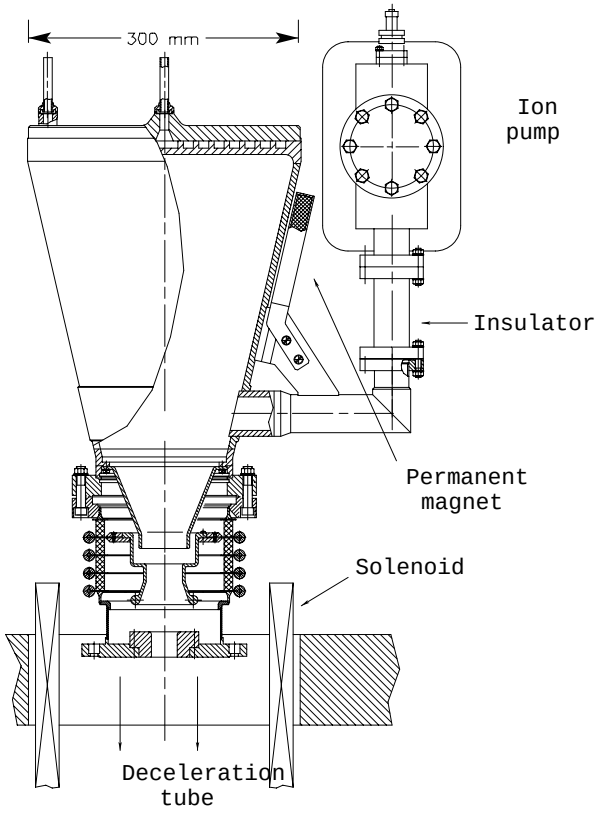

Figure 8.2: Drawing of the collector used in the recirculation tests with an added entrance solenoid

the current loss are understood, the presence of the field will not dramatically change the operation of either the gun or collector. Results of the EBR test are a good basis for predicting their properties at such low magnetic field.

8.3 Cooling interaction region

8.3.1 Choice of magnetic field in the cooling section

Traditional electron cooling devices employ a homogeneous longitudinal magnetic field in the kilogauss range for the beam transport through the cooling region. One of the main reasons is to suppress the transverse velocities arising from the electron beam space charge. In the Recycler system, the space charge effects are much smaller because of the higher beam energy. The following estimate can be written for the beam angular spread, θ, determined by the drift velocities in the combination of the longitudinal magnetic field, H, and the electric field associated with the beam space charge:

$$\theta \approx \frac{2I}{\beta^2\gamma^2 Hac} \quad . \tag{8.2}$$

For the electron beam parameters given in Table 6.1 one needs longitudinal magnetic filed of at least 25 G to keep the beam divergence below 80 μrad needed for optimum cooling. A field value of greater than 30 G satisfies this requirement.

The choice of the longitudinal magnetic field value is determined by three factors:

1. Electron beam divergence due to the drift velocities should be smaller than 80 μrad (as discussed above).

2. Focusing provided by the longitudinal magnetic field should be sufficient to suppress the electron beam instability caused by the beam-wall interaction and other weaker instabilities.

3. Magnetic field flux through the beam cross section in the cooling straight has to be equal to the magnetic flux through the gun cathode.

The second item in this list can be summarized by the following expression:[40]

$$H > \frac{2\gamma\beta mc^2}{e}\sqrt{\frac{2\pi r_e n a^2}{\gamma\beta^2 b^2}} \approx 16\ \mathrm{G}\cdot\sqrt{I/(0.5\ \mathrm{A})} \quad , \tag{8.3}$$

where r_e is the classical electron radius, b is the vacuum chamber radius (5 cm), and n is the electron density. The third requirement puts a practical limit on the longitudinal magnetic field value: if one has a 5 mm diameter cathode and 200 G field at the cathode, the value of the field in the cooling section is 200 G $\times(a/5\ \mathrm{mm})^2 \approx 50$ G for a 5 mm radius beam. The field of 200 G at the cathode seems feasible and, therefore, the choice of 50 G field in the cooling section satisfies all three conditions.

8.3.2 Vacuum requirements

In addition to the above mentioned effects, charge neutralization is also of concern. The electron beam produces ions by ionization of the residual gas in the vacuum chamber. These ions are easily

accumulated in the potential well produced by the electron beam space charge. The electric field of these ions has an effect on the electron beam γ^2 times greater than the beam's own space charge:

$$\theta \approx \left| \frac{2I}{\beta^2\gamma^2 Hac}(1-\alpha\gamma^2) \right| \quad , \tag{8.4}$$

where α is the ratio of the ion density to the electron density. If one wants to keep the electron beam divergence below 80 μrad, one has to have $\alpha \leq 2\%$ ($\gamma \approx 10$). To avoid space-charge neutralization the ions need to be cleared from the beam. Using the cross section for ionization of hydrogen (H_2) by 4.3 MeV electrons $\sigma_i \approx 2 \cdot 10^{-19}$ cm^2, one can easily estimate pressure requirements to keep α below 2 %. This requirement can be expressed in terms of characteristic times:

$$\tau_{escape} \approx \alpha \tau_{comp} \quad , \tag{8.5}$$

where τ_{comp} is the beam space charge compensation time,

$$\tau_{comp} \approx \frac{1}{\sigma_i n_0 \beta c} \quad , \tag{8.6}$$

and $\tau_{escape} \approx L/v_{rms}$, where L is the distance between clearing electrodes (20 m), v_{rms} is an rms ion velocity, and n_0 is the residual gas density. Here we assume that the ions travel along the electron beam with thermal velocities. This assumption most likely overestimates τ_{escape}. For H_2^+ ions at room temperature this yields the residual gas pressure in the cooling section of $\leq 1 \times 10^{-8}$ Torr. Similar calculations for the ions N_2/CO yield partial pressure requirement of $\leq 6 \times 10^{-10}$ Torr. These pressure requirements are by far less demanding than the average Recycler vacuum requirements[5]: $1 \cdot 10^{-10}$ Torr (H_2) and $1.5 \cdot 10^{-11}$ Torr (N_2/CO).

As a possible technical solution consider a lumped vacuum system with a pump at both ends of the 20 m long cooling section. For the beam pipe consider a 4" OD stainless steel pipe degassed at 500 C and conditioned as described in Section 6.2. Pressure along the pipe has a parabolic profile:

$$p(x) = Aq\left(\frac{Lx - x^2}{w} + \frac{L}{S}\right) \quad , \tag{8.7}$$

where A [cm^2/m] is a specific surface area of the pipe, q [Torr-l/s-cm^2] is the surface outgassing rate, w [l/s-m] is the specific conductance of the pipe (460 l/s-m for H_2), S [l/s] is the pumping speed, and x [m] is the coordinate along the beam pipe. The more relevant average pressure is

$$p_{av} = Aq\left(\frac{L^2}{6w} + \frac{L}{S}\right) \quad . \tag{8.8}$$

Assuming a pumping speed S of 30 l/s one can estimate the necessary outgassing rates to achieve the Recycler average pressure: $q \approx 4 \cdot 10^{-14}$ Torr-l/s-cm^2 for H_2 and and $4 \cdot 10^{-15}$ Torr-l/s-cm^2 for (N_2/CO). Such low outgassing rates can be achieved by the method described in Section 6.2. Alternately, one can add more pumps in the cooling section, but such a solution is complicated by the presence of the continuous solenoid.

Note that Eq. 8.7 does not take into account pumping resulting from the ionization caused by the electron beam. The additional pumping can be estimated as

$$S_i = L\sigma_i \frac{I}{e} \quad . \tag{8.9}$$

For H_2 S_i is 1.3 l/s and for N_2/CO it is 5.6 l/s, which makes only a small correction to the pressure distribution.

8.3.3 The effect of the antiproton beam space charge

Since both the antiproton and electron beams are propagating with the same velocity, the effect of the antiproton beam on the electron beam optics is equivalent to the increase of electron beam current. Thus, the average antiproton currents in the Recycler can be as high as 200 mA ($1.4 \cdot 10^{13}$ antiprotons) without any noticeable effects on the electron beam divergence.

8.3.4 Orbit alignment of the antiproton and electron beams

The current plan is to have five sets of the Beam Position Monitors (BPM's) equally spaced along the 20 m long cooling section. Since the Larmour wavelength corresponding to a 50 G magnetic field is 20 m, only one period of oscillations can fit in the cooling section. Consequently, measuring relative antiproton and electron beam positions every 5 m with a 0.5 mm precision will provide 100 μrad orbit alignment. From a signal to noise standpoint, such precision can be easily obtained.

8.4 Electron beam transport

The transport scheme mentioned in Section 8.1 assumes use of a homogenous longitudinal magnetic field in the gun, collector, and in the cooling section, but a lumped focusing system in between. Consider the feasibility of this scheme for the simplest axisymmetric case: an electron is emitted along a field line in a solenoid, exits from the field, travels through a system of lenses and enters into the second solenoid. The question is how to provide a low transverse velocity in the second solenoid? The axial symmetry gives conservation of a particle's generalized angular momentum, which can be written as the Busch theorem:

$$P_\theta(z)r = \frac{e}{2\pi c}\left(\Psi_0 - \Psi(z)\right) \quad , \tag{8.10}$$

where P_θ is the azimuthal momentum, z is the particle's coordinate, r is the radius of the electron trajectory, Ψ and Ψ_0 are the magnetic fluxes at the point considered and on the cathode respectively. The azimuthal velocity at the cathode is assumed to be zero. The theorem dictates that the radial position of an electron determines its azimuthal momentum. Therefore, it is sufficient to put the electron on the proper radius in the second solenoid (where $\Psi = \Psi_0$) to zero the azimuthal component of velocity. If the electron trajectory has a zero radial slope near the second solenoid entrance, the electron will go along the field line without transverse velocity. A system providing simultaneously specific values of both radius and radial slope at the point of the entrance can consist of two lenses. Results of simulation of such a system are shown in Fig. 8.3. The second solenoid is placed in this simulation just after an acceleration tube. This simulation was performed using the SAM code.[41]

The size and position of the first (gun) solenoid and the lenses are determined by the following considerations. First of all, the beam size must be kept significantly smaller than the tube aperture. After the exit from the solenoid $\Psi \ll \Psi_0$, and the electron moves with a constant transverse momentum P_t. If the radial velocity inside the solenoid is zero, the value of P_t is equal to the azimuthal momentum, determined by the Busch theorem:

$$P_t = \frac{e}{2\pi c r_s}\Psi_0 \quad , \tag{8.11}$$

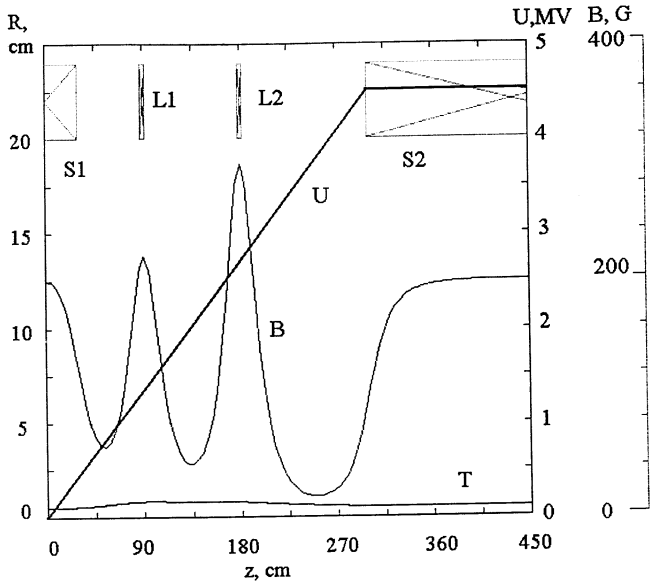

Figure 8.3: Results of a simulation for a beam transport between two solenoids. S1, S2 and L1, L2 are solenoids and lenses, respectively. Curve **B** is the magnetic field on axis. Curve **U** is the potential distribution along the axis. Curve **T** is the particle's trajectory. The trajectory radius is 5 mm in the solenoids and is kept under 8 mm in between.

where r_s is the trajectory radius at the solenoid exit. The beam expansion after the solenoid exit is determined by the ratio of P_t to the full momentum P:

$$r = \left[r_s^2 + \left(\int_{z_s}^{z} \frac{P_t}{P} dz \right)^2 \right]^{1/2} \quad , \tag{8.12}$$

where z_s is the coordinate of the solenoid exit. The P_t value is practically fixed because the value of Ψ_0 is equal to the flux through the beam cross section in the cooling section. The only possibility to decrease the beam size in a specific point is to keep accelerating electrons immersed into the magnetic field up to high enough energy. On the other hand, the higher this energy is, the larger potential difference ΔU_s between the solenoid and acceleration tube electrodes inside is, and the more complicated the high voltage insulation problems are. The arrangement shown in Figure 3.2 is a compromise between these restrictions; the potential difference $\Delta U_s \approx 500$ kV.

The variation of the magnetic field along the axis gives a possibility of aberrations. It means that only one trajectory can have a strictly zero value of the transverse velocity in the second solenoid for a specific setting of the lenses but the momentum of all other particles has a non-zero angle with respect to the beam axis. These angles, found by the simulation using the geometry of Fig. 8.3, are shown in Fig. 8.4 as a function of the beam radius. They are significantly lower than those caused by the thermal velocities (60 μrad).

Note, that the aberrations decrease with the radius of lenses, and the restriction for low enough emmitance growth puts a limit on how small the lens size can be. Further simplification of the transport scheme can be achieved by substituting the solenoidal lenses with the ring-shaped permanent magnets. In this case, an increase in aberrations might be compensated by the method suggested in Ref. [42].

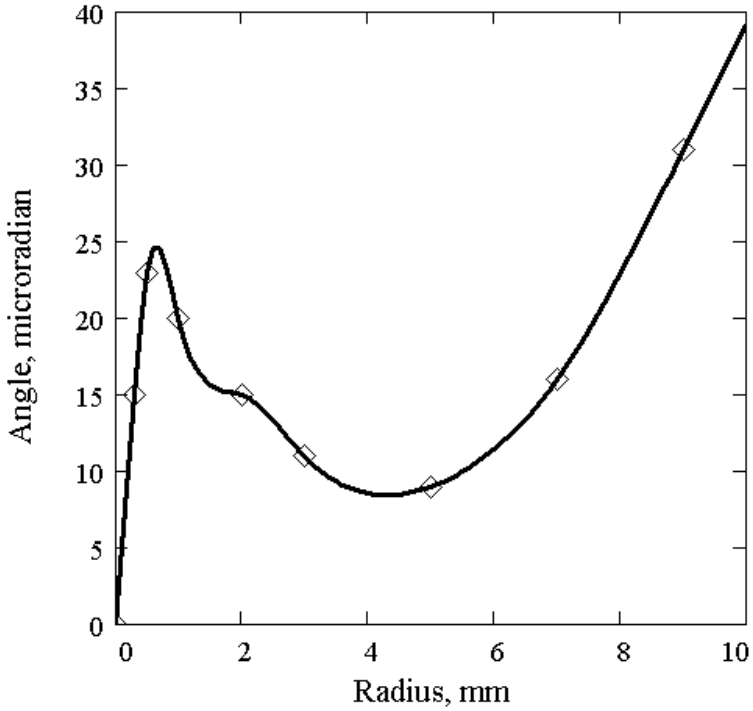

Figure 8.4: Angle between the trajectory and the axis as a function of radius. Lens strength is optimized for the trajectory with r = 5 mm.

Chapter 9

Engineering and Installation Considerations

Present plans for electron cooling in the Recycler ring incorporate a 5 MeV Pelletron accelerator. The Pelletron is an electrostatic accelerator that utilizes the Van de Graaff generator principle to elevate the terminal of the machine to high voltages. This custom built machine uses a chain of charge carrying pellets rather than a typical Van de Graaff belt to carry charge to the terminal. The chain of pellets exhibits wear characteristics that are more favorable than those of conventional belts and ensures cleaner, more stable operation over the long term. The machine is enclosed in a steel tank that conforms to the American Society of Mechanical Engineers standards; it has a large bolted flange at the top through which the accelerator is assembled. The machine is a vertical dual-column structure about 3 meters in diameter and 7.3 meters tall (see Fig. 3.2). These dimensions are in part determined by the amount of sulfur-hexaflouride (SF_6) gas needed to adequately insulate the high voltage terminal. The insulating properties of the gas are enhanced by pressurizing the gas to around 7 atmospheres. The volume of insulating gas necessary to fill the vessel is estimated at 340 cubic meters at STP. The possibility of sudden escape of this gas requires adequate ventilation and/or containment measures in addition to continuous oxygen level monitoring for personnel safety.

A quick opening manway is provided next to the base of the tank along with ports that provided for a generating voltmeter, capacitive pick-ups and an optional capacitive liner. To allow for the possibility of a future increase in tank height, a full diameter flanged joint is included in the lower half of the tank. The insulating column which supports the high potential terminal consist of 1 MV modules made up from laminated alumina ceramic and titanium metal insulating post, stainless steel hoops, and aluminum separator boxes. The hoops establish equipotential planes along the column. Power is provided to the terminal by an insulating rotating shaft that runs from the ground to the terminal. Space is provided for two additional shaft systems for powering optical elements along the two acceleration tubes.

The high voltage terminal is about 2 m in diameter and 1.8 m in height. It is designed to to accommodate both the electron gun and collector as well as their associated power supplies. Dedicated fibre optic links are provided to control and monitor the terminal components at the terminal potential. Two shielded electronic enclosures at terminal ground and a large shielded enclosure for the gun and collector power supplies are provided. Permanent magnet generators provide 11 KVA of power at 400 cps to run the equipment in the terminal. Metal oxide resistors are provided to distribute the high voltage potential along the accelerating tubes and column. The resistor are mounted on the accelerating tubes and column support posts. The accelerating tubes and column are connected electrically along equipotential planes in the column at about 30 cm intervals. The

currents from the accelerating tubes and support columns are measured independently at the column base and can be read from the main control console.

A system is provided for temporarily shorting selected accelerating tubes without entering the pressure vessel. The system consists of stainless steel rods and nylon rods, each about two feet long. They are inserted into the column through a pressure lock at the end of the tank. The shorting rod system provides improved beam performance at lower terminal voltages because high gradients can be held across selected modules. One further important use of the shorting rod system is in troubleshooting accelerator performance. For example, any single 1 MV module in the accelerator can be voltage stressed separately. Voltage stabilization in the system is achieved by employing a corona triode machine stabilizer circuit which uses an error signal from the generating voltmeter in a feedback loop to a corona point array in the Pelletron high potential terminal. The generating voltmeter also measures the electric field at the tank wall facing the terminal to an accuracy of about one percent, depending on SF_6 pressure.

9.1 Sources of radiation

X-rays are produced by the electrons, with emission rates that increase with the atomic number of the target material and even more strongly with electron energy. Below 1 MeV, the emission rate is greatest in the sideward (90°) direction. With increasing electron energy, however, the angular distribution in x-ray emission rate peaks in the forward direction. An important parameter for accelerator shielding design is, therefore, the 90° emission rate $(< 1MeV)$ or the forward (0°) emission rate $(\geq 1MeV)$ from high atomic-number (high-Z) thick targets. The primary source of radiation expected in the Pelletron arrangement will be x-rays that are generated as a result of beam losses.

9.2 Shielding calculations

Shielding calculations in this section will employ the methods and data published in the National Council on Radiation Protection and Measurements Reports No. 51 (NRCP 51) [43]. The report plots measured x-ray and neutron production rates that result when energetic electrons collide with targets (several elements) and uses plots of measured shield attenuation values and inverse distance squared from the target to estimate radiation levels outside of a shielded area. The following calculations estimate the shielding required to reduce radiation levels to an area-occupancy level of one, that is, full occupancy. The x-ray emission rates from a 2 cm diameter, 5 MeV electron beam incident on a thick tungsten (W) target at 0° and 90° to the electron beam direction is given by:

$$D_0(0^\circ, W) = 8 \cdot 10^3 \mathrm{rads} \cdot \mathrm{m}^2 \mathrm{mA}^{-1} \mathrm{min}^{-1} \tag{9.1}$$

$$D_0(90^\circ, W) = 8 \cdot 10^2 \mathrm{rads} \cdot \mathrm{m}^2 \mathrm{mA}^{-1} \mathrm{min}^{-1} \quad . \tag{9.2}$$

Using the experimentally measured maximum beam losses of 10 μA[37],

$$D_0(0^\circ, W) = 80 \mathrm{rads} \cdot \mathrm{m}^2 \mathrm{min}^{-1} \tag{9.3}$$

$$D_0(90^\circ, W) = 8 \mathrm{rads} \cdot \mathrm{m}^2 \mathrm{min}^{-1} \quad . \tag{9.4}$$

These emission rates must be multiplied by the appropriate factors (0.5 and 0.3 for the 0° and 90° directions respectively) to convert them to the equivalent rates for aluminum or concrete targets [43].

$$D_0(0^\circ, Al) = 0.5 \times 80\text{rads} \cdot \text{m}^2\text{min}^{-1} = 40\text{rads} \cdot \text{m}^2\text{min}^{-1} \quad (9.5)$$
$$D_0(90^\circ, Al) = 0.3 \times 8\text{rads} \cdot \text{m}^2\text{min}^{-1} = 2.4\text{rads} \cdot \text{m}^2\text{min}^{-1} \quad (9.6)$$

A similar calculation for an instantaneous beam loss due to a mis-steering or sudden obstruction of the 500 mA, 5 MeV beam shows emission rates of $1.2 \cdot 10^8\text{rads} \cdot \text{m}^2\text{hr}^{-1}$ in the forward direction and $7.2 \cdot 10^6\text{rads} \cdot \text{m}^2\text{hr}^{-1}$ in the transverse direction.

Based on these emission rates one can calculate the shielding transmission ratio, B, i.e the value by which the x-ray absorbed-dose index rate that is incident on the entrance face of the shielding barrier will be diminished by the barrier thickness to the requisite levels $H_m(\text{mrem} \cdot \text{hr}^{-1})$ and dose limit rate at the exit face of the barrier. Here H_m is the maximum permissible dose-equivalent or dose-limit rate.

When primary x-rays dominate the shielding situation

$$B = 1.67 \cdot 10^{-5} \left[\frac{H_m d^2}{DT} \right] \quad (9.7)$$

where,
H_m = the dose-limit rate of (1 mrem/hr);
D = the absorbed-dose index rate $(\text{radsm}^2 \cdot \text{min}^{-1})$ at 1 meter reference distance;
d = distance between x-ray source and reference point (meters);
T = Area occupancy factor;

$$B(0^\circ, 1\text{ mrem/hr}) = 4.18 \cdot 10^{-7} \quad (9.8)$$
$$B(90^\circ, 1\text{ mrem/hr}) = 8.33 \cdot 10^{-6} \quad (9.9)$$

B can be related to the shielding thickness in terms of the number of tenth-value layers of the shielding material that are required to diminish the radiation to H_m or dose-limit levels. A tenth value layer is that thickness through which the x-ray dose equivalent is diminished by a factor of 10. Hence,

$$B = 10^{-n}; or\ n = \log_{10}(1/B) \quad (9.10)$$

A value for an equilibrium tenth-value layer can be conservatively estimated for purposes of calculating shielding-barrier thickness, S.

$$S = T_1 + (n-1)T_e \quad (9.11)$$

Where
S is the shielding-barrier thickness;
T_1 is the first tenth-value layer in the shielding thickness, facing the radiation source;
T_e is the subsequent tenth-value layer, approximately constant in value;

Values of T_1 and T_e for concrete, steel and lead are given in the Appendices of NCRP No.51 as a function of the energy of the electrons incident on a thick radiation producing target. Table 9.1 shows the T_1 values used in the calculation; the T_e values are approximately the same at 5 MeV. Inserting the values for concrete into 9.11 gives:

$$S = 32\text{ cm} + (5.38) \cdot (32\text{ cm}) = 204.16\text{ cm} \sim 6.7\text{ ft(concrete)} \ . \quad (9.12)$$

Table 9.1: X-ray tenth-value layers

Shield	T_1
Concrete (2.35 g cm^{-3})	32 cm
Steel	9.7 cm
Lead	5.5 cm

9.3 Installation of pelletron and electron cooling systems in the Recycler

The research and development issues associated with the medium energy electron cooling effort have led to the planning of a facility at the Wideband Laboratory (Proton East experimental area) for housing a 5 MeV Pelletron and its associated components. This development lab will allow experimentation with high energy electron beam to develop the optics necessary for the cooling straight. In addition, development work on cooling diagnostics, magnetic (solenoidal) field measurements and all issues related to beam recirculation will be conducted at this facility. The final installation of the cooling system will be at the MI-30 service building once the electron cooling system becomes operational. The same Pelletron and electron beamline components will be used at both locations.

Installation of the Pelletron at Wide Band requires no civil construction. The machine will be installed in the controlled area pit and the required shielding blocks will form a cave around the the beam line and the main tank of the machine (see Fig. 9.1). Over-head crane coverage in the building is adequate for the assembly and dismantling of the system. The auxiliary systems for gas handling will be located inside the pit; this includes two dryers and a blower system for transferring the 340 cubic meters of SF_6 gas needed to adequately insulate the high voltage terminal at a pressure of about seven atmospheres. A large capacity SF_6 storage tank will be located just outside the north side of the building and plumbed into the system. Since sulfur-hexaflouride gas is much more dense than air, the area under the tank will need to be instrumented with oxygen monitoring alarms.

The installation of the Pelletron and electron cooling beam-line into the Main Injector tunnel at MI-30 service building requires civil construction.[44] The major difference is that at MI-30 the entire system is at a much lower elevation so that the Pelletron tank can be completely covered by earth. Figure 9.2 shows an elevation of the installation at MI-30. The Pelletron will be supported within a large concrete and steel reinforced pit. The pit will have four levels, two for access to the side manways, one for access to the top flange, and the lower level for access to beam-line components and other mechanical equipment. A hydraulic lifting mechanism will be used to raise and lower the interior service platform when maintenance is necessary. Figure 9.3 is a plan view of the Pelletron installation showing the L-shaped pit area. A thick concrete shielding wall juts into the pit area to provide shielding of the elevator shaft area. the elevator and stairwell allow travel from the pit levels to the above grade service building. The service building will be extended to provide a control room and a pump room for insulating gas. A reservoir tank for the gas will be placed between the service building and the MI berm. Another elevation view is shown in Figure 9.4. After the Pelletron tank is installed, a precast concrete roof slab will be lowered over the pit opening and sealed in place. Earth fill will form a berm over the concrete roof slab to provide the necessary shielding.

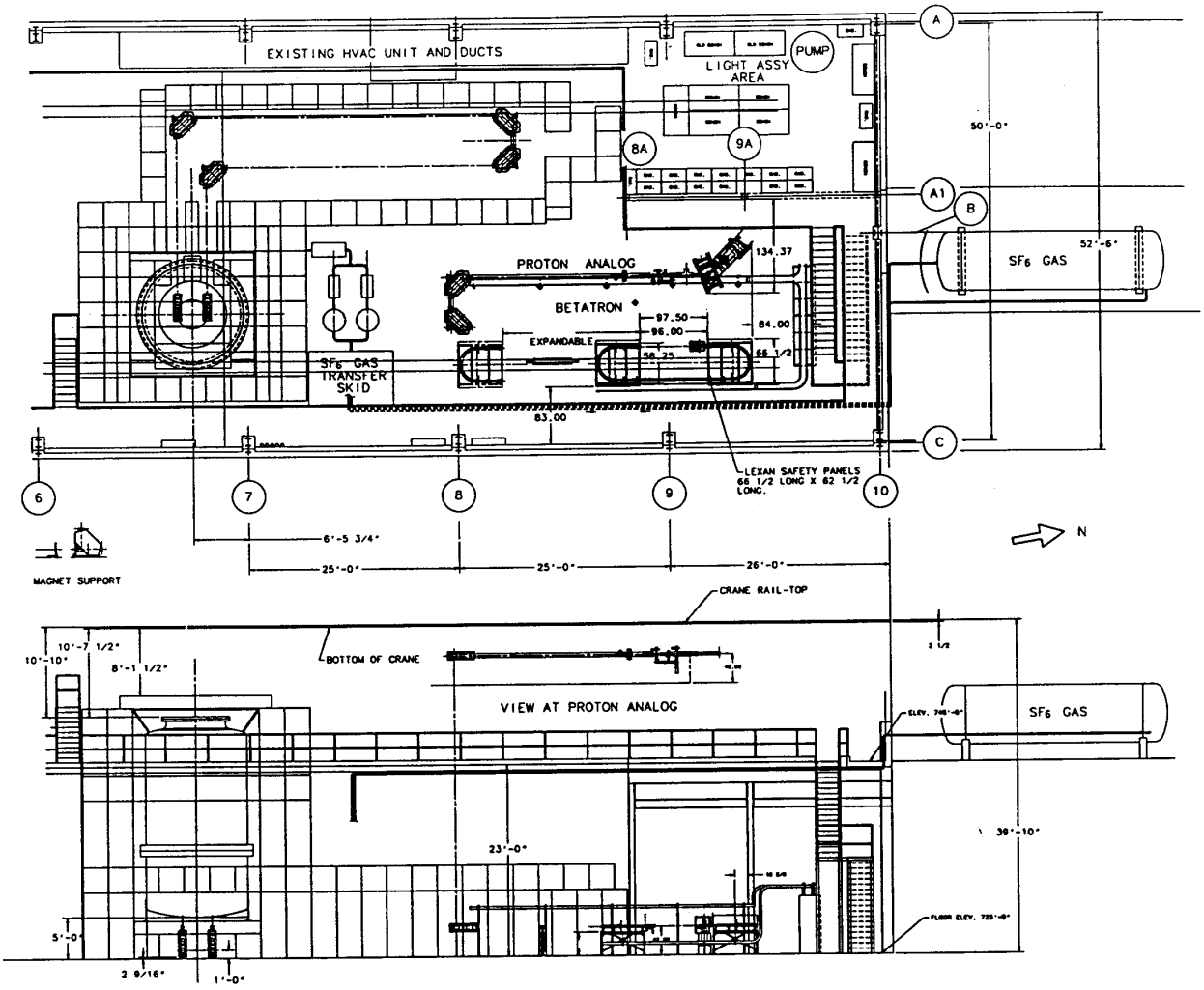

Figure 9.1: Layout of Pelletron and electron beamline in Wideband Laboratory in the Proton East area

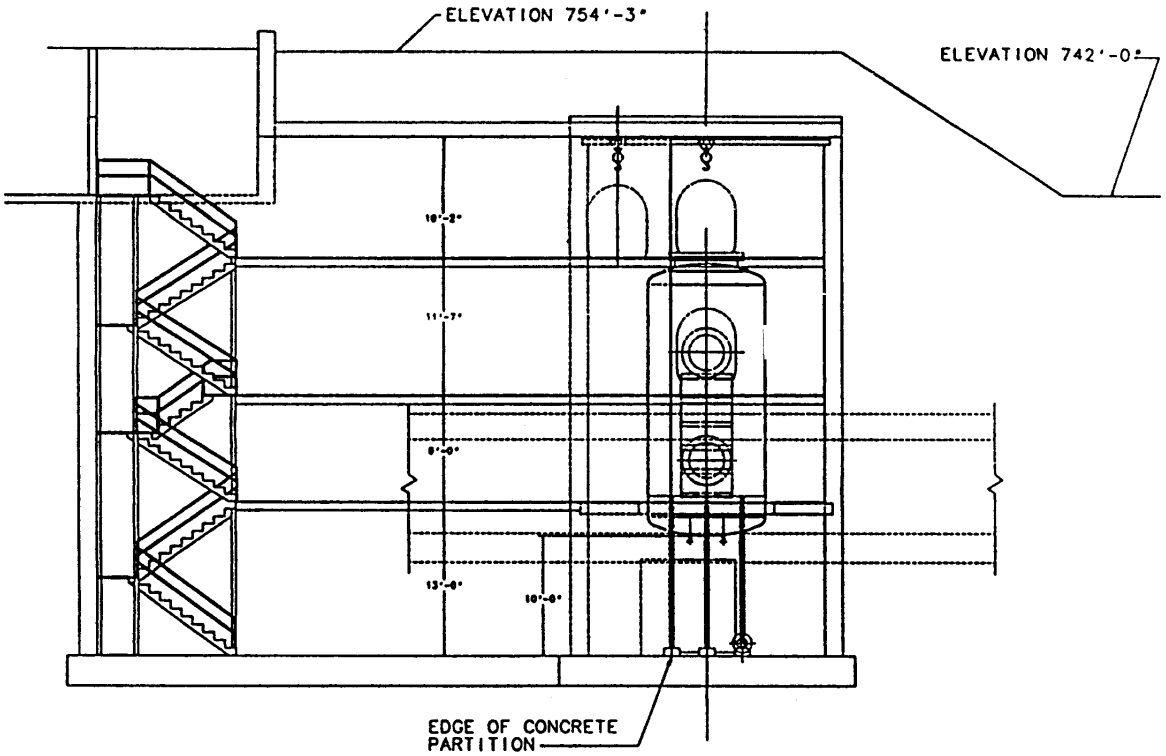

Figure 9.2: Elevation view of Pelletron installation at the MI-30 straight section

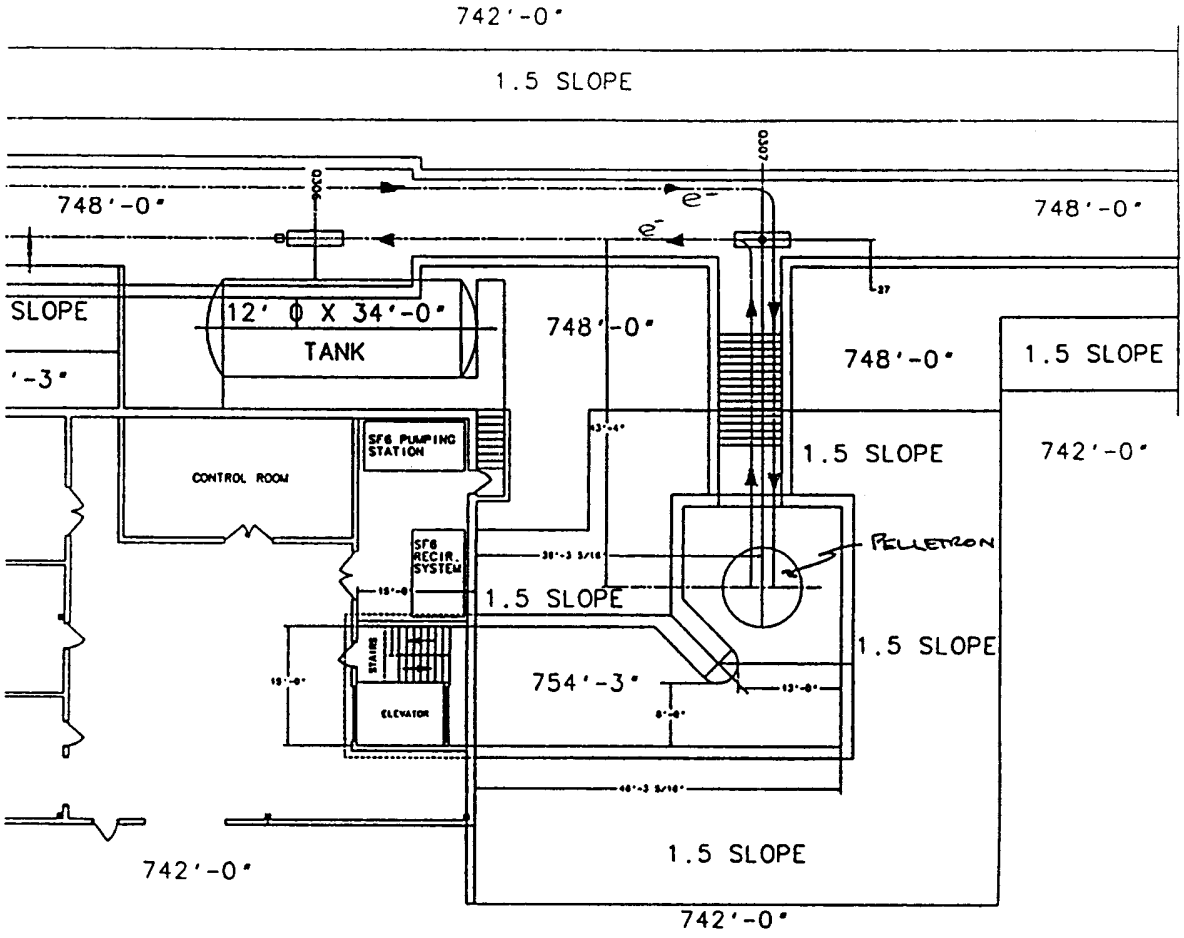

Figure 9.3: Layout of the electron cooler at the MI-30

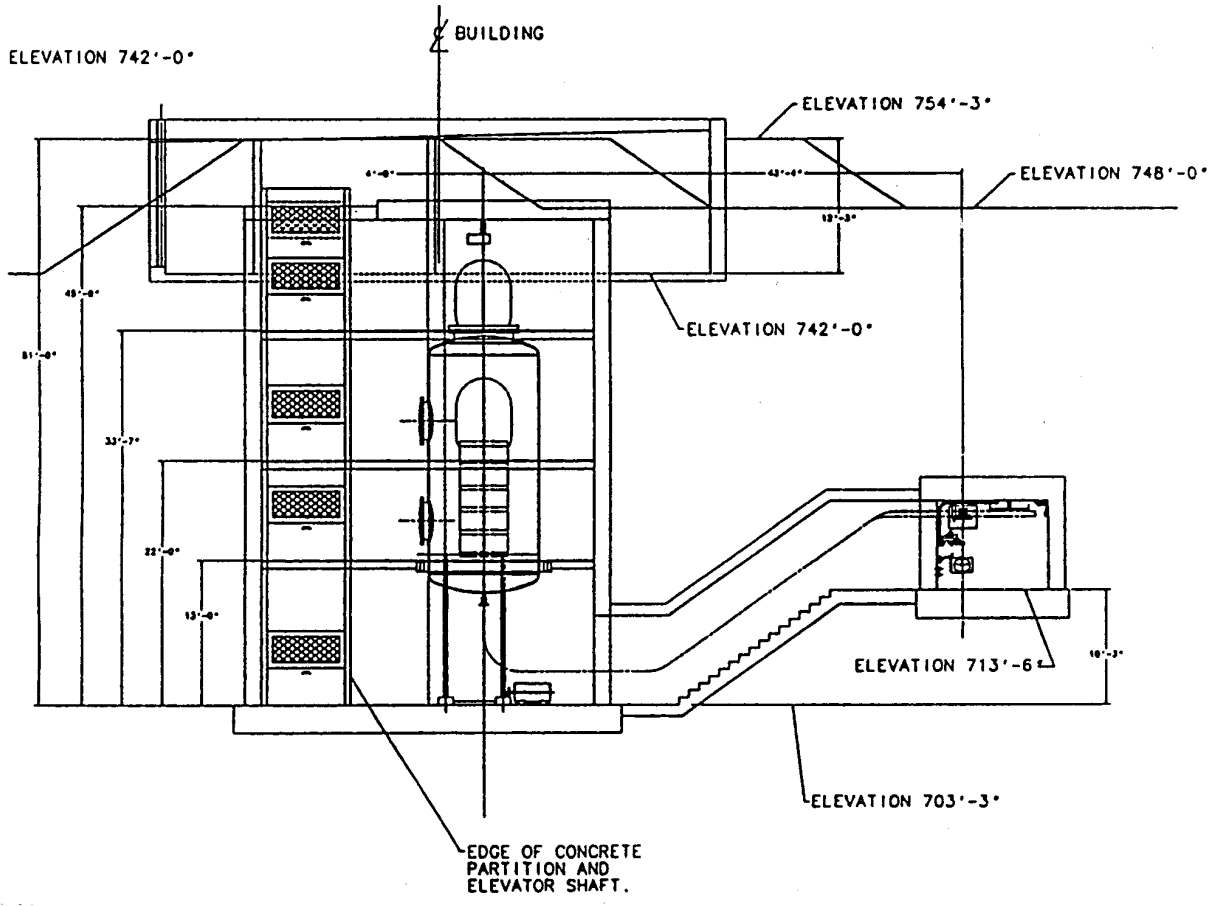

Figure 9.4: Elevation of Pelletron and electron beamline at the MI-30 straight section

Bibliography

[1] D. B. Cline *et al*.,"Intermediate Energy Electron Cooling for Antiproton Sources Using a Pelletron Accelerator", IEEE Trans. Nucl. Sci., **NS-30**, no. 4 (1983) p2370

[2] Delbert J. Larson,"Intermediate Energy Electron Cooling for Antiproton Sources", PhD dissertation, U. Wisconsin, Madison WI (1986)

[3] A. M. Budker, Atomnaja Energija, **22** (5), p246 (1967).

[4] I. N. Meshkov, Phys. Part. Nucl., **25** (6), p631 (1994).

[5] Gerry Jackson, "The Fermilab Recycler Ring Technical Design Report", FERMILAB-TM-1991, unpublished internal note (Nov. 96)

[6] Run II Handbook, available from internet,
`http://www-bd.fnal.gov/lug/runII_handbook/RunII_index.html`

[7] S. Y. Lee and K. Y. Ng, "Beam Manipulation in the Recycler with Electron Cooling", FERMILAB-FN-663 (Jan. 1998)

[8] H. Poth, "Electron Cooling: Theory, Experiment, Applications", Phys. Rept. **196**, Nos. 3 & 4, North Holland (1990) pp 135–297

[9] A. Burov and J. A. MacLachlan, "Optimization of Parameters in Medium Energy Electron Cooling", in preparation

[10] Ya. Derbenev and A. N. Skrinsky,"The Kinetics of Electron Cooling of Beams in Heavy Particle Storage Rings",Patr. Acc. **8** (1977) pp 1–20

[11] J. A. MacLachlan, "Cooling Models, Rates, *etc*.", Proc. Workshop on Medium Energy Electron Cooling (MEEC97), Budker Inst. Novosibirsk, (February 1997)

[12] J. Maclachlan, NIM, Sec. A, **391**, p. 131 (1997)

[13] S. Nagaitsev, NIM, Sec. A, **391**, p. 142 (1997)

[14] Ya. Derbenev, private communication (1998).

[15] see web page
`www-bd.fnal.gov/lug/tev33/TeV33.html`

[16] see web page
`www-bd.fnal.gov/lug`

[17] see web page
`www.fermi3.fnal.gov/welcome.html`

[18] John P. Marriner, priv. comm.

[19] James D. Bjorken and Sekazi K. Mtingwa, "Intrabeam Scattering", Part. Acc. **13** (1983) pp 115–143

[20] A. Piwinsky, Proc. 9th Int'l Conf. High Energy Acc., Stanford (1974) p 405

[21] A. Burov, "Electron Cooler Impedances", Part. Acc., **57**, p. 131 (1997).

[22] V. V. Parkhomchuk, private communication (1997).

[23] R.A. Salimov *et al*. Proc. EPAC, Rome, 1988

[24] L. R. Elias and G. Ramian, IEEE Trans. Nucl. Sci. **NS-32** No. 5 (1985), p. 1732

[25] J.R. Adney *et al*. IEEE Proceedings of the 1989 Particle Accelerator Conference, pp. 348-350, (1989)

[26] A. Sharapa, A. Shemyakin, and S. Nagaitsev, "Electron Gun and Collector for the Fermilab High Energy Electron Cooling", accepted for publication in NIM

[27] A. N. Sharapa and A. V. Shemyakin, NIM, **404** (1998), pp. 185-189

[28] M. Steck *et al.,* "Electron cooling of heavy ions at the Heidelberg cooler storage ring TSR", Proc. of the Workshop on Electron cooling and new cooling techniques, Legnaro, Italy, 15-17 May, 1990, edited by R. Calabrese and L. Tecchio, World Scientific (1991)

[29] R.Ley *et al.,* "The new electron beam collector for LEAR", Proc. of the Workshop on Electron cooling and new cooling techniques, Legnaro, Italy, 15-17 May, 1990, edited by R. Calabrese and L. Tecchio, World Scientific (1991)

[30] Y. Tito Sasaki, "A survey of vacuum cleaning procedures: A subcommittee report of the American Vacuum Society Recommended Practice Committee", J. Vac. Sci. Technol. **A9(3)** (May/Jun 1991) pp 2025-2035

[31] J. A. MacLachlan, "Modeling Electron Transport Optics with Protons", in Proc. of Workshop on Medium Energy Electron Cooling, MEEC97, Novosibirsk (1997)

[32] W. Kells, "Detector of Microwave Radiation from Cooler Electron Beam", Fermilab TM-798 (1978)

[33] W. Kells, "Laser Diagnostics for Electron Cooling Beam", Fermilab TM-771 (1978)

[34] H. Poth, "Electron Cooling", CERN Accelerator School, CERN 87-03 (21 April 1987) p562

[35] M. E. Veis *et al*. "Electron beam technique for high voltage electron cooling", Proc. Workshop on Medium Energy Electron Cooling (MEEC97), Budker Inst. Novosibirsk, p.125, (February 1997)

[36] Jerry Ramian, UCSB (private communication, July 1998)

[37] A. C. Crawford and S. Nagaitsev, "Successful MeV-Range Beam Recirculation", proc. 1998 EPAC, Stockholm (1998)

[38] V. A. Lebedev and A. N. Sharapa, "Formation of an electron beam with low transverse velocities in systems with a longitudinal magnetic field", Sov. Phys. Tech. Phys., 32 (1987), pp594–595

[39] D. G. Myakishev, M. A. Tiunov, and V. P. Yakovlev, "Code SuperSAM for calculation of electron guns with high beam area convergence", Proc. XV ICHEA (Hamburg, 1992), Int. J. Mod. Phys. A (Proc. Suppl.) **2B**(1993) Vol. II, pp 915-917

[40] N. Dikansky, S. Nagaitsev, and V. Parkhomchuk, "Electron Beam Focusing System", Proceedings of MEEC96 workshop, Fermilab (1996)

[41] B. M. Fomel, M. A. Tiunov, and V. P. Yakovlev, "SAM - an interactive code for evaluation of electron guns", Preprint INP 96-11, Novosibirsk (1996)

[42] S. Nagaitsev and Ya. Derbenev "Immersed gun and collector with a Pelletron", Proc. Workshop on Medium Energy Electron Cooling (MEEC97), Budker Inst. Novosibirsk (February 1997) p197

[43] Radiation Protection Design Guidelines for 0.1-100 MeV Particle Accelerator Facilities. NCRP Report No.51

[44] P. Hurh, "Physical Installation of Pelletron and Electron Cooling System", from MEEC96 Workshop at Fermilab (Feb. 96), in Fermilab-TM-1998 (Sept. 97)

[45] MEB E-Cool Design Report, IUCF (1992).

[46] V. V. Parkhomchuk, from MEEC96 Workshop at Fermilab (Feb. 96), in Fermilab-TM-1998 (Sept. 97)

Appendix A

Optimum electron density distribution

In Section 4.2.2 the electron beam was assumed homogeneous within the circle $r \leq a$; the radius a was then optimized. However, the electron density can vary arbitrarily in the transverse xy plane, both in the radial $r = \sqrt{x^2 + y^2}$ and poloidal $\phi = \arccos(x/r)$ directions. There should be an optimum distribution giving the shortest cooling time at a given electron current and loss percentage.

This problem can be resolved in two steps. First, the optimum density distribution $n(\vec{r}_\perp)$ can be found within the circle $r \leq a$; second, the radius a can be optimized. Using the same units as in Section 4.2.2, the cooling time for a given particle with the stop-point $\vec{r}_\perp$ can be expressed as

$$\tau = v_z \sqrt{J_x J_y} J_e / n(\vec{r}_\perp) \tag{A.1}$$

with

$$\int_{r<a} d^2 r n(\vec{r}_\perp) = \pi a^2 = 2\pi J_e \ . \tag{A.2}$$

The normalization of Eq. A.2 is needed to establish the identity of the units in this and the earlier treatment. It follows that for the fixed cooling time t, the particles with

$$v_z > \bar{v} = n(\vec{r}_\perp) t / (J_e \sqrt{J_x J_y}) \tag{A.3}$$

are effectively lost for cooling. With $g(J_x, J_y, v)$ to denote the particle distribution over the transverse actions J_x, J_y and the longitudinal velocity v, normalized as

$$\int_0^\infty \int_0^\infty dJ_x dJ_y \int_0^\infty dv_z g(J_x, J_y, v) = 1 \ , \tag{A.4}$$

the inside part of the loss percentage Δ_{in} is expressed

$$\Delta_{in} = \iint_{J_x + J_y < J_e} dJ_x dJ_y \int_{\bar{v}}^\infty dv_z g(J_x, J_y, v) \ . \tag{A.5}$$

To find the optimum distribution within the fixed radius a, the variational principle can be used; for the optimum, any small redistributions $\delta n(\vec{r}_\perp)$ of the density do not influence the losses (Eq. A.5) in the first order of $\delta n(\vec{r}_\perp)$. Note that the redistribution does not increase the total electron current:

$$\iint_{r<a} d^2 r \delta n(\vec{r}_\perp) = 0 \ . \tag{A.6}$$

The variation of the density results in a change of $\bar{v}$ (Eq. A.3), the lower limit of the loss integral in Eq. A.5, causing a variation of the integral itself:

$$\delta\Delta_{in} = -\iint_{J_x+J_y<J_e} dJ_x dJ_y g(J_x, J_y, \bar{v})\delta n(x,y)t/\sqrt{J_x, J_y} \quad . \tag{A.7}$$

In the integration over the actions, the density is taken at the stop-point of the particle; in the adopted units

$$x = \sqrt{2J_x}, \quad y = \sqrt{2J_y} \quad .$$

Converting from the integration over actions to the integration over the coordinates, the loss variation follows. The losses variation is zero at the optimum, so that

$$\delta\Delta_{in} \propto \iint_{r<a} dxdy g(J_x, J_y, \bar{v})\delta n(x,y) = 0 \quad . \tag{A.8}$$

The last condition has to be satisfied for any density redistribution restricted only by the requirement of electron current conservation (Eq. A.6). This can be fulfilled only when the particle distribution is constant at the cooling boundary:

$$g(J_x, J_y, \bar{v}) = \text{const.} \tag{A.9}$$

This equation gives the condition for optimum distribution of the electron density. For a given particle distribution g, it imposes a restriction on the limiting longitudinal velocity $\bar{v}$ and thus on the electron density $n(x,y) = \bar{v}J_e\sqrt{J_x J_y}/t$.

For a Gaussian distribution

$$g(J_x, J_y, v) = \sqrt{2/\pi}\exp(-J_x - J_y - v^2/2) \quad , \tag{A.10}$$

the optimum condition (Eq. A.9) results in

$$J_x + J_y + \bar{v}^2/2 = J_m \quad , \tag{A.11}$$

where J_m is a constant. The electron density can be obtained from this equation, while the constant J_m is found from the normalization (Eq. A.2). The electron density associated with the marginal velocity $\bar{v}$ (A.3) is found from here:

$$\begin{aligned} n(\vec{r}_\perp) = &\quad n_r(r)\sin\phi\cos\phi \\ n_r(r) = &\quad \begin{cases} JJ_e\sqrt{2(J_m - J)}/t & \text{if } J \le J_e \\ 0 & \text{otherwise} \end{cases} \\ \int_0^{J_e} n_r dJ = &\quad \pi J_e, \quad J = r^2/2 \end{aligned} \tag{A.12}$$

The profile of the optimum radial distribution n_r is presented in Fig. A.1.

It follows from here that for the given constant $J_m \ge J_e$, the beam cooling time is determined by

$$t = \int_0^{J_e} J\sqrt{2(J_m - J)}dJ/\pi \quad . \tag{A.13}$$

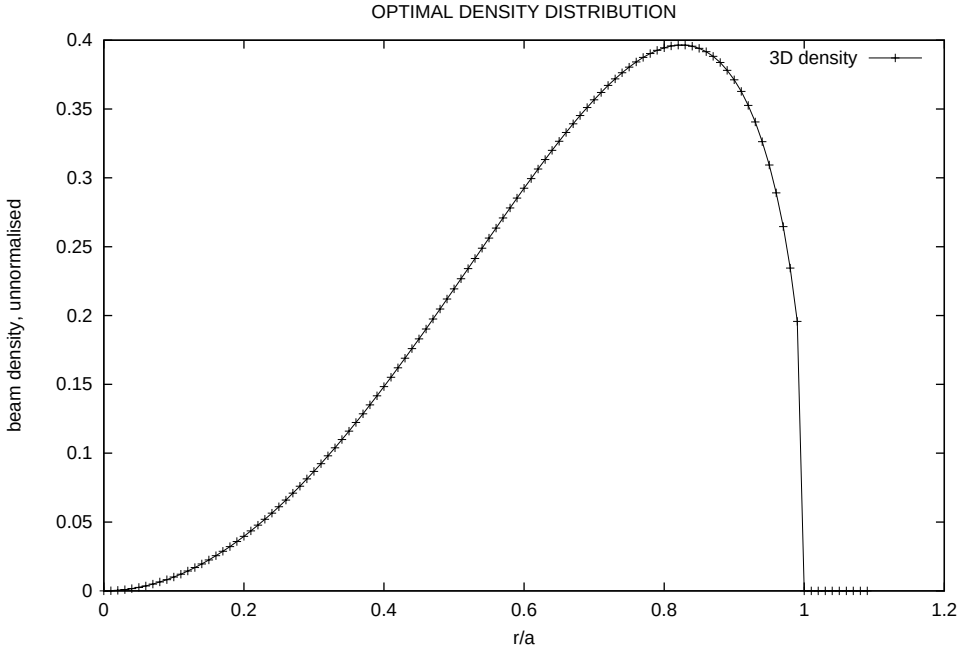

Figure A.1: Profile of the optimum radial distribution of the electron beam, unnormalized.

Then, the inside part of the losses (Eq. A.5) can be expressed as

$$\Delta_{in} = \sqrt{\frac{2}{\pi}} \exp(-J_m) \int_0^{J_e} \frac{dJJ}{\sqrt{2(J_m - J)}} = \sqrt{2\pi} \exp(-J_m) \frac{\partial t}{\partial J_m} \quad . \tag{A.14}$$

The total losses consist of the inside part (Eq. A.14) and the outside part (Eq. 4.29):

$$\Delta_t = \sqrt{2\pi} \exp(-J_m) \frac{\partial t}{\partial J_m} + J_e \exp(-J_e) \quad . \tag{A.15}$$

It now can be shown that at the optimum the introduced constant

$$J_m = J_e \quad . \tag{A.16}$$

First, minimization of the total losses for the given time t requires $J_m = J_e + \mathcal{O}(1)$. Hence the cooling time can be written as

$$t = \frac{4\sqrt{2}}{15\pi} J_m^{5/2} \quad . \tag{A.17}$$

Then, if $J_e < J_m$, the total losses (Eq. A.15) can be minimized by increasing J_e up to its maximum $J_e = J_m$, while the time t (Eq. A.17) is not changed.

Thus, the final expressions for the cooling time and the total losses as functions of the electron beam radius $a = J_e^2/2$ become

$$\begin{array}{rcl} \Delta_t & = & \frac{4}{3\pi} J_e^{3/2} \exp(-J_e) + J_e \exp(-J_e) \\ t & = & \frac{4\sqrt{2}}{15\pi} J_e^{5/2} \quad . \end{array} \tag{A.18}$$

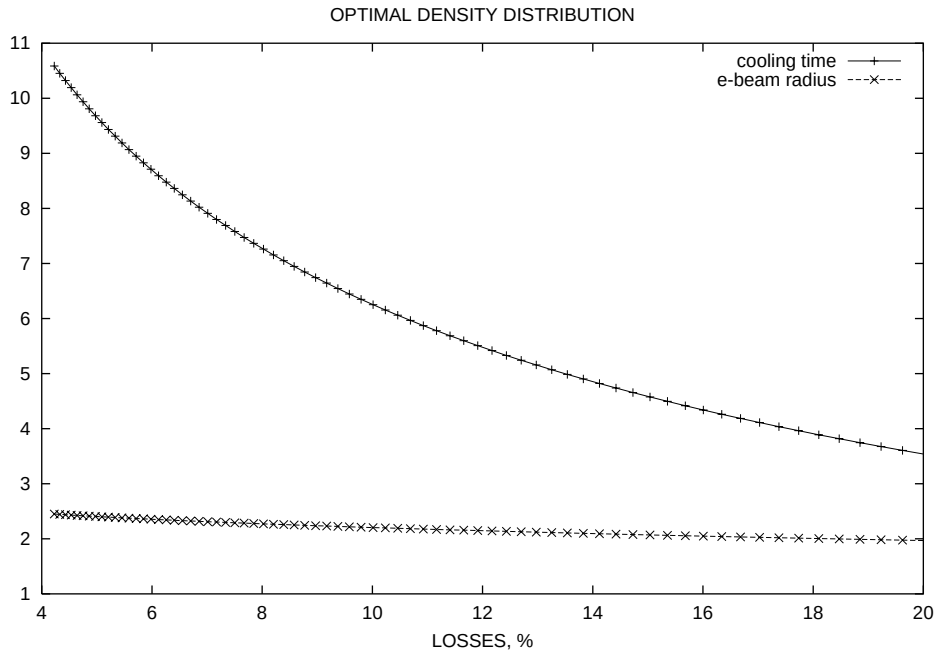

Figure A.2: Optimum radius of the electron beam and the time of cooling required by the given loss percentage. The time is in the units of the parameter t_0 (Eq. 4.22), the electron beam radius is in the units of the rms amplitude of the cooled beam $x_m = \sqrt{2\epsilon\beta_f/(\beta\gamma)}$.

The result is a dependence of the cooling time required on the given loss percentage. This dependence, together with the corresponding dependence of the optimum electron radius, is shown in Fig. A.2.

It can be concluded that the optimization of the electron beam density gives rather modest gain over the case of the homogeneous density with the optimized radius. At the accepted loss of 5%, the beam cooling time for these two cases differs by a factor of 1.6.

Appendix B

Considerations for lumped focusing of electrons in the cooling straight

The cooling electron beam can be focused either by means of a constant solenoidal magnetic field or with thin solenoidal lenses for a compensation of the space charge repulsion as in reference[45]; both variants have been discussed for the Recycler[13]. The tolerances for the latter variant need specific consideration.

Assuming the lenses to be separated by the distances l_l, the angle θ_{sc} acquired by the electron beam boundary is

$$\theta_{sc} = \frac{\lambda r_e l_l}{\beta^3 \gamma^3 a} \ , \tag{B.1}$$

with λ standing for the electron linear density. For the parameters listed in Table 4.4 and $l_l = 1$ m, Eq. B.1 gives $\theta_{sc} = \ 1.5\ \mu$rad, corresponding to the lens focusing distance $f_l = a/(2\theta_{sc}) = 7$ km. Hence, the space charge effect is so weak at these parameters, that even one lens for the total cooler length would be enough to keep the angle below the tolerable level.

It was noted in [46], that the electron beam focused by the thin lenses would be unstable due to the wall image charges. The instability is convective with the space increment rate

$$G = \sqrt{2\lambda r_e/\gamma}/(\beta b) \ , \tag{B.2}$$

where b is the aperture radius. For the parameters discussed, it gives $G^{-1} = 6$ m which is comparable with the total cooling length.

In this case, the tolerable beam offset x_{in} and angle θ_{in} at the entrance of the cooler are determined by the dependance of the instability growth factor on the cooler length l_c:

$$x_{in} \leq \theta_e G^{-1} \exp(-G l_c), \quad \theta_{in} \leq \theta_e \exp(-G l_c) \tag{B.3}$$

which gives $x_{in} \leq 10\,\mu$m and $\theta_{in} \leq 2\,\mu$rad in the case under consideration. An offset of the lenses is not a tight parameter because of the long focal length. It could be more important to control the lens angle α. This angle drives an electron beam angle $\theta_l = \alpha\sqrt{d_l/(2f_l)}$, where d_l is a thickness of the lens. Assuming the lens angles to be independent random values with the rms α_{rms}, an average angle acquired by the electron beam at the instability length G^{-1} can be found:

$$\theta_l = \alpha_{rms}\sqrt{\frac{d_l}{2G f_l l_l}} \ ; \tag{B.4}$$

because $f_l \propto l_l^{-1}$, it does not depend on the lens separation l_l. To be tolerable, this angle has to be small at the end of the cooler, giving the requirement

$$\alpha_{rms} \leq \theta_e \sqrt{\frac{2Gf_l l_l}{d_l}} \exp(-Gl_c + 1) \quad . \tag{B.5}$$

According to the previous calculations, $\theta_e = 4 \cdot 10^{-5}$; for the thickness $d_l = 10$cm it comes out $\alpha_{rms} \leq 4 \cdot 10^{-3}$. The numbers obtained in this chapter are summarized in Tab. B.1:

Table B.1: THIN-LENS OPTICS

Parameter	Symbol	$\beta_f = 200$m	$\beta_f = 20$m	Unit
Minimal number of lenses	N_l	1	3	
Instability growth length	G^{-1}	6		m
Beam entrance offset	x_{in}	≤ 10	≤ 20	μm
Beam entrance angle	θ_{in}	≤ 2	≤ 4	μrad
Lens rms angle	α_{rms}	≤ 4		mrad